Doctoral Thesis

Theoretical studies on cosmological implications of the electroweak symmetry breaking

Masanori Tanaka

Department of Physics, Osaka University,

Toyonaka, Osaka, 560-0043, Japan

Acknowledgements

I would like to express my sincere gratitude to my supervisor, Prof. Shinya Kanemura, for providing me with a lot of instruction and advise to physics and life. Thanks to his tremendous supports, I have been able to complete this thesis. I would also like to appreciate Prof. Tetsuya Onogi, Prof. Takahiro Sumi, Prof. Ryosuke Sato and Prof. Kei Yagyu for the careful reading my thesis and the helpful comments. I am much obliged to Prof. Tomo Takahashi, Dr. Ryo Nagai, Dr. Katsuya Hashino for their fruitful and stimulating collaborations. I am grateful to the faculty members of the particle physics theory group at Osaka University, Prof. Tatsuma Nishioka, Prof. Satoshi Yamaguchi, Prof. Minoru Tanaka, Prof. Hidenori Fukaya, Prof. Norihiro Iizuka and Prof. Yutaka Hosotani, and the secretaries, Ms. Kazumi Asano and Ms. Akiko Takao, for their support of my research activities. I appreciate my colleagues in the group, Mr. Takayuki Sumimoto, Mr. Hiroki Kawakami, Mr. Kento Katayama and Mr. Yushi Mura for many exciting discussions and talks. I would like to thank my mother and my grandfather for their kind support and encouragement.

Abstract

Although the standard model (SM) in particle physics is consistent with the results in collider experiments, it cannot explain several cosmological observations such as the baryon asymmetry of the Universe (BAU) and the existence of dark matter. In order to solve these problems, we should consider new physics. When we consider new physics models with extensions of the Higgs sector from the SM, aspects of the electroweak symmetry breaking can be drastically changed. Especially, dynamics of the electroweak phase transition (EWPT) at the early Universe can be changed. In the SM, the EWPT is crossover. On the other hand, the EWPT can be a first-order in extended Higgs models. We are able to observe remnants of the first-order EWPT by using cosmological observations.

The first-order EWPT plays an important role to solve problems such as the BAU. The electroweak baryogenesis is a promising scenario to explain the baryon asymmetry. In this scenario, the baryon asymmetry can be produced when the first-order EWPT occurred. It indicates that testing first-order EWPT is important.

In general, in extended Higgs models with the strongly first-order EWPT, the triple Higgs boson coupling hhh deviates from the SM prediction about 20–30%. It implies that we can test the strongly first-order EWPT at future collider experiments; i.e., International Linear Collider (ILC) and High-Luminocity LHC (HL-LHC). On the other hand, there is a possibility that a special shape of gravitational waves (GWs) can be produced by the first-order phase transition. The first-order phase transition at the early Universe occurs via the vacuum bubble nucleation. Then, characteristic GWs can be produced by vacuum bubble collisions. Therefore, the first-order EWPT can be tested by GW observations. For the first-order EWPT, the predicted GW spectrum has a peak around 10^{-3}–10^{-1} Hz. Such GWs may be detected at future space-based interferometers such as the Laser Interferometer Space Antenna (LISA) and DECi-hertz Interferometer Gravitational wave Observatory (DECIGO).

In this thesis, we first discuss the dynamics of the EWPT in the two Higgs doublet model as an example of renormalizable extended Higgs models. We show the prediction on the triple Higgs boson coupling and GW spetrum in this model. We also show that new scalar bosons, whose masses are lighter than 2 TeV, must exist in order to realize the scenario of electroweak baryogenesis. In addition, we discuss how we can know a typical mass scale of new scalar bosons by the combination of the measurement of hhh coupling with GW observations.

We then discuss the EWPT in a new effective field theory (EFT). As already mentioned, the SM is consistent with results in the LHC. Furthermore, no signatures for new particles have been observed. For these reasons, the framework of the Standard Model Effective Field Theory (SMEFT) is often used. In the SMEFT, higher dimensional operators composed of field contents in the SM are introduced to describe new physics beyond the SM. Whereas, there is a possibility that large quantum corrections in Higgs couplings can be realized by heavy new particles. Such effects are often called as the non-decoupling effects. The non-decoupling effects are important to realize the strongly first-order EWPT. Unfortunately, the SMEFT is not a good framework to describe new physics with the non-decoupling effects. It means that we need a new EFT instead of the SMEFT. In recent, the nearly aligned Higgs Effective Field Theory (naHEFT) is proposed as a good candidate. The naHEFT can describe new physics with the non-decoupling effects. In this thesis, model independent predictions on the hhh coupling and GW spectra are shown by using the naHEFT.

Finally, we discuss the relation between the first-order EWPT and primordial black holes. If the

first-order EWPT occurs at the early Universe, a large energy density fluctuation may be realized. As a result, primordial black holes can be formed. It means that the first-order EWPT may be tested by current and future PBH observations. We discuss the PBH formation in the naHEFT to obtain model independent results. The mass of PBHs produced by the EWPT is about 10^{-5} of the solar mass. Such PBHs may be observed by microlensing observations such as Subaru Hyper Suprime Cam (HSC), Optical Gravitational Lensing Experiment (OGLE), PRime-focus Infrared Microlensing Experiment (PRIME) and Nancy Grace Roman (Roman) Space Telescople. It means that we may be able to test the first-order EWPT by using microlensing observations. We show complementarity of PBH observations, future GW observations and collider experiments to test the first-order EWPT.

Contents

Chapter 1

Introduction

The Standard Model in particle physics is a theory which successfully explains experimental results in various experiments such as collider experiments, flavor experiments and cosmological observations [1]. Interactions with particles in the SM are determined by the gauge principle. Masses of particles in the SM are given by the Higgs mechanism [2–6]. The Higgs mechanism is based on the spontaneous electroweak symmetry breaking (EWSB). The EWSB occurred at the early Universe is called as the electroweak phase transition (EWPT). According to the lattice simulations, the EWPT in the SM is not a first-order [7, 8]. On the other hand, the EWPT can be a first-order when we consider extended Higgs models. If the first-order EWPT occurs at the early Universe, remnants of the first-order EWPT may be observed by using cosmological observations and collider experiments.

In the SM, an isospin doublet scalar field is only introduced to realize the EWSB. Although this assumption is minimal, there is no principle to determine the structure of the Higgs sector like the gauge principle characterizing the interactions with elementary particles. In addition, several phenomena beyond the SM (BSM) have been already confirmed by cosmological observations, i.e., the baryon asymmetry of the Universe (BAU), neutrino oscillations and the existence of dark matter. These facts indicate that extensions of the Higgs sector from the SM are natural ways to solve the BSM phenomena. Phenomenological consequences of extended Higgs models at current and future collider experiments have been thoroughly investigated. For instance, the collider phenomenology in two Higgs doublet model [9–24], the SM with singlet scalar fields with a scalar mixing [25–32], the inert doublet scalar field [21, 33–36], the SM with triplet scalar fields [37–41] have been examined.

The extended Higgs models may solve BSM phenomena such as the BAU. To generate the observed baryon asymmetry from a baryon-symmetric early Universe, we need a mechanism which satisfies Sakharov's conditions [42]. For example, the electroweak baryogenesis (EWBG) is a promising scenario satisfying Sakharov's conditions [43]. In the EWBG, the baryon asymmetry can be generated when the first-order EWPT proceeds [43]. The sphaleron process, which violates baryon numbers, plays an important role to generate the baryon asymmetry in the EWBG [44,45]. In order to explain the observed baryon asymmetry via the EWBG, the sphaleron process decouples after the first-order EWPT [43]. This condition is often called as the sphaleron decoupling condition. We call the first-order EWPT satisfying the sphaleron decoupling condition as the strongly first-order EWPT. The EWPT in extended Higgs models with an additional doublet scalar field [46–58], a singlet scalar field with scalar mixing [59–65] or without scalar mixing [66–69] have been analyzed.

We can obtain several predictions in the collider phenomenology from the sphaleron decoupling

condition. For instance, the triple Higgs boson coupling hhh deviates from the SM prediction by 20–30 % to satisfy the sphaleron decoupling condition in several extended Higgs models like the two Higgs doublet model [50]. The hhh coupling can be measured precisely at future collider experiments. For example, the hhh coupling are measured at 50 % accuracy at the HL-LHC [70]. At future lepton colliders such as the ILC with 1 TeV center mass energy, the hhh coupling can be measured at 10 % accuracy [71]. It means that the first-order EWPT may be tested by future collider experiments where the hhh coupling can be precisely measured.

The EWBG predicts not only characteristic collider signatures but also cosmological phenomena. When the first-order phase transition occurs at the early Universe, stochastic gravitational waves (GWs) can be produced [72]. The first-order phase transition at the early Universe occurs via the nucleation and expansion of vacuum bubbles. Characteristic spectrum of GWs can be produced via the dynamics of the vacuum bubbles [73]. For the first-order EWPT, the predicted GW spectrum has a peak around 10^{-3}–10^{-1} Hz. Such characteristic GWs may be detected at future space-based interferometers such as the Laser Interferometer Space Antenna (LISA) [74] and the DECi-hertz Interferometer Gravitational wave Observatory (DECIGO) [75]. Predictions on GWs produced by the first-order EWPT have been thoroughly investigated in various extended Higgs models [56, 57, 61, 65, 68, 69, 72, 76–88] By using future GW observations, we may be able to test the first-order EWPT.

The strongly first-order EWPT, which is important to realize the EWBG, requires the large deviation in the hhh coupling. This fact is confirmed in renormalizable extended Higgs models and effective field theories (EFTs). In the THDMs, the large deviation in hhh coupling can be realized by quantum corrections from heavy additional scalar bosons [9]. Such large quantum corrections to Higgs couplings are often called as the non-decoupling effects. The relation between the strongly first-order EWPT and the deviation in the hhh coupling is also discussed in effective field theories (EFTs) [89]. The Standard Model Effective Field Theory (SMEFT) is often used in order to obtain model independent results. The EWPT in the SMEFT has been analyzed in the literatures [76, 79, 80, 84, 88–92]. Although the SMEFT is a proper EFT to describe new physics that has decoupling properties, it cannot describe extended Higgs models with the non-decoupling effects [93, 94]. It means that a new EFT framework describing models with the non-decoupling effects is required.

In this thesis, we first discuss the EWPT in extended Higgs models. Especially, we focus on the two Higgs doublet model (THDM) as an example of renormalizable extended Higgs models. We precisely evaluate the sphaleron decoupling condition in the THDM. The predictions on the hhh coupling and GW spectra are evaluated by using the precise sphaleron decoupling condition. We show that upper bounds on new additional scalar fields can be obtained by combining the sphaleron decoupling condition and the unitarity bound. It is well known that the unitarity bound gives upper bounds on masses of new scalar fields [14, 19, 95, 96]. However, the mass upper bounds cannot be determined by using only the unitarity bound in a case where the discovered Higgs boson is SM-like. We show that the mass upper bounds can be determined by combining the sphaleron decoupling condition and the unitarity bound even if the discovered Higgs boson has SM-like properties. In addition, we show that the typical mass scale of new scalar fields may be determined by using the measurement of the hhh coupling and GW observations.

We next discuss the dynamics of the EWPT in a new EFT, which is the nearly aligned Higgs EFT (naHEFT). The naHEFT is an extension of the Higgs EFT [97–110]. The Higgs EFT may be able to describe extended Higgs models with the non-decoupling effects [93, 94]. We show that the naHEFT can appropriately describe extended Higgs models with the strongly first-order EWPT.

Finally, we discuss a relation between the first-order EWPT and primordial black holes (PBHs).

PBHs can be generated by a large energy density fluctuation at the early Universe [111–113]. So far, various possibilities of the PBH formation via the first-order phase transition have been discussed [87, 114–122]. In our analysis, we focus on the PBH formation mechanism proposed by Liu et al. [120]. For the PBH formation discussed in Ref. [120], the large density fluctuation can be realized because of the delay of the first-order phase transition. Since the delay of the phase transition only depends on the structure of the effective potential, the abundance of PBHs can be determined in any models with the first-order EWPT. Properties of PBHs produced by the first-order EWPT were discussed by using the SMEFT framework [87]. In our analysis, we utilize the effective potential in the naHEFT in order to obtain model independent results. The mass of PBHs formed by the EWPT is about 10^{-5} of the solar mass. Such PBHs may be observed by microlensing observations such as Subaru HSC, OGLE, PRIME and Roman Space Telescope. We discuss complementarity of PBH observations, future GW observations and collider experiments to test the first-order EWPT.

The structure of this thesis is as follows. In Chapter 2, we review the standard model in particle physics. In Chapter 3, we give a brief review for extended Higgs models and effective field theories. In addition, we explain the details of the first-order phase transition. In Chapter 4, we discuss the EWPT in extended Higgs models. We mainly focus on the two Higgs doublet model in this chapter. In Chapter 5, we define the naHEFT and discuss its phenomenology. In Chapter 6, we discuss the relation between PBHs and the first-order EWPT. Finally, we give the grand summary in Chapter 7.

Chapter 2

The standard model in particle physics

2.1 Particle contents in the standard model

The SM possesses the gauge symmetry $SU(3)_C \times SU(2)_L \times U(1)_Y$ Particle contents in the SM are shown in Tab. 2.1. The subscripts L and R represent the chirality. The subscript i indicates the generation. Numbers shown in Tab. 2.1 are the representation of each gauge group. The $U(1)_Y$ charge Y and the third component of the weak isospin I_3 are related to the observed electric charge Q by Nisjima-Gell-mann formula [123, 124]:

$$Q = I_3 + Y. \tag{2.1.1}$$

This formula is related to the spontaneous electroweak symmetry breaking (EWSB) $SU(2)_L \times U(1)_Y \to U(1)_{\rm EM}$. In the SM, the EWSB is occurred by a isospin doublet scalar field Φ shown in Tab. 2.1. The Higgs field can give masses of fermions and gauge bosons. In this thesis, we focus on the part related to the electroweak symmetry $SU(2)_L \times U(1)_Y$. We call a model with the EW symmetry and a isospin doublet scalar field as Weinberg-Salam theory [125–127].

2.2 Higgs mechanism

Although masses of fermions and gauge bosons are forbidden by the gauge symmetry, the Higgs mechanism can give the masses. The Higgs mechanism is realized by a Higgs boson in the SM. As shown in Tab. 2.1, the Higgs boson can be expressed by

$$\Phi = \begin{pmatrix} \phi^+ \\ \phi^0 \end{pmatrix} = \frac{1}{\sqrt{2}} \begin{pmatrix} \phi_1 + i\phi_2 \\ \phi_3 + i\phi_4 \end{pmatrix} \quad (\phi_i \in \boldsymbol{R}). \tag{2.2.1}$$

In Weinberg-Salam theory, the Higgs potential at the tree-level is given by

$$\begin{aligned} V(\Phi) &= -\mu^2 \Phi^\dagger \Phi + \lambda (\Phi^\dagger \Phi)^2 \\ &= \lambda \left\{ \left(\Phi^\dagger \Phi\right) - \frac{\mu^2}{2\lambda} \right\}^2 - \frac{\mu^2}{4\lambda}, \end{aligned} \tag{2.2.2}$$

where we assume $\mu^2 > 0$. The last term is a constant. Since the parameter μ^2 is not negative, the Higgs potential has a minimum value. Then, the Higgs field should satisfy the following condition at the minimum value

$$|\Phi|^2 = \frac{\mu^2}{2\lambda}. \tag{2.2.3}$$

Table 2.1: Particle contents in the SM.

	$\ell_L^{(i)} = \begin{pmatrix} \nu_L^{(i)} \\ e_L^{(i)} \end{pmatrix}$	$e_R^{(i)}$	$q_L^{(i)} = \begin{pmatrix} u_L^{(i)} \\ d_L^{(i)} \end{pmatrix}$	$u_R^{(i)}$	$d_R^{(i)}$	$\Phi = \begin{pmatrix} \phi^+ \\ \phi^0 \end{pmatrix}$
$SU(3)_C$	**1**	**1**	**3**	**3**	**3**	**1**
$SU(2)_L$	**2**	**1**	**2**	**1**	**1**	**2**
$U(1)_Y$	–1/2	–1	+1/6	+2/3	–1/3	+1/2

This condition characterize the topological structure of the vacuum. By using the expression for the Higgs field given in Eq. (2.2.1)), we can obtain

$$\sum_{i=1}^{4} \phi_i^2 = \frac{\mu^2}{\lambda}. \tag{2.2.4}$$

This result indicates that the topological structure of the vacuum in the SM corresponds to S^3. It means that any stable topological solitons cannot exist in Weinberg-Salam theory [128]. Conversely, there is a possibility that unstable particle-like solutions in field equations can exist, i.e., electroweak sphalerons [44, 45].

The Higgs field around the vacuum can be parameterized by

$$\Phi = \frac{1}{\sqrt{2}} \begin{pmatrix} w^+ \\ v + h + ia \end{pmatrix}. \tag{2.2.5}$$

The fluctuation around the vacuum can be expressed by using fields $\boldsymbol{\pi} = (\pi_1, \pi_2, \pi_3)$ as

$$\Phi = e^{\frac{i\boldsymbol{\sigma}\cdot\boldsymbol{\pi}(x)}{v}} \frac{1}{\sqrt{2}} \begin{pmatrix} 0 \\ v + h \end{pmatrix}. \tag{2.2.6}$$

Since the Weinberg-Salam theory is invariant under the gauge symmetry $SU(2)_L$, effects from the factor $e^{\frac{i\boldsymbol{\sigma}\cdot\boldsymbol{\pi}(x)}{v}}$ cannot appear in any physical quantities. Therefore, it is sufficient to consider the following expression when we discuss phenomenology around the vacuum

$$\Phi = \frac{1}{\sqrt{2}} \begin{pmatrix} 0 \\ v + h \end{pmatrix}. \tag{2.2.7}$$

We here confirm that gauge bosons can acquire their masses by the Higgs mechanism. The kinetic term of the Higgs field can be expressed by using the expression (2.2.7) as

$$|D_\mu \Phi|^2 = \left| \left(\partial_\mu + ig\frac{1}{2}\vec{\sigma}\cdot\vec{W}_\mu - ig'\frac{1}{2}B_\mu \right) \frac{1}{\sqrt{2}} \begin{pmatrix} 0 \\ v + h \end{pmatrix} \right|^2, \tag{2.2.8}$$

$$\vec{\sigma}\cdot\vec{W}_\mu = \begin{pmatrix} W_\mu^3 & W_\mu^1 - iW_\mu^2 \\ W_\mu^1 + iW_\mu^2 & -W_\mu^3 \end{pmatrix}, \quad W_\mu^\pm = \frac{W_\mu^1 \mp iW_\mu^2}{\sqrt{2}}, \tag{2.2.9}$$

where $\sigma_i\,(i = 1, 2, 3)$ is the Pauli matrix. g and g' are the gauge couplings for $SU(2)_L$ and $U(1)_Y$.

Then, we can obtain

$$\begin{aligned}|D_\mu\Phi|^2 &= \left|\frac{1}{\sqrt{2}}\begin{pmatrix}0\\ \partial_\mu h\end{pmatrix} + \frac{ig'}{2}\begin{pmatrix}0\\ B_\mu\frac{1}{\sqrt{2}}(v+h)\end{pmatrix} + \frac{ig}{2}\begin{pmatrix}W^+_\mu(h+v)\\ -W^3_\mu\frac{1}{\sqrt{2}}(v+h)\end{pmatrix}\right|^2 \\ &= \frac{g^2}{4}W^+_\mu W^{-\mu}(h+v)^2 + \frac{1}{2}\partial_\mu h\partial^\mu h + \frac{g'^2}{8}B_\mu B^\mu(h+v)^2 \\ &\quad - \frac{gg'}{4}B^\mu W^3_\mu(h+v)^2 + \frac{g^2}{8}W^3_\mu W^{3\mu}(h+v)^2. \end{aligned} \tag{2.2.10}$$

We define Z_μ, A_μ and θ_W as follows;

$$\begin{aligned} Z_\mu &= W^3_\mu\cos\theta_W - B_\mu\sin\theta_W, \\ A_\mu &= W^3_\mu\cos\theta_W + B_\mu\sin\theta_W, \\ \tan\theta_W &= \frac{g'}{g}, \end{aligned} \tag{2.2.11}$$

where Z_μ, A_μ and θ_W represent the Z boson field, the photon field and Weinberg angle, respectively. Then, we can express the kinetic term of the Higgs field in terms of Z_μ and A_μ as

$$|D_\mu H|^2 = \frac{1}{2}\partial_\mu h\partial^\mu h + \frac{g^2}{4}(h+v)^2W^-_\mu W^{+\mu} + \frac{g^2+g'^2}{4}(h+v)^2Z_\mu Z^\mu + 0\cdot A_\mu A^\mu(h+v)^2 \tag{2.2.12}$$

Thus, the masses of $W^\pm_\mu$, Z_μ and A_μ are given by

$$m_W = \frac{1}{2}gv, \tag{2.2.13}$$

$$m_Z = \frac{1}{2}\sqrt{g^2+g'^2}\,v, \tag{2.2.14}$$

$$m_A = 0. \tag{2.2.15}$$

We next confirm the masses of fermions. We first consider the masses of leptons. The renormalizable interaction terms between the Higgs doublet field and leptons, which are invariant under the gauge group $SU(2)_L\times U(1)_Y$, can be given by

$$\mathcal{L}^{\text{lepton}}_{\text{yukawa}} = -y^\ell_{ij}(\overline{\ell^{(i)}_L}\Phi)e^{(j)}_R + \text{h.c.}, \tag{2.2.16}$$

where y^ℓ_{ij} are Yukawa coupling constants for leptons. As already mentioned, the subscript i indicates the generation. After the EWSB, the interaction terms can be expressed by

$$\mathcal{L}^{\text{lepton}}_{\text{yukawa}} = -\frac{y^\ell_{ij}}{\sqrt{2}}v\overline{e^{(i)}_L}e^{(j)}_R - \frac{y^\ell_{ij}}{\sqrt{2}}h\overline{e^{(i)}_L}e^{(j)}_R + \text{h.c.}. \tag{2.2.17}$$

We here define mass eigenstates for leptons by using unitary matrices U and V as

$$\begin{aligned} e^{(j)}_L &\to e^{m(j)}_L = V^\dagger_{ji}e^{(i)}_L, \\ e^{(i)}_R &\to e^{m(i)}_R = U^\dagger_{ij}e^{(j)}_R. \end{aligned} \tag{2.2.18}$$

Then, we can obtain

$$y^\ell_{ij}\overline{e^{(i)}_L}\ell^{(j)}_R = \overline{e^{m(a)}_L}V^\dagger_{ai}y^\ell_{ij}U_{jb}\ell^{m(b)}_R. \tag{2.2.19}$$

By defining U and V to diagonalize $V^\dagger_{ai} y^\ell_{ij} U_{jb}$, we obtain

$$\mathcal{L}^{\rm lepton}_{\rm yukawa} = -\frac{v}{\sqrt{2}} Y^\ell_i \overline{e^{m(i)}_L} e^{m(i)}_R - \frac{1}{\sqrt{2}} Y^\ell_i \overline{e^{m(i)}_L} e^{m(i)}_R h. \tag{2.2.20}$$

Therefore, the masses for leptons can be expressed by

$$M^\ell_i = \frac{v}{\sqrt{2}} Y^\ell_i. \tag{2.2.21}$$

Since the SM does not have right handed neutrino, the masses of neutrino are zero.

The masses of quarks can be discussed in the same way as in the lepton case. The Yukawa interaction terms for quarks can be given by

$$\mathcal{L}^{\rm quark}_{\rm yukawa} = -y^d_{ij} \overline{q^{(i)}_L} \Phi d_R - y^u_{ij} \overline{q^{(i)}_L} \Phi_C u_R + \text{h.c.}, \tag{2.2.22}$$

where Φ_C is the charge conjugate of the Higgs doublet field, which is defined by $\Phi_C = i\sigma_2 \Phi$. We define two unitary matrices $\tilde{U}$ and $\tilde{V}$ to obtain mass eigenstates for quarks as

$$\begin{aligned} &u^{m(j)}_L = \tilde{V}^\dagger_{(u)ji} u^{(i)}_L, \quad d^{m(j)}_L = \tilde{V}^\dagger_{(d)ji} d^{(i)}_L, \\ &u^{m(i)}_R = \tilde{U}^\dagger_{(u)ij} u^{(i)}_R, \quad d^{m(i)}_R = \tilde{U}^\dagger_{(d)ij} d^{(j)}_R, \\ &\tilde{V}^\dagger_{(u,d)ai} y^{u,d}_{ij} U_{(u,d)jb} = Y^{u,d}_a \delta_{ab}. \end{aligned} \tag{2.2.23}$$

Then, the masses of quarks can be given by

$$M^{u,d}_a = \frac{v}{\sqrt{2}} Y^{u,d}_a. \tag{2.2.24}$$

In the SM, the masses of quarks and leptons are proportional to the vacuum expectation value v. As we will see later, the SM prediction is consistent with the results at the Large Hadron Collider experiments.

2.3 CKM matrix and CP violation

We here give a review for the CP violation in the SM.

In the previous section, we have discussed the mass eigenstates for quarks. We here discuss the weak-charged current part. The weak-charged current part for quarks is expressed by

$$\mathcal{L}_{W^\pm} \propto W^+_\mu \overline{u}^{(i)}_L \gamma^\mu d^{(i)}_L + \text{h.c.}. \tag{2.3.1}$$

When the flavor eigenstates in $\mathcal{L}_{W^\pm}$ are replaced by the mass eigenstates, we can obtain

$$\mathcal{L}_{W^\pm} \propto W^+_\mu \overline{u}^{(i)}_L \gamma^\mu d^{(i)}_L + \text{h.c.} \to W^+_\mu \overline{u}^{m(i)}_L \gamma^\mu (\tilde{V}_{(u)} \tilde{V}^\dagger_{(d)})_{ij} d^{m(j)}_L + \text{h.c.}. \tag{2.3.2}$$

In general, $\tilde{V}_{(u)} \tilde{V}^\dagger_{(d)}$ is not a diagonal matrix. Therefore, the flavor violation can be induced via the weak-charged current. The matrix $V^{\rm CKM} \equiv \tilde{V}_{(u)} \tilde{V}^\dagger_{(d)}$ is often called as Cabibbo-Kobayashi-Maskawa (CKM) matrix [129, 130]. In the SM, there is a CP violation phase in the CKM matrix.

For the weak-neutral current, the flavor violation cannot appear because of the CKM matrix is a unitary matrix. Thus, the flavor changing neutral current (FCNC) is suppressed in the SM. This mechanism is often called as Glashow-Iliopoulous-Maiani (GIM) mechanism [131].

2.4 Theoretical constraints on the Higgs sector

In this section, we discuss the theoretical constraints on the Higgs sector. These constraints are used in our numerical analysis discussed after Chapter 3.

2.4.1 Perturbative unitarity

We here explain the concept of perturbative unitarity.

When the perturbative expansion is violated, the S-matrix cannot satisfy $S^\dagger S = 1$. Substituting $S = 1 + iT$ into the above condition, we can obtain [132]

$$T^\dagger T = -i(T - T^\dagger). \tag{2.4.1}$$

We here consider the matrix element for two-particle scattering with the initial state $|i\rangle = |p_1 p_2\rangle$ and the final state $|f\rangle = |q_1 q_2\rangle$. Then, we can obtain the following condition for the scattering amplitude

$$-i\left[\mathcal{M}\left(i \to f\right) - \mathcal{M}^*\left(f \to i\right)\right] = \sum_n \left(\prod_{i=1}^n \int \frac{d^3k_i}{(2\pi)^3}\frac{1}{2E_i}\right) \mathcal{M}^*\left(f \to \{k_i\}\right)\mathcal{M}\left(i \to \{k_i\}\right), \tag{2.4.2}$$

where the scattering amplitude is defined by

$$\langle f|iT|i\rangle = (2\pi)^4\delta^4(p_1 + p_2 - q_1 - q_2)i\mathcal{M}(i \to f). \tag{2.4.3}$$

Considering the forward scattering ($p_i = q_i$), we can obtain

$$2\mathrm{Im}\mathcal{M}(p_1, p_2 \to p_1, p_2) = 2E_{\rm cm}p_{\rm cm}\sigma_{\rm tot}(p_1, p_2 \to \text{anything}), \tag{2.4.4}$$

where $E_{\rm cm}$ and $p_{\rm cm}$ is the total center-of-mass energy and the momentum in the center-of-mass frame, respectively. $\sigma_{\rm tot}(p_1, p_2 \to \text{anything})$ is the total cross section for the process $p_1, p_2 \to$ anything. In the case where $E_{\rm cm}$ is much larger than masses of any particles ($E_{\rm cm} \simeq 2|p_{\rm cm}|$), Eq. (2.4.4) implies

$$\frac{1}{E_{\rm cm}^2}\mathrm{Im}\mathcal{M}(p_1, p_2 \to \text{anything}) = \sigma_{\rm tot}(p_1, p_2 \to \text{anything}) \geq \sigma(p_1, p_2 \to p_1, p_2). \tag{2.4.5}$$

The cross section for two-body scattering $\sigma(p_1, p_2 \to p_1, p_2)$ is expressed by

$$\sigma(p_1, p_2 \to p_1, p_2) = \frac{1}{E_{\rm cm}^2}\int d\cos\theta \frac{\mathcal{M}^2(p_1, p_2 \to p_1, p_2)}{32\pi^2}. \tag{2.4.6}$$

When we use the partial wave expansion, the scattering amplitude for two-body scattering can be expressed by

$$\mathcal{M} = 16\pi\sum_{J=0}^{\infty}(2J+1)P_J(\cos\theta)a_J, \tag{2.4.7}$$

where $P_J(\cos\theta)$ is Legendre polynomials. Since we here consider the forward scattering ($\theta = 0$), the Legendre polynomials satisfy $P_J(\cos\theta = 1)1$. As a result, Eq. (2.4.5) implies

$$\sum_{J=0}^{\infty}(2J+1)\left[\mathrm{Im}(a_J) - |a_J^2|\right] \geq 0. \tag{2.4.8}$$

Therefore, we can obtain

$$|\mathrm{Re}(a_J)| \leq \eta, \tag{2.4.9}$$

where $\eta = 1$ [133, 134] or $1/2$ [135].

Before the discovery of the Higgs boson with 125 GeV, the upper bound on the Higgs mass was obtained by using the condition (2.4.9) with $\eta = 1$ [133, 134]. This upper bound is often called as Lee-Quigg-Thacker bound, which is about 1 TeV. The authors of Ref. [133, 134] considered two-body scatterings for channels ($W_L^+W_L^-$, Z_LZ_L, hh, Z_Lh) in the SM, where W_L and Z_L are longitudinal components of gauge bosons.

After the discover of the Higgs boson, the unitarity bound (2.4.9) can be used to determined upper bounds on masses of new particles. For example, upper bounds for masses of additional scalar bosons in the THDM was discussed [95]. The upper bounds cannot be obtained in the case where the couplings of discovered Higgs boson to fermions and gauge bosons are SM-like.

2.4.2 Vacuum stability

We next discuss bounds from the vacuum stability.

In the SM, there are two parameters μ^2 and λ as shown in Eq. (2.2.2). The parameter λ should satisfy

$$\lambda > 0. \tag{2.4.10}$$

This condition is required to guarantee that the Higgs potential has a global minimum only at the VEV $v \simeq 246\,\mathrm{GeV}$ (we call this vacuum as the EW vacuum). If the condition Eq. (2.4.10) is not satisfied, the EW vacuum is a false vacuum. It means that the vacuum in our Universe may be changed.

If we consider the structure of the Higgs potential at large field values, renormalization scale or field value dependence of the parameter λ should be taken into account. In the SM, the vacuum stability at the next-to-next-to leading order is discussed [136]. According to the analysis in Ref. [136], the Higgs potential in the SM may be a metastable. However, the energy scale μ, where the vacuum stability is broken, strongly depends on the value of the top quark mass m_t.

The vacuum stability bound in various extended Higgs models has been also discussed. For instance, the vacuum stability in the THDM is discussed in Refs. [137–140]. In the following analysis, we utilize the vacuum stability as a theoretical constraints on extended Higgs models.

2.5 Experimental constraints on the Higgs sector

In this section, we review experimental constraints on the Higgs sector.

2.5.1 Electroweak precise measurement

The oblique parameters are useful to parametrize new physics effects in electroweak observables. The oblique parameters $S\,T$ and U are defined by two point functions of gauge bosons. The two point function $\Pi_{XY}(q^2)$ are defined by the following equation [141]

$$ig^{\mu\nu}\Pi_{XY}(q^2) + (q^\mu q^\nu \text{ term}) \equiv \int d^4x e^{-iqx}\langle J_X^\mu(x) J_Y^\nu(0)\rangle, \tag{2.5.1}$$

where $J^\mu_X(x)$ $(X = 1, 2, 3, Q)$ are currents coupling to the EW gauge bosons, which are defined by

$$\begin{aligned}&\mathcal{L}_{W^+} + \mathcal{L}_{W^-} + \mathcal{L}_Z + \mathcal{L}_A \\ &\quad = \frac{e}{\sqrt{2}s_W} W^+_\mu J^\mu_+ + \frac{e}{\sqrt{2}s_W} W^-_\mu J^\mu_- + \frac{e}{s_W c_W} Z_\mu (J^\mu_3 - s^2_W J^\mu_Q) + eA_\mu J^\mu_Q, \end{aligned} \tag{2.5.2}$$

with

$$J^\mu_\pm = J^\mu_1 \pm i J^\mu_2. \tag{2.5.3}$$

We consider the Taylor expansion for $\Pi_{XY}(q^2)$ in terms of the external momentum q^2 as

$$\Pi_{XY}(q^2) = \Pi_{XY}(0) + q^2 \Pi'_{XY}(0) + O(q^4). \tag{2.5.4}$$

Since the $O(q^4)$ terms are proportional to the inverse of squared masses of new particle, these terms can be negligible.

Then, the oblique parameters S, T and U are defined as [141]

$$\alpha S \equiv 4e^2 \left[\Pi'_{33}(0) - \Pi'_{3Q}(0)\right], \tag{2.5.5}$$

$$\alpha T \equiv \frac{e^2}{s^2_W c^2_W m^2_Z} \left[\Pi_{11}(0) - \Pi_{33}(0)\right], \tag{2.5.6}$$

$$\alpha U \equiv 4e^2 \left[\Pi'_{11}(0) - \Pi'_{33}(0)\right]. \tag{2.5.7}$$

Considering S, T and U in terms of the two point functions of the gauge fields $W^\mu_\pm$, Z^μ and A^μ, we can obtain [142]

$$\frac{\alpha}{4s^2_W c^2_W} S = -\,\mathrm{Re}\left[\frac{\Pi_{ZZ}(m^2_Z) - \Pi_{ZZ}(0)}{m^2_Z} - \frac{c^2_W - s^2_W}{c_W s_W} \frac{\Pi_{Z\gamma}(m^2_Z)}{m^2_Z} - \frac{\Pi_{\gamma\gamma}(m^2_Z)}{m^2_Z}\right], \tag{2.5.8}$$

$$\alpha T = -\,\mathrm{Re}\left[\frac{\Pi_{WW}(0)}{m^2_W} - \frac{\Pi_{ZZ}(0)}{m^2_Z}\right], \tag{2.5.9}$$

$$\begin{aligned}\frac{\alpha}{4s^2_W} U = -\,\mathrm{Re}\Bigg[&\frac{\Pi_{WW}(m^2_W) - \Pi_{WW}(0)}{m^2_W} - c^2_W \frac{\Pi_{ZZ}(m^2_Z) - \Pi_{ZZ}(0)}{m^2_Z} \\ &-2 s_W c_W \frac{\Pi_{Z\gamma}(m^2_Z)}{m^2_Z} - s^2_W \frac{\Pi_{\gamma\gamma}(m^2_Z)}{m^2_Z}\Bigg].\end{aligned} \tag{2.5.10}$$

The parameter T is related to ρ parameter via

$$\rho - 1 = \alpha T. \tag{2.5.11}$$

The measured value of ρ parameter is [1]

$$\rho = 1.00038 \pm 0.00020. \tag{2.5.12}$$

The oblique parameter S, T and U have been investigated at LEP experiments. The experimental constraints on these parameters are given by [143]

$$S = 0.04 \pm 0.11, \quad T = 0.09 \pm 0.14 \quad U = -0.02 \pm 0.11. \tag{2.5.13}$$

The SM predictions for these parameters are consistent with these experimental results at 95% confidence level. Therefore, the oblique parameters can give strong constraints on new physics.

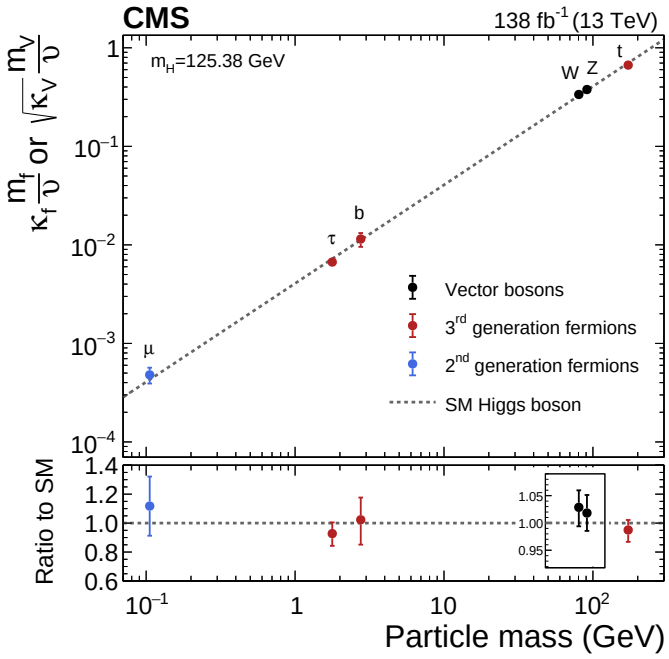

Figure 2.1: Higgs coupling constants for quarks, leptons and gauge bosons. The black dotted line is the prediction in the SM. The results in the LHC are consistent with the SM prediction. This figure is taken from Ref. [144].

2.5.2 Measurements of Higgs couplings

When we consider extended Higgs models, the Higgs boson couplings can deviate from the SM prediction. Such deviations can be parameterized by the κ framework [145]. In the κ framework, the couplings of the observed Higgs boson to gauge bosons and fermions are expressed by

$$g_{hVV} = \kappa_V g^{\rm SM}_{hVV}, \quad g_{hff} = \kappa_f g^{\rm SM}_{hff}, \tag{2.5.14}$$

where V and f indicate the gauge bosons (i.e., $W^\pm$ and Z) and the fermions (i.e., t and τ). $g^{\rm SM}_{hVV}$ and $g^{\rm SM}_{hff}$ are the couplings of the discovered Higgs bosons to the gauge bosons and the fermions in the SM, respectively. If the discovered Higgs boson is SM-like, the factor κ_V and κ_f satisfy $\kappa_V = \kappa_f = 1$ at the tree level. We often call the case satisfying $\kappa_V = \kappa_f = 1$ as *the alignment limit*.

In Fig. 2.1, measured Higgs boson couplings to fermions and gauge bosons are shown. This figure is taken from Ref. [144]. The black dotted line is the SM prediction. The constraints on κ_t, κ_Z, κ_W, κ_b and κ_μ in Fig. 2.1 are determined by the measurement of the branching ratio for the Higgs boson decay. Since $2m_t > m_h$, the constraint on κ_t is indirectly determined by measuring the radiative correction in the decay $h \to \gamma\gamma$ [144]. As we can see, the SM prediction is consistent with the LHC result. This fact gives strong constraints on new physics. Especially, new physics satisfying the conditions $\kappa_V \simeq 1$ and $\kappa_f \simeq 1$ can be an allowed candidate.

Although the measured Higgs couplings are consistent with the LHC results, several Higgs couplings can deviate from the SM prediction. For instance, the triple Higgs boson coupling hhh can deviate from the SM prediction. In the SM, hhh coupling can appear after the EWSB. The

triple Higgs boson coupling can be approximately evaluated by using the effective potential.

$$\left.\frac{\partial^3 V_{\rm eff}(h)}{\partial h^3}\right|_{h=0} = \lambda_{hhh}^{\rm SM}\left(1-\frac{\Delta\lambda_{hhh}}{\lambda_{hhh}^{\rm SM}}\right), \quad \Delta\lambda_{hhh} \equiv \lambda_{hhh}^{\rm new} - \lambda_{hhh}^{\rm SM}, \tag{2.5.15}$$

where $\lambda_{hhh}^{\rm SM}$ is the triple Higgs boson coupling in the SM, which is given by

$$\lambda_{hhh}^{\rm SM} \simeq \frac{3m_h^2}{v}\left(1-\frac{m_t^4}{\pi^2 m_h^2 v^2}\right). \tag{2.5.16}$$

Since the radiative correction from the top quark is leading in the SM, we only consider the effect from the top quark. $\lambda_{hhh}^{\rm new}$ is the triple Higgs boson coupling in extended Higgs models. If models with extended Higgs sectors are considered, the triple Higgs boson coupling can deviate from the SM prediction. The deviation is parameterized by $\Delta\lambda_{hhh}$.

The current constraints on the hhh coupling are at 95 % confidence level

$$-1.4 < \frac{\Delta\lambda_{hhh}}{\lambda_{hhh}^{\rm SM}} < 5.3 \quad \text{(ATLAS [146])}, \tag{2.5.17}$$

$$-2.24 < \frac{\Delta\lambda_{hhh}}{\lambda_{hhh}^{\rm SM}} < 5.49 \quad \text{(CMS [144])}. \tag{2.5.18}$$

As we can see, the large deviation in hhh coupling can be allowed. Actually, such large deviation can be realized by quantum corrections from heavy new particles, i.e., two Higgs doublet models [9]. As discussed later, the large deviation in the triple Higgs boson coupling is related to the first-order EWPT [50, 89].

For future collider experiments, hhh coupling can be measured precisely. At the HL-LHC, hhh coupling can be measured at 50 % accuracy at the 68 % confidence level [70]. In addition, at future lepton collider such as energy upgraded versions of the ILC with 500 GeV and 1 TeV center mass energy, it is expected that hhh coupling can be measured by 27% and 10% accuracies at the 68 % confidence level, respectively [71].

Chapter 3

Extended Higgs models

In this chapter, we give a brief review for extended Higgs models. We here focus on the two Higgs doublet models, $O(N)$ scalar singlet model and the inert doublet model as examples for renormalizable extended Higgs models. Then, we explain why we need effective field theory frameworks to discuss phenomenology in model independent ways. Finally, we give a review for the first-order electroweak phase transition.

3.1 Review of two Higgs doublet models

We here give a brief review for the two Higgs doublet models (THDMs). It has been discussed by many theorists whether the THDMs with CP violation can explain the baryon asymmetry of the Universe or not [51,86,147,148]. On the other hand, the CP violation is strongly constrained by the electric dipole moment experiments [149,150]. In recently, it has been shown that the CP-violating THDMs may be able to explain the BAU without contradicting the EDM experiments [86, 147, 151, 152]. Therefore, investigating the dynamics of the EWPT in the THDMs is important.

In this section, we discuss the EWPT in the THDMs. Since the dynamics of the EWPT is not much changed by CP violation in the THDMs [54, 153], we focus on the THDMs without the additional CP phase for simplicity.

3.1.1 Definition of the two Higgs doublet model

We consider the CP-conserving THDMs with a softly broken Z_2 symmetry $\Phi_1 \to \Phi_1$, $\Phi_2 \to -\Phi_2$. The Higgs potential in the THDMs is given by [9]

$$\begin{aligned} V_{\text{tree}}^{\text{THDM}}(\Phi_1,\Phi_2) = {} & m_1^2|\Phi_1|^2 + m_2^2|\Phi_2|^2 - \left(m_{12}^2\Phi_1^\dagger\Phi_2 + \text{h.c.}\right) \\ & + \frac{\lambda_1}{2}|\Phi_1|^4 + \frac{\lambda_2}{2}|\Phi_2|^4 + \lambda_3|\Phi_1|^2|\Phi_2|^2 + \lambda_4\left|\Phi_1^\dagger\Phi_2\right|^2 + \left[\frac{\lambda_5}{2}\left(\Phi_1^\dagger\Phi_2\right)^2 + \text{h.c.}\right], \end{aligned} \tag{3.1.1}$$

where m_{12}^2 and λ_5 can be complex numbers. For simplicity, we assume that m_{12}^2 and λ_5 are real. The doublet fields Φ_i $(i = 1, 2)$ are parameterized as

$$\Phi_i = \begin{bmatrix} w_i^+ \\ \frac{1}{\sqrt{2}}(v_i + h_i + z_i) \end{bmatrix} \quad (i = 1, 2), \tag{3.1.2}$$

	Φ_1	Φ_2	Q_L	L_L	u_R	d_R	e_R
Type-I	+	−	+	+	−	−	−
Type-II	+	−	+	+	−	+	+
Type-X	+	−	+	+	−	−	+
Type-Y	+	−	+	+	−	+	−

Table 3.1: Z_2 charge assignment in each type of the THDM.

where v_1 and v_2 are the vacuum expectation values (VEVs) of each doublet with $v = \sqrt{v_1^2 + v_2^2} \simeq 246\,\mathrm{GeV}$. Also, we define the ratio of the VEVs as $\tan\beta = v_2/v_1$. The mass parameters m_1^2 and m_2^2 can be reduced by the tadpole conditions

$$\left.\frac{\partial V_{\rm tree}^{\rm THDM}}{\partial h_1}\right|_{\rm min} = \left.\frac{\partial V_{\rm tree}^{\rm THDM}}{\partial h_2}\right|_{\rm min} = 0. \tag{3.1.3}$$

In this model, there are five mass eigenstates; two CP-even states (h, H), a CP-odd state (A) and charged state $(H^\pm)$. These mass eigenstates are obtained by introducing the mixing angle α and β

$$\begin{pmatrix} h_1 \\ h_2 \end{pmatrix} = R(\alpha)\begin{pmatrix} H \\ h \end{pmatrix}, \quad \begin{pmatrix} z_1 \\ z_2 \end{pmatrix} = R(\beta)\begin{pmatrix} z \\ \zeta \end{pmatrix}, \quad \begin{pmatrix} w_1^+ \\ w_2^+ \end{pmatrix} = R(\beta)\begin{pmatrix} w^+ \\ H^+ \end{pmatrix}, \tag{3.1.4}$$

with

$$R(\theta) = \begin{pmatrix} \cos\theta & -\sin\theta \\ \sin\theta & \cos\theta \end{pmatrix}. \tag{3.1.5}$$

The fields z and $w^\pm$ are the Nambu-Goldstone bosons, whose degrees of freedom are absorbed by the longitudinal components of Z and $W^\pm$ bosons. In this paper, we identify the field h as the discovered Higgs boson, whose mass is 125GeV.

The squared masses of the charged fields $H^\pm$ and CP-odd field A are given by

$$m_{H^\pm}^2 = M^2 - \frac{\lambda_4 + \lambda_5}{2}v^2, \tag{3.1.6}$$

$$m_A^2 = M^2 - \lambda_5 v^2, \tag{3.1.7}$$

where M^2 is defined by $M^2 = m_{12}^2/(\sin\beta\cos\beta)$, which plays an important role to realize the first order EW phase transition at the early Universe. The masses of the CP-even field H and h are given by

$$m_H^2 = M_{11}^2\cos^2(\beta-\alpha) + M_{22}^2\sin^2(\beta-\alpha) - M_{12}^2\sin 2(\beta-\alpha), \tag{3.1.8}$$

$$m_h^2 = M_{11}^2\sin^2(\beta-\alpha) + M_{22}^2\cos^2(\beta-\alpha) + M_{12}^2\sin 2(\beta-\alpha), \tag{3.1.9}$$

with

$$M_{11}^2 = \left(\lambda_1\cos^4\beta + \lambda_2\sin^4\beta\right)v^2 + \frac{1}{2}\lambda_{345}v^2\sin^2 2\beta, \tag{3.1.10}$$

$$M_{22}^2 = M^2 + \frac{1}{4}\left(\lambda_1 + \lambda_2 - 2\lambda_{345}\right)v^2\sin^2 2\beta, \tag{3.1.11}$$

$$M_{12}^2 = -\frac{1}{2}\left(\lambda_1\cos^2\beta - \lambda_2\sin^2\beta - \lambda_{345}\cos^2 2\beta\right)v^2\sin 2\beta, \tag{3.1.12}$$

$$\tan 2(\beta-\alpha) = -\frac{2M_{12}^2}{M_{11}^2 - M_{22}^2}, \tag{3.1.13}$$

	ζ_u	ζ_d	ζ_e
Type-I	$+\cot\beta$	$+\cot\beta$	$+\cot\beta$
Type-II	$+\cot\beta$	$-\tan\beta$	$-\tan\beta$
Type-X	$+\cot\beta$	$+\cot\beta$	$-\tan\beta$
Type-Y	$+\cot\beta$	$-\tan\beta$	$+\cot\beta$

Table 3.2: Mixing factors of Yukawa interactions in the THDM in each type

where $\lambda_{345} \equiv \lambda_3 + \lambda_4 + \lambda_5$. The free parameters in this model are given by

$$m_H, \quad m_A, \quad m_{H^\pm}, \quad \tan\beta, \quad M^2, \quad \sin(\beta-\alpha). \tag{3.1.14}$$

In this model, the coupling constants of the discovered Higgs boson with the gauge bosons and fermions can deviate from the SM prediction because of the scalar mixing between the CP-even scalar fields h and H. The deviation in the coupling of the Higgs to the gauge bosons at the tree level is expressed by

$$\frac{g_{hVV}^{\rm THDM}}{g_{hVV}^{\rm SM}} = \kappa_V = \sin(\beta-\alpha), \tag{3.1.15}$$

where $g_{hVV}^{\rm THDM}$ is the coupling of the Higgs boson to the gauge bosons in the THDM. For the couplings of the Higgs to fermions, the deviation in the couplings are given by

$$\frac{g_{hff}^{\rm THDM}}{g_{hff}^{\rm SM}} = \kappa_f = \sin(\beta-\alpha) + \zeta_f \cos(\beta-\alpha), \tag{3.1.16}$$

where $g_{hVV}^{\rm THDM}$ is the coupling of the Higgs boson to the fermion f in the THDM. The expression of ζ_f in each type of the THDMs is summarized in Tab. 3.2.

3.1.2 Triple Higgs boson coupling in the two Higgs doublet models

The deviation in the triple Higgs boson coupling in the THDMs at the one-loop level is approximately given by [9]

$$\frac{\Delta\lambda_{hhh}^{\rm THDM}}{\lambda_{hhh}^{\rm SM}} \simeq \sum_{\Phi=H,A,H^\pm} \frac{n_\Phi m_\Phi^4}{12\pi^2 m_h^2 v^2}\left(1-\frac{M^2}{m_\Phi^2}\right)^3, \tag{3.1.17}$$

where n_Φ and m_Φ are the degree of freedoms and the masses of the additional Higgs bosons, respectively. In the parameter region with $\sin(\beta-\alpha)\simeq 1$, the masses $m_\Phi\,(\Phi = H, A, H^\pm)$ can be expressed by

$$m_\Phi^2 \simeq M^2 + \lambda_\Phi v^2 \quad (\Phi = H, A, H^\pm), \tag{3.1.18}$$

where λ_Φ is the linear combination of λ_i in the Higgs potential given in Eq. (3.1.1). Then, we can consider two cases; (1) $\lambda_\Phi v^2 \ll M^2$ and (2) $\lambda_\Phi v^2 \gtrsim M^2$. The deviation in the triple Higgs boson coupling can be expressed in each case as follows

$$\frac{\Delta\lambda_{hhh}^{\rm THDM}}{\lambda_{hhh}^{\rm SM}} \simeq \sum_{\Phi=H,A,H^\pm} \frac{n_\Phi m_\Phi^4}{12\pi^2 m_h^2 v^2}\left(1-\frac{M^2}{m_\Phi^2}\right)^3 \simeq \begin{cases} \displaystyle\sum_\Phi \frac{n_\Phi \lambda_\Phi^3 v^4}{12\pi^2 m_h^2 m_\Phi^2} & (\lambda_\Phi v^2 \ll M^2) \\ \displaystyle\sum_\Phi \frac{n_\Phi m_\Phi^4}{12\pi^2 m_h^2 v^2} & (\lambda_\Phi v^2 \gtrsim M^2) \end{cases}. \tag{3.1.19}$$

In the case with $\lambda_\Phi v^2 \ll M^2$, the deviation in the hhh coupling is proportional to the inverse of the square masses m_Φ^2. Hence, new physics effects on the hhh coupling by the additional Higgs bosons are getting small as the masses of the additional Higgs bosons in the THDMs are heavy. Such behavior is often called as the decoupling behavior. On the other hand, in the case with $\lambda_\Phi v^2 \gtrsim M^2$, the deviation in the hhh coupling is proportional to the fourth power of m_Φ^2. It means that the heavy additional Higgs bosons can give large quantum corrections in the hhh coupling. We often call such large effects in Higgs couplings as the non-decoupling effects [9]. In order to realize the large deviation in the hhh coupling in the THDMs, the non-decoupling effects are important.

The hhh coupling in extended Higgs models is also evaluated not only the one-loop level but also the two-loop level by using the effective potential approximation [20, 21, 154, 155]. The two-loop corrections by new scalar bosons, which are about 20 % of the one-loop corrections, enhance the deviation in the hhh coupling [20, 21].

3.1.3 Non-decoupling effects in Higgs boson couplings

Not only the hhh coupling but also other Higgs couplings can also deviate from the SM prediction via the quantum corrections by heavy additional Higgs bosons in the THDMs. For instance, the hZZ coupling in the SM at the one-loop level is given by [9]

$$g_{hZZ}^{\rm SM} = \frac{2m_Z^2}{v}\left(1 - \frac{5m_t^2}{32\pi^2 v^2}\right). \tag{3.1.20}$$

On the other hand, the deviation in the hZZ coupling at the one-loop level in the THDMs with $\sin(\beta-\alpha)=1$ is given by

$$\kappa_Z^{1\ell} \simeq \sum_\Phi \frac{n_\Phi m_\Phi^2}{64\pi^2 v^2} - \sum_\Phi \frac{n_\Phi m_\Phi^2}{96\pi^2 v^2}\left(1 - \frac{M^2}{m_\Phi^2}\right)^2. \tag{3.1.21}$$

In the decoupling situation ($m_\Phi \sim M$), the second term in Eq. (3.1.21) vanishes. Therefore, the radiative corrections to the hZZ coupling are small in the decoupling region. On the contrary, the loop corrections are maximal in the non-decoupling region ($M \simeq 0$). This behavior is the same as the deviation in the hhh coupling. As a result, the hZZ coupling can deviate from the SM prediction about $O(1)\%$.

The $h\gamma\gamma$ coupling can also deviate from the SM prediction via the heavy charged Higgs boson $H^\pm$ in the THDMs. The value of $\kappa_\gamma^{1\ell}$ in the THDM is given by [156]

$$(\kappa_\gamma^{1\ell})^2 \simeq \left|1 + \frac{\mathcal{A}_{\rm THDM}}{\mathcal{A}_{\rm SM}}\right|^2, \tag{3.1.22}$$

where

$$\mathcal{A}_{\rm SM} = \kappa_W A_1(\tau_W) + \frac{4}{3}\kappa_t A_{1/2}(\tau_t), \tag{3.1.23}$$

$$\mathcal{A}_{\rm THDM} = \frac{v}{m_{H^\pm}^2} g_{hH^+H^-} A_0(\tau_{H^\pm}). \tag{3.1.24}$$

In the alignment limit ($\kappa_W = \kappa_t = 1$), the value of $\mathcal{A}_{\rm SM}$ is given by $\mathcal{A}_{\rm SM} = -6.498$. The parameter τ_i is defined as $\tau_i = m_h^2/(4m_i^2)$ for the particle i. The function $A_0(\tau)$, $A_{1/2}(\tau)$ and $A_1(\tau)$ are defined

by

$$A_0(\tau) = -[\tau - f(\tau)]\tau^{-2}, \tag{3.1.25}$$
$$A_{1/2}(\tau) = 2[\tau + (\tau - 1)f(\tau)]\tau^{-2}, \tag{3.1.26}$$
$$A_1(\tau) = -[2\tau^2 + 3\tau + 3(2\tau - 1) - f(\tau)]\tau^{-2}, \tag{3.1.27}$$

with

$$f(\tau) \simeq \begin{cases} \arcsin^2 \sqrt{\tau} & (\tau \leq 1) \\ -\frac{1}{4}\left[\log \frac{1+\sqrt{1-\tau^{-1}}}{1-\sqrt{1-\tau^{-1}}} - i\pi\right] & (\tau > 1). \end{cases} . \tag{3.1.28}$$

$g_{hH^+H^-}$ in Eq. (3.1.3) corresponds to the coupling in the Lagrangian of the THDMs $\mathcal{L}_{\rm THDM} \ni g_{hH_+H_-}hH^+H^-$. In the case with $\sin(\beta-\alpha)=1$, $g_{hH^+H^-}$ is given by [11]

$$g_{hH^+H^-} = -\frac{m_h^2}{v} - \frac{2m_{H^\pm}^2}{v}\left(1 - \frac{M^2}{m_{H^\pm}^2}\right). \tag{3.1.29}$$

This result means that the deviation in the $h\gamma\gamma$ coupling is a constant in the non-decoupling limit ($M = 0$). In the decoupling region ($m_{H^\pm} \simeq M$), the deviation in the $h\gamma\gamma$ coupling is proportional to $m_{H^\pm}^{-2}$. Therefore, the deviation is small in the large $m_{H^\pm}$ region in the decoupling case. The $h\gamma\gamma$ coupling can deviate from the SM prediction about $O(1)\%$.

3.1.4 Experimental constraints on the two Higgs doublet models

The THDMs have been thoroughly investigated by collider experiments. The THDMs with $m_{H^\pm} < 78\,\text{GeV}$ are ruled out by the LEP experiments [157]. In addition, the lower bounds on the masse of the additional Higgs bosons are determined by the measurements of $A \to \tau\overline{\tau}$ and $A \to t\bar{t}$ processes at the LHC experiments. For instance, in the type-I THDM with $\tan\beta = 1$, the mass region $m_\Phi < 600\,\text{GeV}$ ($\Phi = H$, A, $H^\pm$) is excluded. In the type-II THDM with $\tan\beta < 2$ ($\tan\beta > 10$), the mass region $m_\Phi < 350\,\text{GeV}$ ($m_\Phi < 400\,\text{GeV}$) is ruled out.

The mass $m_{H^\pm}$ are strongly constrained by flavor experiments [143]. In the type-I THDM with $\tan\beta \leq 1.5$, $m_{H^\pm} < 300\,\text{GeV}$ is constrained by the $B_s \to \mu\mu$ process measurement. In the type-II THDM, the region $m_\Phi < 590\,\text{GeV}$ is ruled out independently of $\tan\beta$ by the $B \to X_s\gamma$ process.

If $\sin(\beta-\alpha) \neq 1$, the Higgs couplings to gauge bosons and fermions can deviate from those in the SM. As shown in Fig. 2.1, κ_V and κ_f are strongly constrained by the LHC experiments. Therefore, the results in the LHC give constraints on the scalar mixing angle $\sin(\beta-\alpha)$. In the type-I THDM with $\tan\beta = 1$ ($\tan\beta = 2$), $|\cos(\beta-\alpha)| > 0.18$ (0.25) is excluded. For the type-II THDM with $\tan\beta = 1$ ($\tan\beta = 2$), $|\cos(\beta-\alpha)| > 0.09$ (0.11) is ruled out. These results indicates that the Higgs couplings to gauge bosons and fermions should be the SM-like.

Another important parameters in discussing constraints on the Higgs sector is the oblique parameters S, T and U [141]. The two-point function of W and Z bosons in the THDMs are calculated in Refs. [158–160]. According to these theoretical calculations and the measurement of ρ parameter [161], the following conditions should be required approximately

$$m_{H^\pm} \simeq m_A \quad \text{or} \quad m_{H^\pm} \simeq m_H \text{ with } \sin(\beta-\alpha) \simeq 1. \tag{3.1.30}$$

These conditions can be satisfied when the Higgs potential possesses a custodial symmetry [162–164].

3.1.5 Theoretical constraints on the two Higgs doublet models

We here discuss theoretical constraints on the THDM. The unitarity bound is a useful tool to determine constraints on the THDM. The elastic scatterings of the following channels have been considered [9];

$$\begin{aligned} &W_L^+W_L^-,\ W_L^+H^-,\ H^+W_L^-,\ H^+H^-, Z_LZ_L,\ Z_LA,\\ &AA,\ Z_Lh,\ Z_LH,\ Ah,\ AH,\ hh,\ hH,\ HH. \end{aligned} \tag{3.1.31}$$

As shown the above, the longitudinal component of the gauge bosons is important when we discuss the unitarity bound. According to the equivalent theorem [165, 166], the elastic scattering process including longitudinal component of the gauge bosons can be replaced by the Nambu-Goldstone boson at the high energy. Then, 14 processes shown in (3.1.31) can be expressed as [95]

$$\begin{aligned} &w^+w^-,\ w^+G^-,\ G^+w^-,\ G^+G^-, zz,\ z\zeta,\\ &\zeta\zeta,\ zh,\ zH,\ \zeta h,\ \zeta H,\ hh,\ hH,\ HH. \end{aligned} \tag{3.1.32}$$

The eigenvalues of S matrix for the above processes are given by [95]

$$a_\pm = \frac{1}{16\pi}\left[\frac{3}{2}(\lambda_1+\lambda_2) \pm \sqrt{\frac{9}{4}(\lambda_1-\lambda_2)^2 + (2\lambda_3+\lambda_4)^2}\right], \tag{3.1.33}$$

$$b_\pm = \frac{1}{16\pi}\left[\frac{1}{2}(\lambda_1+\lambda_2) \pm \sqrt{\frac{1}{4}(\lambda_1-\lambda_2)^2 + \lambda_4^2}\right], \tag{3.1.34}$$

$$c_\pm = d_\pm = \frac{1}{16\pi}\left[\frac{1}{2}(\lambda_1+\lambda_2) \pm \sqrt{\frac{1}{4}(\lambda_1-\lambda_2)^2 + \lambda_5^2}\right], \tag{3.1.35}$$

$$e_1 = \frac{1}{16\pi}\left(\lambda_3 + 2\lambda_4 - 3\lambda_5\right), \tag{3.1.36}$$

$$e_2 = \frac{1}{16\pi}\left(\lambda_3 - \lambda_5\right), \tag{3.1.37}$$

$$f_+ = \frac{1}{16\pi}\left(\lambda_3 + 2\lambda_4 + 3\lambda_5\right), \tag{3.1.38}$$

$$f_- = \frac{1}{16\pi}\left(\lambda_3 + \lambda_5\right), \tag{3.1.39}$$

$$f_1 = f_2 = \frac{1}{16\pi}\left(\lambda_3 + \lambda_4\right). \tag{3.1.40}$$

The unitarity bound is given by

$$|a_\pm|,\ |b_\pm|,\ |c_\pm|,\ |d_\pm|,\ |e_{1,2}|,\ |f_\pm|,\ |f_{1,2}| < \eta, \tag{3.1.41}$$

where we take $\eta = 1/2$ [135]. In the following, we use the unitarity bound given in Eq. (3.1.41) as a theoretical constraint.

Another theoretical constraint is the vacuum stability bound. The vacuum stability bound at the tree level in the THDM is given by [137, 140, 167]

$$\lambda_1 > 0, \quad \lambda_2 > 0, \quad \sqrt{\lambda_1\lambda_2} + \lambda_3 + \min(0,\ \lambda_4+\lambda_5,\ \lambda_4-\lambda_5) > 0. \tag{3.1.42}$$

If this condition is not satisfied, the EW vacuum ($\sqrt{v_1^2+v_2^2} \simeq 246\,\mathrm{GeV}$) is not a global minimum.

3.2 Review of $O(N)$ scalar singlet model

We here consider the model with additional N singlet real scalar fields S_i, which have a global $O(N)$ symmetry. We call this model as the $O(N)$ scalar singlet model in the following. The Higgs potential in this model is given by [77, 168]

$$V_{O(N)}(\Phi, \vec{S}) = -\mu^2 \Phi^\dagger \Phi + \lambda (\Phi^\dagger \Phi)^2 + \frac{\mu_S^2}{2} |\vec{S}|^2 + \frac{\lambda_S}{4!} |\vec{S}|^4 + \lambda_{\Phi S} |\vec{S}|^2 \Phi^\dagger \Phi, \tag{3.2.1}$$

where $(\vec{S})^{\mathrm{T}} = (S_1, S_2, \cdots S_N)$ is a vector under the $O(N)$ symmetry. We here assume $\mu_S^2 \geq 0$ to avoid that the additional singlet scalar fields get the vacuum expectation values $\langle S_i \rangle = 0$.

The EWPT in the $O(N)$ scalar singlet model has been thoroughly investigated [68, 69, 77, 168, 169]. Since the additional singlet scalar fields stabilize because of the symmetry, these can be a candidate of dark matter [77]. In the $O(N)$ scalar singlet model with $N = 1$, the phenomenology at future hadron collider is discussed by Curtin, Meade and Yu [169]. The authors showed that the direct production of the additional singlet field is difficult even at future 100 TeV hadron colliders since the singlet field only interact with the SM Higgs. On the other hand, it was also shown that the indirect test via the measurement of the triple Higgs boson coupling can be useful to explore the scalar singlet field.

For theoretical constraints, the unitarity bound is expressed by [69]

$$\frac{1}{32\pi} \left[3\lambda + (N+2)\lambda_S + \sqrt{\{3\lambda - (N+2)\lambda_S\}^2 + 4N\lambda_{\Phi S}^2} \right] < \frac{1}{2}. \tag{3.2.2}$$

In our analysis, we use this bound as a theoretical constraint in the $O(N)$ scalar singlet model.

3.3 Requirement of the effective field theory describing new physics

According to the current LHC experiment results, the SM is a successful theory. On the other hand, the SM cannot explain several cosmological observations such as the baryon asymmetry of the Universe. Various models with extended Higgs sectors have been considered to explain these observations. These extended Higgs models are strongly constrained by collider experiments. In particular, the typical mass scale of new particles should generally be larger than the EW scale. The effects on low energy observations from new particles can be well described by using the framework of the effective field theory (EFT). In this section, we discuss the implication of the EFT. Then, two famous EFT frameworks – the Standard Model EFT (SMEFT) and the Higgs EFT (HEFT) – are reviewed.

3.3.1 Review of the standard model effective field theory

The new physics effects on low energy observations can be studied by introducing higher mass dimensional operators to the SM. This systematic framework is the SMEFT. These higher mass dimensional operators are originated from the effects of integrated out heavy new particles. The contributions from heavy new particles are getting small when we take the limit where the masses of new particles are sufficiently heavier than the EW scale. This fact is based on the decoupling theorem [170].

The SMEFT is a good EFT framework which effectively describes decoupling new physics models. In the SMEFT, the effects from new physics are expressed by polynomials of the fields in the SM, which transform linearly under the EW symmetry. For the dimension-six operators in the SMEFT with one generation of fermions, there are 59 independent operators which conserve the baryon number [171]. In the case with three generations of fermions, there are 2499 operators in the SMEFT [172]. A systematic method to relate the dimension-six operators with specific renormalizable models is established (see Ref. [173]).

Constraints from the higher dimensional operators including the fermion and the gauge fields in the SMEFT has been discussed thoroughly [174]. To obtain constraints on operators involving only the Higgs field (i.e., $|\Phi|^6/\Lambda^2$), it is important to measure the Higgs self-coupling constant such as the triple Higgs boson coupling [175]. As mentioned in Chapter 2, the current constraint of the triple Higgs boson coupling is not stringent. Therefore, the operators involving only the Higgs field may give a large deviation in Higgs couplings from the SM prediction. In addition, such operators play an important role to realize the strongly first-order EWPT. The dynamics of the EWPT is also discussed in the literatures [76, 88–92, 176].

3.3.2 Review of the Higgs effective field theory

The SMEFT is used as a useful EFT framework in order to discuss model independent phenomenology in extended Higgs models. On the other hand, the Higgs EFT is also discussed as a good candidate for new EFT framework. In the Higgs EFT, new physics effects are expressed by polynomials of the fields in the SM, which transform non-linearly under the EW symmetry. We here compare the part of the SMEFT that only includes the Higgs field and the Nambu-Goldstone bosons with the same part in the Higgs EFT. In the SMEFT, the part depending only the Higgs field and the Nambu-Goldstone bosons is expressed by [94]

$$\mathcal{L}_{\rm SMEFT} \ni A(|\Phi|^2)\left|\partial_\mu \Phi\right|^2 + B(|\Phi|^2)\left(\partial_\mu |\Phi|^2\right)^2 - V(\Phi) + O(\partial^4), \tag{3.3.1}$$

where Φ is the Higgs doublet field in the SM. The form factors $A(|\Phi|^2)$ and $B(|\Phi|^2)$ can parameterize new physics effects. In the SM, the form factors take $A(|\Phi|^2) = 1$ and $B(|\Phi|^2) = 0$. The function $V(\Phi)$ is the Higgs potential. The important property of the SMEFT is that $A(|\Phi|^2)$, $B(|\Phi|^2)$ and $V(\Phi)$ are analytic at the origin $|\Phi|^2 = 0$. On the other hand, the same part in the Higgs EFT is expressed by

$$\mathcal{L}_{\rm HEFT} \ni \frac{1}{2}K(h)\partial_\mu h \partial^\mu h + \frac{v^2}{2}F(h){\rm Tr}\left[\partial_\mu U \partial^\mu U\right] + V(h), \tag{3.3.2}$$

where the matrix U is defined in terms of the Nambu-Goldstone bosons $\vec{\pi}$ as

$$U = \exp\left[i\frac{\vec{\sigma}\cdot\vec{\pi}}{v}\right]. \tag{3.3.3}$$

The form factors $K(h)$ and $F(h)$ include new physics effects. The function $V(h)$ is the Higgs potential. In the SM, the form factors satisfy $K(h) = 1$ and $F(h) = 1$. In the Higgs EFT, $K(h)$, $F(h)$ and $V(h)$ need not be analytic except for $h = 0$. It means that the Higgs EFT can be convert into the SMEFT. However, the opposite is not always possible. This fact is shown in Ref. [177].

As shown in subsection 3.1.2, heavy new particles can give large quantum corrections in Higgs couplings such as hhh coupling. The non-decoupling effects in hhh coupling come from the radiative correction to the Higgs potential, which is so-called the Coleman-Weinberg potential [178]. As well

known, the Coleman-Weinberg potential includes the logarithmic functions. Therefore, the Higgs EFT is a proper EFT framework when we consider new physics with the non-decoupling effects. Conversely, the SMEFT may not be a good framework when we discuss new physics with the non-decoupling effects. Actually, it has been shown that the non-decoupling effects in hhh coupling cannot be described by the SMEFT [93, 94].

Considering extensions of the Higgs EFT, we can obtain a new EFT which is able to describe new physics with the non-decoupling effects. In recently, a candidate for the new EFT has been proposed in Ref. [179]. We explain the new EFT in Chapter 5.

3.4 Dynamics of the first-order phase transition

In this section, we give a review for the details of the first-order phase transition. We first explain the scenario of EW baryogenesis where the first-order phase transition plays an important role. In addition, we explain the sphaleron process which is the baryon number violating process. Then, we describe how to determine the vacuum bubble nucleation rate. The sphaleron decoupling condition, which is a criterion to realize the EW baryogenesis, is also discussed. Finally, we define parameters characterizing the first-order phase transition. Gravitational waves from the first-order phase transition can be parameterized by these parameters.

3.4.1 Importance of the first-order EW phase transition

Dynamics of the EWPT is still unknown. If the EWPT is a first-order, the BAU may be able to be solved via the mechanism of EWBG [43].

The ratio of the baryon number to the photon number is measured by the cosmic microwave background (CMB) and light element abundances related to the big bang nucleosynthesis (BBN) at 95% confidence level [1]:

$$\frac{n_b}{n_\gamma} \simeq (6.5 - 5.8) \times 10^{-10} \quad \text{(BBN)}, \tag{3.4.1}$$

$$\frac{n_b}{n_\gamma} \simeq (6.12 \pm 0.04) \times 10^{-10} \quad \text{(CMB)}. \tag{3.4.2}$$

The observation results cannot be explained in the standard cosmology model. We here consider the case that the Universe satisfies $n_b/n_\gamma = 0$ as the initial condition. At the early Universe with $T < 1\,\text{GeV}$, number densities of nucleons n_b and anti-nucleons $n_{\bar{b}}$ are given by

$$\frac{n_b}{n_\gamma} \simeq \frac{n_{\bar{b}}}{n_\gamma} \simeq \left(\frac{m_p}{T}\right)^{3/2} \exp\left[-\frac{m_p}{T}\right], \tag{3.4.3}$$

where m_p is the mass of protons. When $T < 20\,\text{MeV}$, the nucleons and anti-nucleons are decoupled. Then, n_b and $n_{\bar{b}}$ take the following values [180]

$$\frac{n_b}{n_\gamma} \simeq \frac{n_{\bar{b}}}{n_\gamma} \simeq 10^{-18}. \tag{3.4.4}$$

The above number is smaller than the observed baryon number (3.4.2). This fact implies that the BAU cannot be explained within the framework of the standard cosmology. Therefore, a mechanism to produce the baryon asymmetry is required.

In order to generate the baryon asymmetry from the baryon symmetric Universe, a mechanism satisfying Sakharov's condition is required [42]. Sakharov's condition is composed of three conditions [42];

1. Baryon number violation
2. C and CP violation
3. Departure from the thermal equilibrium

The necessity of the first condition is trivial to explain the baryon asymmetry from the baryon symmetric Universe. In order to explain why the second condition is required, we consider a process $X + A \to B + C$, which violates baryon numbers n. If the C symmetry is respected, the C-conjugated process $X^C + A^C \to B^C + C^C$ occurs with the same possibility. The process $X^C + A^C \to B^C + C^C$ violates the baryon number $-n$. Thus, the net baryon numbers disappears. The necessity of the CP violation is also shown by the same argument as for the C symmetry. Therefore, the C and CP violations are needed to generate the baryon asymmetry. If the system is in thermal equilibrium, the baryon number density and the anti-baryon number density have the same density distribution. Then, the net baryon number is vanished by the pair annihilation of baryons and anti-baryons. It means that the third condition is also required to produce the baryon asymmetry.

In the scenario of EWBG, Sakharov's condition can be satisfied by the following mechanisms [43];

1. Sphaleron process
2. C and CP violation in extensions of Higgs sectors
3. Strongly first-order EWPT

The sphaleron process is a vacuum transition process at finite temperatures. This process violates the baryon and lepton numbers via the chiral anomaly [181, 182]. In the EW theory, the sum of baryon and lepton numbers $B + L$ is not conserved. The current for $B + L$ is expressed by using the field strength for the $SU(2)_L$ gauge field $W^a_{\mu\nu}$ and $U(1)_Y$ gauge field $B_{\mu\nu}$ as

$$\partial_\mu J^\mu_{B+L} = \frac{n_f}{32\pi}\left(g^2\epsilon^{\mu\nu\rho\sigma}W^a_{\mu\nu}W^a_{\rho\sigma} + g'^2 B_{\mu\nu}B_{\rho\sigma}\right), \tag{3.4.5}$$

where g and g' are the gauge couplings for $SU(2)_L$ and $U(1)_Y$, respectively. Since the $U(1)_Y$ part is not important, we neglect the part in the following. The constant n_f is the number of generations. Using Eq. (3.4.5), we can obtain

$$\Delta(B + L) = N_f\left[N_{CS}(t = +\infty) - N_{CS}(t = -\infty)\right], \tag{3.4.6}$$

where $N_{CS}(t)$ is the Chern-Simons number, which is defined as

$$N_{CS}(t) = \frac{g^2}{16\pi^2}\int_t d^3x\epsilon_{ijk}\left(W^a_i\partial_j W^a_k + \frac{1}{3}\epsilon^{abc}W^a_i W^b_j W^c_k\right). \tag{3.4.7}$$

The field W^a_i is the $SU(2)_L$ gauge field. Degenerate classical vacua are distinguished by the integer N_{CS}. These vacua are often called as topologically distinct vacua. Eq. (3.4.6) indicates that $B + L$ can be changed when the vacuum transition process occurs.

Since there are energy barriers between the topological distinct vacua, it is difficult to occur the vacuum transition process frequently. The height of the energy barrier is characterized by energies of sphalerons. The sphalerons are non-perturbative solutions in field equations for the EW gauge and Higgs fields [44, 45]. At the zero temperature, the vacuum transition can be realized via the quantum tunneling [182]. The tunneling rate $\Gamma_{\rm tunneling}$ is given by

$$\Gamma_{\rm tunneling} \propto \exp\left[-\frac{8\pi^2}{g^2}\right]. \tag{3.4.8}$$

Therefore, such vacuum transition hardly occurs.

At finite temperatures, thermal fluctuations can induce the vacuum transition via the sphalerons. These processes are called as the sphaleron process. The sphaleron transition rate at the temperature T in the broken phase ($v(T) \neq 0$) is given by [183]

$$\Gamma^{\rm br}_{\rm sph}(T) \simeq \left[2\mathcal{N}_{\rm tr}(T)\mathcal{N}_{\rm rot}(T)\mathcal{V}_{\rm rot}\frac{\omega_-(T)}{gv(T)}\right] T^4 \left(\frac{\alpha_W}{4\pi}\right)^4 \left(\frac{4\pi v(T)}{gT}\right)^7 \kappa(T) e^{-E_{\rm sph}(T)/T}, \tag{3.4.9}$$

where $\mathcal{N}_{\rm tr}$ and $\mathcal{N}_{\rm rot}$ are the normalization factors for the zero mode related to the translation and the rotation, respectively. The factor $\mathcal{V}_{\rm rot}$ is the volume of the rotation group, which is given by $\mathcal{V}_{\rm rot} = 8\pi^2$. The factor ω_- is the frequency for the negative mode around sphalerons. α_W is defined by $\alpha_W = \alpha/\sin^2\theta_W$. The factor κ is the fluctuation determinant around sphalerons. $E_{\rm sph}(T)$ is an energy of sphalerons at finite temperatures, which can be expressed by

$$E_{\rm sph}(T) = \frac{4\pi v(T)}{g}\mathcal{E}(T). \tag{3.4.10}$$

The factor $\mathcal{E}$ depends on details of models. Eq. (3.4.10) indicates that the Boltzmann suppression factor in the sphaleron transition rate (3.4.9) disappears at the symmetric phase ($v(T) = 0$). Therefore, the sphaleron process rapidly occurs in the symmetric phase. It is expected that the sphaleron process plays an important role to explain the BAU.

Since the sphaleron energy characterizes the sphaleron transition rate, determination of the sphaleron energy is important. In general, the sphaleron energy depends on the details of extended Higgs models. The sphaleron solutions in extended Higgs models have been calculated in the literatures [49, 59, 62, 83, 85, 184–191]. The sphaleron energy at the zero temperature can be determined indirectly via the measurement of the hhh coupling in several extended Higgs models [190].

3.4.2 Bubble nucleation at the early Universe

The first-order phase transition at the early Universe proceeds via the nucleation and expansion of vacuum bubbles. The nucleation rate of the vacuum bubbles $\Gamma(T)$ is given by [192]

$$\Gamma(T) \simeq T^4 \left(\frac{S_3(T)}{2\pi T}\right)^{3/2} \exp\left[-\frac{S_3(T)}{T}\right], \tag{3.4.11}$$

where $S_3(T)$ is three-dimensional action for bounce solutions, which is defined by

$$S_3(T) = \int d^3x \left[\frac{1}{2}\left(\vec{\nabla}\phi_b\right)^2 + V_{\rm eff}\left(\phi_b, T\right)\right]. \tag{3.4.12}$$

The field ϕ_b is the bounce solution, which is determined by solving the following field equation with the boundary conditions

$$\frac{d^2\phi_b}{dr^2} + \frac{2}{r}\frac{d\phi_b}{dr} - \frac{\partial V_{\rm eff}}{\partial \phi_b} = 0, \quad \left.\frac{d\phi_b}{dr}\right|_{r=0} = 0, \quad \phi_b|_{r=\infty} = 0. \tag{3.4.13}$$

Calculating the bounce solutions in extended Higgs models, we utilize the public code *CosmoTransitions* [193]. In order to complete the first-order phase transition by today, at least one vacuum bubble must be nucleated in the horizon. A temperature at which one vacuum bubble is nucleated in the horizon is called as the nucleation temperature T_n, which is defined by

$$\left.\frac{\Gamma(T)}{H^4(T)}\right|_{T=T_n} = 1, \tag{3.4.14}$$

where $H(T)$ is the Hubble constant, which is given by

$$H(T) \simeq 1.66\,\frac{\sqrt{g_*(T)}T^2}{M_{p\ell}}. \tag{3.4.15}$$

The factor $g_*(T)$ is the effective degrees of freedom at temperatures T. The factor $M_{p\ell}$ is the Planck mass, which is given by $M_{p\ell} \simeq 1.22 \times 10^{19}\,\text{GeV}$.

The condition Eq. (3.4.14) means that a single vacuum bubble can be nucleated in a single Hubble volume at the nucleation temperature. If the condition $\Gamma(T)/H^4(T) \geq 1$ is not satisfied at any temperatures, the phase transition cannot be completed by today. It means that we may observe several areas in our Universe where the vacuum expectation value of the Higgs field is zero. Since we have not observe such regions, the phase transition should be completed by today.

3.4.3 Sphaleron decoupling condition

The sphaleron process plays an important role to produce the baryon asymmetry, i.e., EW baryogenesis [43] and leptogenesis [194]. In this section, we focus on the scenario of EW baryogenesis.

In the EW baryogenesis, the chiral asymmetry can be produced via the dynamics between the expanding vacuum bubble walls and the plasma. The produced chiral asymmetry can be transformed into the baryon number via the sphaleron process. Then, the generated baryon number is injected into the insider of the vacuum bubbles. If the sphaleron process can be decoupled inside the vacuum bubbles, the washout of the baryon number can be avoided. As a result, the observed baryon asymmetry can be produced.

As we mentioned, the sphaleron process should be decoupling after the phase transition in order to success the scenario of EWBG. The condition avoiding the washout of produced baryon number is given by [43, 52, 183]

$$-\frac{dN_B}{N_B dt} \simeq \frac{13}{2}N_f\left[2\mathcal{N}_{\rm tr}(T)\mathcal{N}_{\rm rot}(T)\mathcal{V}_{\rm rot}\frac{\omega_-(T)}{gv(T)}\right]T\left(\frac{\alpha_W}{4\pi}\right)^4\left(\frac{4\pi v(T)}{gT}\right)^7\kappa(T)e^{-E_{\rm sph}(T)/T} < H(T). \tag{3.4.16}$$

Transforming the above inequality, we can obtain

$$\begin{aligned}\frac{E_{\rm sph}(T)}{T} > 38.849 &- \frac{1}{2}\ln\frac{g_*(T)}{106.75} + \ln\kappa(T) + \ln\left[2\mathcal{N}_{\rm tr}(T)\mathcal{N}_{\rm rot}(T)\frac{\omega_-(T)}{gv(T)}\right] \\ &+ 7\ln\left(\frac{v(T)}{T}\right) - \ln\left(\frac{T}{100\,\text{GeV}}\right).\end{aligned} \tag{3.4.17}$$

In general, the factors $g_*(T)$, $\mathcal{N}_{\rm tr}(T)$, $\mathcal{N}_{\rm rot}(T)$ and $\omega_-(T)$ depend on temperatures and details of extended Higgs models. For instance, the temperature and model dependences of the factors $\mathcal{N}_{\rm tr}(T)$ and $\mathcal{N}_{\rm rot}(T)$ have been evaluated in the minimal supersymmetric standard model [52]. However, effects on the sphaleron decoupling condition from these dependences are logarithmic. Hence, we can expect that the dependences are negligible. In this thesis, we use the values of $g_*(T)$, $\mathcal{N}_{\rm tr}(T)$, $\mathcal{N}_{\rm rot}(T)$ and $\omega_-(T)$ in the SM at the zero temperature. We take $\mathcal{N}_{\rm tr}(T=0) \simeq 7.6$ and $\mathcal{N}_{\rm rot}(T=0) \simeq 11.2$ [195]. In addition, we take $\omega_-(T)^2 \simeq 0.65\, g^2 v(T)^2$ [195] and $\kappa \simeq 0.12$ [196]. Then, the condition (3.4.17) is expressed by

$$\frac{v(T)}{T} > \frac{g}{4\pi \mathcal{E}(T)} \left[41.65 + 7 \ln \frac{v(T)}{T} - \ln \frac{T}{100\,{\rm GeV}} \right] \equiv \zeta_{\rm sph}(T). \tag{3.4.18}$$

In the following, this condition is used when we discuss the feasibility of EWBG. The similar condition has been calculated by several theorists [52, 60, 188]. In the SM with a scalar singlet field, the value of $\zeta_{\rm sph}(T)$ is about 1.2 [60]. The value of $\zeta_{\rm sph}(T)$ is often taken as the unity as the approximate sphaleron decoupling condition.

3.4.4 Gravitational waves from the first-order phase transition

If the first-order phase transition occurs at the early Universe, the vacuum bubbles are produced. The vacuum bubbles can collide with each other as these expands. Then, characteristic GWs can be predicted. The GWs from the first-order phase transition can be characterized by four quantities; latent heat of the phase transition, duration of the phase transition, nucleation temperature and vacuum bubble wall velocity. α is the normalized released latent heat by radiative energy density, which is defined by

$$\alpha \equiv \frac{\epsilon(T_n)}{\rho_{\rm rad}(T_n)}, \tag{3.4.19}$$

where $\rho_{\rm rad}(T) = (\pi^2/30) g_* T^4$, and $\epsilon(T)$ is given by

$$\epsilon(T) = \Delta V_{\rm eff} - T \frac{\partial \Delta V_{\rm eff}}{\partial T}, \quad \Delta V_{\rm eff} = V_{\rm eff}(\varphi_-(T), T) - V_{\rm eff}(\varphi_+(T), T), \tag{3.4.20}$$

where φ_+ and φ_- denote the true and false vacua, respectively. The parameter β/H corresponds to the inverse of the duration of phase transition, which is defined by

$$\frac{\beta}{H} = \tilde{\beta} \equiv T_n \left. \frac{d}{dT} \left(\frac{S_3}{T} \right) \right|_{T=T_n}, \tag{3.4.21}$$

where S_3 is the three-dimensional Euclidian action.

If the first-order phase transition occurs in the early Universe, GWs can be produced due to the vacuum bubble dynamics. The GWs from the first-order EWPT have three sources: collisions of the vacuum bubbles, compressional waves (sound waves) and magnetohydrodynamics turbulence. The GW amplitude from the collisions of the vacuum bubbles, which is obtained by using the envelope approximation [197], is given by

$$\Omega_{\rm env}(f) h^2 = 1.67 \times 10^{-5} \left(\frac{H}{\beta} \right)^2 \left(\frac{\kappa_\varphi \alpha}{1+\alpha} \right)^2 \left(\frac{100}{g_*} \right)^{1/3} \left(\frac{0.11\, v_w^3}{0.42 + v_w^2} \right) \left(\frac{3.8\, (f/f_{\rm env})^{2.8}}{1 + 2.8 (f/f_{\rm env})^{3.8}} \right)^{7/2}. \tag{3.4.22}$$

where v_w is the wall velocity. In this thesis, we take the value of v_w as a free parameter. The factor κ_φ is the efficiency factor, which is given by

$$\kappa_\varphi \simeq \frac{1}{1+0.715\alpha}\left(0.715\,\alpha + \frac{4}{27}\sqrt{\frac{3\alpha}{2}}\right) \quad \text{with} \quad v_w = 1. \tag{3.4.23}$$

The peak frequency $f_{\rm env}$ is given by

$$f_{\rm env} = 1.65\times 10^{-5}\,{\rm Hz}\left(\frac{0.62}{1.8-0.1v_w+v_w^2}\right)\left(\frac{\beta}{H}\right)\left(\frac{T_n}{100\,{\rm GeV}}\right)\left(\frac{g_*}{100}\right)^{1/6}. \tag{3.4.24}$$

The amplitude of the GWs from sound wave is given by [198]

$$\Omega_{\rm sw}(f)h^2 = 2.65\times 10^{-6} v_w \left(\frac{H}{\beta}\right)\left(\frac{\kappa_v\alpha}{1+\alpha}\right)^2\left(\frac{100}{g_*}\right)^{1/3}(f/f_{\rm sw})^3\left(\frac{7}{4+3(f/f_{\rm sw})^2}\right)^{7/2}, \tag{3.4.25}$$

The factor κ_v is the fraction of the released latent heat contributing to sound wave formation, which is given by [199]

$$\kappa_v(v_w,\alpha) \simeq \begin{cases} \dfrac{c_s^{11/5}\kappa_A\kappa_B}{(c_s^{11/5}-v_w^{11/5})\kappa_B + v_w c_s^{6/5}\kappa_A} & (v_w < c_s), \\ \kappa_B + (v_w-c_s)\delta\kappa + \dfrac{(v_w-c_s)^3}{(v_J-c_s)^3}\left[\kappa_C-\kappa_B-(v_J-c_s)\delta\kappa\right] & (c_s < v_w < v_J), \\ \dfrac{(v_J-1)^3 v_J^{5/2} v_w^{-5/2}\kappa_C\kappa_D}{[(v_J-1)^3-(v_w-1)^3]v_J^{5/2}\kappa_C + (v_w-1)^3\kappa_D} & (v_J < v_w), \end{cases} \tag{3.4.26}$$

where

$$\begin{aligned} \kappa_A &\simeq v_w^{6/5}\frac{6.9\,\alpha}{1.36-0.037\sqrt{\alpha}+\alpha}, \quad \kappa_B \simeq \frac{\alpha^{2/5}}{0.017+(0.997+\alpha)^{2/5}}, \\ \kappa_C &\simeq \frac{\sqrt{\alpha}}{0.135+\sqrt{0.98+\alpha}}, \qquad \kappa_D \simeq \frac{\alpha}{0.73+0.083\sqrt{\alpha}+\alpha}, \end{aligned} \tag{3.4.27}$$

$$c_s = 1/\sqrt{3} \simeq 0.577, \tag{3.4.28}$$

$$v_J = \frac{\sqrt{2\alpha/3+\alpha^2}+1/\sqrt{3}}{1+\alpha}, \tag{3.4.29}$$

$$\delta\kappa \simeq -0.9\ln\frac{\sqrt{\alpha}}{1+\sqrt{\alpha}}. \tag{3.4.30}$$

The peak frequency $f_{\rm sw}$ is given by [198]

$$f_{\rm sw} = 1.9\times 10^{-2}{\rm mHz}\frac{1}{v_w}\left(\frac{\beta}{H}\right)\left(\frac{T_n}{100{\rm GeV}}\right)\left(\frac{g_*}{100}\right)^{1/6}. \tag{3.4.31}$$

The leading contribution among the three sources is the GWs from sound waves (for instance, see Ref. [69]).

The GW amplitude from magnetohydrodynamics turbulence is given by [200, 201]

$$\Omega_{\rm turb}(f)h^2 = 3.35\times10^{-4}\left(\frac{H}{\beta}\right)\left(\frac{\kappa_{\rm turb}\,\alpha}{1+\alpha}\right)^{\frac{3}{2}}\left(\frac{100}{g_*}\right)^{1/3} v_w \frac{(f/f_{\rm turb})^3}{(1+(f/f_{\rm turb}))^{11/3}\,(1+8\pi f/h)}. \tag{3.4.32}$$

The efficiency factor $\kappa_{\rm turb}$ is given by $\kappa_{\rm turb} = \epsilon\kappa_{\rm sw}$ with $\epsilon \simeq 0.05\,\%$. The peak frequency $f_{\rm turb}$ is given by

$$f_{\rm turb} = 2.7\times10^{-5}\,{\rm Hz}\,v_w^{-1}\left(\frac{\beta}{H}\right)\left(\frac{T_n}{100\,{\rm GeV}}\right)\left(\frac{g_*}{100}\right)^{1/6}. \tag{3.4.33}$$

To examine parameter regions where GWs can be detected at LISA and DECIGO, we use the signal-to-noise ratio for the observation of the GW spectrum, which is discussed in Ref. [202]. The criterion is such that the signal-to-noise ratio for the GW spectrum is larger than 10, which is adopted in the analysis in Chapter 6.

Chapter 4

EW phase transition in renormalizable extended Higgs models

4.1 EW phase transition in the two Higgs doublet models

In this section, we discuss the EWPT in the two Higgs doublet models. We first discuss the sphaleron decoupling condition in the two Higgs doublet model. Then, we discuss the phenomenology at collider experiments and gravitational wave observations.

4.1.1 EW phase transition in the two Higgs doublet model

In order to discuss the phase transition, the effective potential at finite temperatures is important. The effective potential in the THDM is given by

$$V_{\rm eff}(\varphi_1,\varphi_2,T) = V_{\rm tree}^{\rm THDM}(\varphi_1,\varphi_2) + V_{\rm CW}(\varphi_1,\varphi_2) + \frac{T^4}{2\pi^2}\sum_i n_i J_i\left(\frac{m_i^2(\varphi_1,\varphi_2)}{T^2}\right), \tag{4.1.1}$$

where $V_{\rm CW}$ is the Coleman-Weinberg potential [178]. The third term in Eq. (4.1.1) is the thermal corrections to the effective potential [203]. The function $J_i(x)$ is defined by

$$J_i(x) = \int_0^\infty dk k^2 \ln\left[1 - {\rm sign}(n_i)\exp\left(-\sqrt{k^2+x}\right)\right], \tag{4.1.2}$$

where

$${\rm sign}(n_i) = \begin{cases} 1 & (n_i > 0) \\ -1 & (n_i < 0) \end{cases}. \tag{4.1.3}$$

As well known, the infrared divergence can appear in the zero mode of Matsubara frequencies of boson fields [203]. In order to avoid the divergence, we should include thermal corrections to masses of boson particles. There are two famous methods to include the higher order thermal corrections; (1) Parwani scheme [204] (2) Arnold-Espinosa scheme [205]. Since the Parwani scheme can appropriately describe the phase transition at relatively low temperatures, we here take the Parwani scheme. In the Parwani scheme, we should replace the field dependent masses of boson fields in Eq. (4.1.1) with the thermal masses

$$m_i^2(\varphi_1,\varphi_2,T) \to M_i^2(\varphi_1,\varphi_2,T) = m_i^2(\varphi_1,\varphi_2) + \Pi_i(T), \tag{4.1.4}$$

where $\Pi_i(T)$ is the thermal correction to the mass of particle i. The detail of the calculation for $\Pi_i(T)$ is discussed in Appendix A. We here consider the phase transition in the three scenarios of the THDMs:

1. Alignment with degenerated masses
2. Alignment with mass differences
3. Non-alignment

In the following, we discuss the EW phase transition in each scenario.

In order to realize the scenario of electroweak baryogenesis, the sphaleron decoupling condition should be satisfied. Since the sphaleron energy depends on the detail of models, the sphaleron solutions should be calculated to evaluate the constraint on the THDM from the sphaleron decoupling condition. It is difficult to get the sphaleron solutions without the simplification of the field equations. It is economical to simplify the field equations by using an ansatz, which has the symmetry and other properties of the sphaleron [1]. Here, we take the following ansatz

$$W_i^a(\vec{\xi}) = \frac{v(T)}{2}\left[\epsilon^{aij}n_j\frac{1-R(\xi)\cos\theta(\xi)}{\xi} + (\delta_{ai}-n_an_i)\frac{R(\xi)\sin\theta(\xi)}{\xi}\right], \tag{4.1.5}$$

$$\Phi_1(\vec{\xi}) = \frac{v_1(T)}{\sqrt{2}}S_1(\xi)e^{in_a\sigma^a\phi_1(\xi)}\begin{pmatrix}0\\1\end{pmatrix}, \tag{4.1.6}$$

$$\Phi_2(\vec{\xi}) = \frac{v_2(T)}{\sqrt{2}}S_2(\xi)e^{in_a\sigma^a\phi_2(\xi)}\begin{pmatrix}0\\1\end{pmatrix}, \tag{4.1.7}$$

where $\vec{\xi} = gv(T)\vec{r}/2$, $\xi = |\vec{\xi}|$ and $v(T) = \sqrt{v_1(T)^2+v_2(T)^2}$. The radial functions R, S_1 and S_2 satisfy the following boundary conditions

$$\begin{aligned}&\lim_{\xi\to0}R(\xi)\to-1,\ \lim_{\xi\to0}S_1(\xi)\to0,\ \lim_{\xi\to0}S_2(\xi)\to0,\\ &\lim_{\xi\to\infty}R(\xi)\to1,\ \lim_{\xi\to\infty}S_1(\xi)\to1,\ \lim_{\xi\to\infty}S_2(\xi)\to1.\end{aligned} \tag{4.1.8}$$

Here, we take $\theta(\xi)=\pi$ and $\phi_i(\xi)=\pi/2$ $(i=1,2)$ as taken in Ref. [189]. Then, the sphaleron energy at finite temperatures $E_{\rm sph}(T)$ is given by

$$E_{\rm sph}(T) = \frac{4\pi v(T)}{g}\mathcal{E}(T), \tag{4.1.9}$$

$$\begin{aligned}\mathcal{E}(T) = \int d\xi\Bigg[&\frac{1}{2}\left(\frac{\partial R}{\partial\xi}\right)^2 + \frac{1}{4\xi^2}(1-R(\xi))^2 + \frac{v_1(T)^2\xi^2}{v(T)^2}\left\{\left(\frac{\partial S_1}{\partial\xi}\right)^2 + \frac{1}{2\xi^2}S_1^2(1-R(\xi))^2\right\}\\ &+\frac{v_2(T)^2\xi^2}{v(T)^2}\left\{\left(\frac{\partial S_2}{\partial\xi}\right)^2 + \frac{1}{2\xi^2}S_2^2(1-R(\xi))^2\right\} + \frac{8\xi^2}{g^2v(T)^4}\left\{V_{\rm eff}(S_1,S_2,T) - V_{\rm eff}(v_1,v_2,T)\right\}\Bigg],\end{aligned} \tag{4.1.10}$$

where $V_{\rm eff}$ is the effective potential at finite temperatures.

[1] In recent, it was shown that the sphaleron solutions can be obtained by using the method of the gradient flow without assuming any ansatz [206].

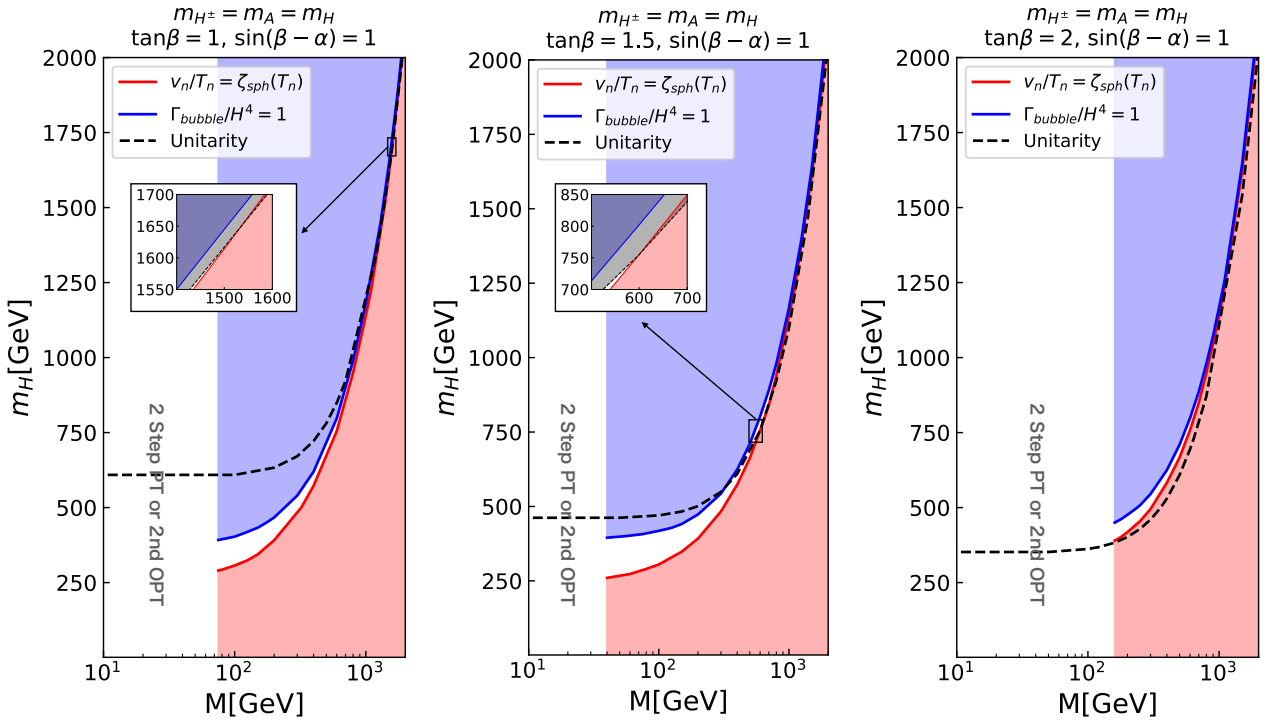

Figure 4.1: The parameter region where the strong first order EW phase transition can be realized in Scenario 1. In the red region, the sphaleron decoupling condition cannot be satisfied. The blue region is constrained by the completion condition for the phase transition. The black region is excluded by the perturbative unitarity bound. In the green region, the EW phase transition is two step phase transition in which the first step phase transition is second order phase transition. If the value of $\tan\beta$ is large, the strong first order EW phase transition cannot be realized.

By substituting the ansatz in Eq. (4.1.7) into the field equations for the gauge and Higgs fields, we can obtain the differential equations for the functions R, S_1 and S_2 as

$$\frac{\partial^2 R}{\partial \xi^2} + \frac{1}{\xi^2} R(1-R^2) + (1-R)\left\{ \frac{v_1(T)^2}{v(T)^2}(S_1)^2 + \frac{v_2(T)^2}{v(T)^2}(S_2)^2 \right\} = 0, \tag{4.1.11}$$

$$2\xi^2 \frac{\partial^2 S_\alpha}{\partial \xi^2} + 4\xi \frac{\partial S_\alpha}{\partial \xi} - S_\alpha (1-R)^2 - \frac{8\xi^2}{g^2 v_\alpha(T)^2 v(T)^2} \frac{\partial V_{\rm eff}(S_1, S_2, T)}{\partial S_\alpha} = 0 \quad (\alpha = 1, 2), \tag{4.1.12}$$

with the boundary conditions described in Eq. (4.1.8). By combining $\mathcal{E}(T)$ in Eq. (4.1.10) with the sphaleron decoupling condition in Eq. (3.4.18), we can discuss the sphaleron decoupling condition in the THDM.

Scenario1: Alignment with degenerated masses

In Fig. 4.1, we show the parameter region where the strong first order EW phase transition can be satisfied with several theoretical constraints. In the red region, the sphaleron decoupling condition cannot be satisfied. The blue parameter region is excluded by the completion condition for the phase transition. This condition is expressed as

$$\frac{\Gamma(T)}{H^4(T)} \leq 1. \tag{4.1.13}$$

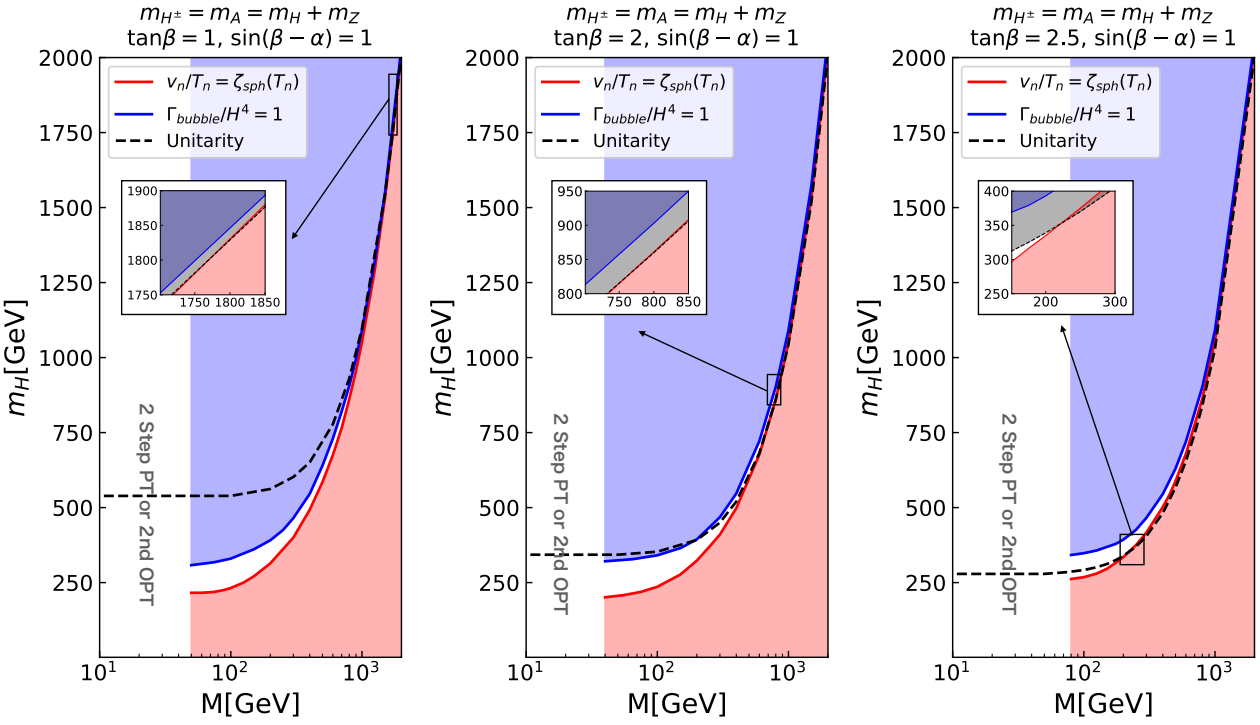

Figure 4.2: The parameter region where the strong first order EW phase transition can be realized in the THDM with $m_{H^\pm} = m_A = m_H + m_Z$, $\sin(\beta-\alpha) = 1$ and $\tan\beta = 1,\ 2,\ 2.5$. The definition of each colored region is the same in Fig. 4.1. As in Fig. 4.1, if the value of $\tan\beta$ is large, the strong first order EW phase transition cannot be realized.

If this condition cannot be satisfied, the phase transition does not finish by today. In the green region, the EW phase transition can be a two step phase transition where the first step phase transition is second order. To realize the scenario of EW baryogenesis, the first step phase transition should be first order. Therefore, the EW baryogenesis cannot be realized in the green parameter region. The black region is constrained by the perturbative unitarity bound in Eq. (3.1.41). From Fig. 4.1, upper bounds on the masses of additional Higgs bosons can be constrained by the unitarity bound and the sphaleron decoupling condition. If there is a mass difference between additional Higgs bosons or $\sin(\beta-\alpha) \neq 1$, the mass upper bounds can be determined by only the unitarity bound. This fact is called as *the new no-lose theorem*, which has been discussed in the literatures [14, 19, 29, 96]. Our result shows that upper bounds on additional Higgs bosons can be obtained by combining the unitarity bound with the sphaleron decoupling condition even if the discovered Higgs boson is SM-like.

Scenario2: Alignment with a relatively small mass difference

In Fig. 4.2, we show the result of the THDM with a relatively small mass difference. As an example, we here consider the THDM with $m_{H^\pm} = m_A = m_H + m_Z$ and $\sin(\beta-\alpha) = 1$. As we can see, when the mass difference is relatively small, upper bounds on masses of additional Higgs bosons can be determined by the unitarity bound and the sphaleron decoupling condition.

In Fig. 4.3, we consider the THDM with $m_{H^\pm} = m_A = m_H + 1.5\,m_Z$, $\tan\beta = 1.5$ and $\sin(\beta-\alpha) = 1$. According to Fig. 4.2 and Fig. 4.3, the mass upper bounds are determined by only the

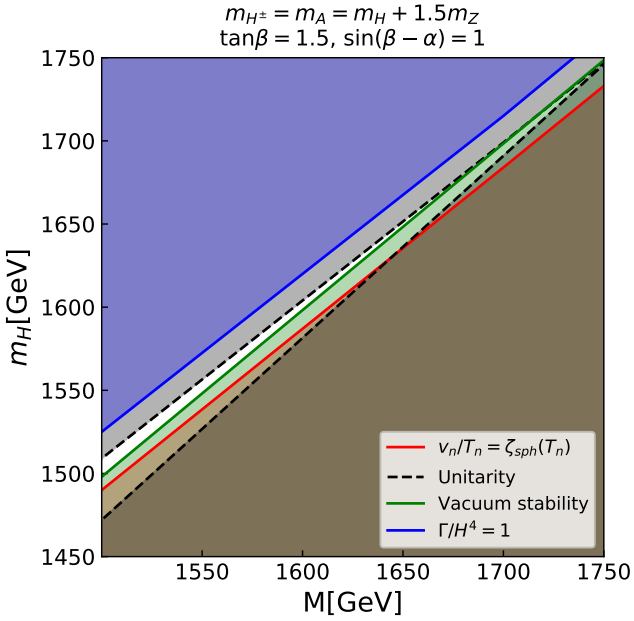

Figure 4.3: The parameter region where the strong first order EW phase transition with the theoretical constraints. The mass upper bound is determined by the unitarity bound without the sphaleron decoupling condition. By combining the vacuum stability bound and the unitarity bound, we can get the mass upper bound.

unitarity bound when the mass difference is getting large. This reason is as follows. When we consider the difference between $m^2_{H^\pm}$ and m^2_H in the case with $m_{H^\pm} = m_A = m_H + 1.5\,m_Z$ and $\sin(\beta-\alpha) = 1$ as an example, we can obtain

$$m^2_{H^\pm} - m^2_H = 3m_H m_Z = \widetilde{\lambda} v^2, \tag{4.1.14}$$

where $\widetilde{\lambda}$ is a linear combination of λ_i $(i = 1, \cdots 5)$ in the Higgs potential given in Eq. (3.1.1). Eq. (4.1.14) indicates that the large m_H cannot be taken while keeping the value of $\widetilde{\lambda}$ small. As a result, the mass upper bounds on additional Higgs bosons can be determined by the unitarity bound when the additional Higgs bosons in the THDM have a mass difference.

Scenario3: Non-alignment

In Fig. 4.4, we show the result in the THDM with or without alignment. When we consider the non-alignment case $\sin(\beta-\alpha) \neq 1$, the mass upper bound lowers. Actually, in the THDM with $m_H = m_{H^\pm} = m_A$, $\tan\beta = 1$ and $\sin(\beta-\alpha) = 1$, the mass upper bound is around 1.6 TeV. On the other hand, in the case without alignment $\sin(\beta-\alpha) = 0.999$, the mass upper bound is around 1.2TeV. It means that the strong first order EW phase transition prefers the alignment limit $\sin(\beta-\alpha) = 1$.

In this subsection, we have analyzed the EWPT in the THDMs. We have shown that even if the discovered Higgs boson is SM-like, the masses of additional Higgs bosons can be determined by combining the unitarity bound and the sphaleron decoupling condition. We have confirmed the

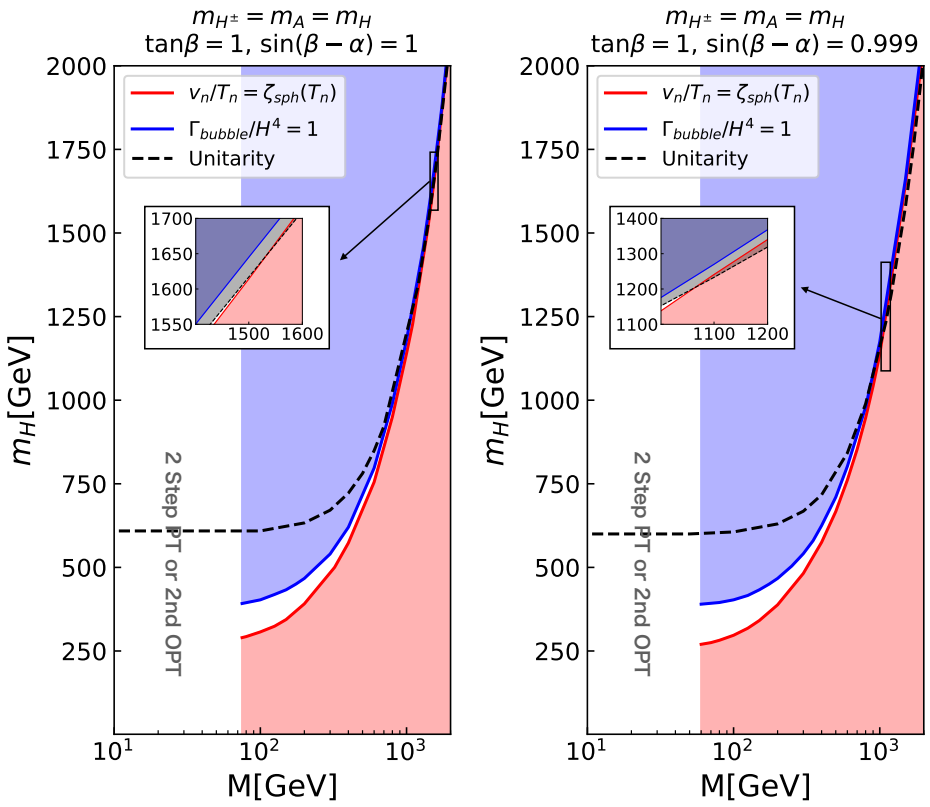

Figure 4.4: The parameter region satisfying the theoretical constraints with $\sin(\beta-\alpha) = 1$ and $\sin(\beta-\alpha) \neq 1$. It lowers in the $\sin(\beta-\alpha) \neq 1$ case that the mass upper bound determined by the sphaleron decoupling condition and the unitarity bound.

upper bound is given by

$$m_\Phi < 1.6 - 2 \text{ TeV} \quad (\Phi = H, A, H^\pm). \tag{4.1.15}$$

This bound means that if we cannot detect a new particle whose mass is below the upper bound in Eq. (4.2.1), the scenario of EW baryogenesis cannot be realized. For this reason, our result plays an important role to test the feasibility of EW baryogenesis at future collider experiments.

4.1.2 Phenomenology in extended Higgs models with relatively heavy additional Higgs bosons

In the previous subsection, we have obtained the upper bounds on masses of additional Higgs bosons in Eq. (4.2.1). This bound means the THDM with relatively heavy Higgs boson $\sim O(1)$ TeV may realize the strong first order EW phase transition. On the other hand, testing such models is difficult at future collider experiments such as HL-LHC and the ILC. Then, how can we know the mass scale of new Higgs bosons?

In order to show how to know the mass scale, we focus on the correlation between the triple Higgs boson coupling hhh and the gravitational waves from the first order EW phase transition. In this paper, we consider three benchmark scenarios to reveal the correlation. The benchmarks are shown in Tab. 4.1. We note that BM0 cannot be allowed by the experimental constraints from the LHC and the flavor physics [143]. But, we dare to show the GW spectrum in BM0 for comparison. Also, we show the deviation in the triple Higgs boson coupling in each benchmark in Tab. 4.1.

	$m_{H^\pm}$	m_A	m_H	M	$\tan\beta$	$\Delta\lambda^{1\ell}_{hhh}/\lambda^{\rm SM}_{hhh}$	$\Delta\lambda^{2\ell}_{hhh}/\lambda^{\rm SM}_{hhh}$	v_n/T_n
BM0	373GeV	373GeV	373GeV	50GeV	1	71.5%	86.4%	3.80
BM1	464GeV	464GeV	373GeV	200GeV	1.8	80.2%	112%	2.60
BM2	891GeV	891GeV	800GeV	720GeV	1.8	80.2%	125%	2.37

Table 4.1: Benchmark scenarios with $\sin(\beta-\alpha)=1$. $\Delta\lambda^{1\ell}_{hhh}/\lambda^{\rm SM}_{hhh}$ is the deviation in the triple Higgs boson coupling at the one-loop level. $\Delta\lambda^{2\ell}_{hhh}/\lambda^{\rm SM}_{hhh}$ is that at the two-loop level.

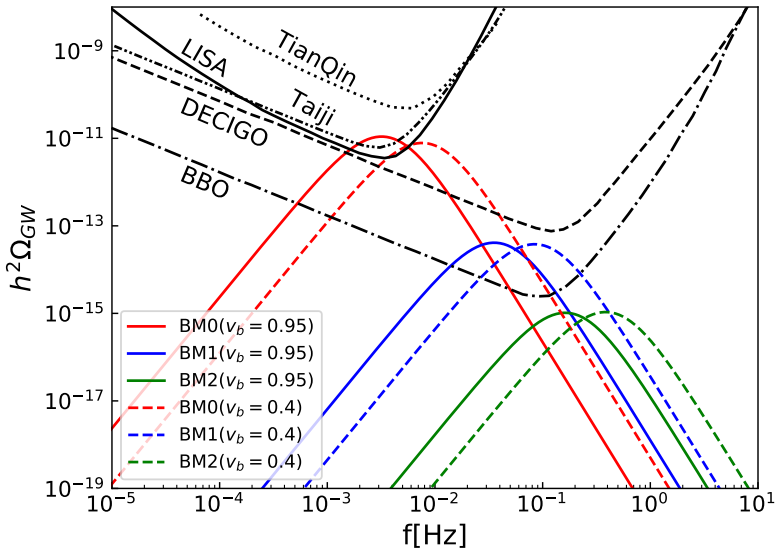

Figure 4.5: Predicted GW spectra in the benchmarks shown in Table 4.1.

In Fig. 4.5, we show the predicted GW spectra in the benchmarks in Tab. 4.1. The black lines are the sensitivity curves in BBO [207], DECIGO [75], LISA [74], Taiji [208], TianQin [209]. The solid (dashed) lines are the case where the wall velocity v_b is 95% (40%) of the light speed. According to Fig. 4.5, the peak of the GW spectra in BM1 is higher than that of BM2. On the other hand, the predicted triple Higgs boson couplings in BM1 and BM2 are the same values. It means that we may be able to know the mass scale of new particles as follows:

1. The peaked GW spectrum is observed and the large hhh coupling is measured
   → Relatively *light* new scalar bosons may exist

2. The peaked GW spectrum is not observed and the large hhh coupling is measured
   → Relatively *heavy* new scalar bosons may exist

This fact plays an important role when we test extended Higgs models with heavy additional Higgs bosons. As we mentioned in the introduction, testability of relatively light Higgs bosons have been thoroughly investigated by using the results at current and future collider experiments. Conversely, testing the existence of relatively heavy new scalar fields might be difficult at near future collider experiments. On the other hand, we have shown that the extended Higgs models with heavy new scalar fields may predict the peaked GWs and the large triple Higgs bosons coupling. It means that the mass scale of new scalar fields may be searched by observing the peaked GWs and triple Higgs boson coupling at future space-based interferometers or collider experiments.

In addition, we have analyzed the prediction on the hhh coupling in the THDMs with relatively heavy additional Higgs bosons like BM2. In order to satisfy the sphaleron decoupling condition in the THDMs with $m_\Phi > 700\,\mathrm{GeV}$ ($\Phi = H, A, H^\pm$), $\Delta^{\mathrm{THDM}}_{hhh}/\lambda^{\mathrm{SM}}_{hhh} > 60\%$ is required at the one-loop level. At the two-loop level, $\Delta^{\mathrm{THDM}}_{hhh}/\lambda^{\mathrm{SM}}_{hhh} > 80\%$ is required to satisfy the sphaleron decoupling condition in the THDMs with $m_\Phi > 700\,\mathrm{GeV}$. When we have obtained the constraint on the hhh coupling from the sphaleron decoupling condition at the two-loop level, the two-loop corrections to the effective potential at finite temperatures. It means that the hhh coupling should deviate from the SM prediction to realize the scenario of the EWBG in the THDMs with relatively heavy additional Higgs bosons.

4.2 Summary

We have shown that the masses of additional Higgs bosons can be determined by combining the unitarity bound and the sphaleron decoupling condition even if the discovered Higgs boson is SM-like. We have confirmed the upper bound is given by

$$m_\Phi < 1.6 - 2\ \mathrm{TeV} \quad (\Phi = H, A, H^\pm). \tag{4.2.1}$$

If we cannot discover a new particle whose mass is below the upper bound in Eq. (4.2.1), the scenario of EW baryogenesis may not be realized. Our result plays an important role to test the feasibility of EW baryogenesis at future collider experiments.

In addition, we have discussed phenomenology in the THDMs. We have shown that the typical mass scale of new scalar fields can be determined by future GW observations and collider experiments. It means that we are able to know mass scale indirectly even if exploring models with relatively heavy new scalar fields may be difficult at near future collider experiments.

Chapter 5

Nearly aligned Higgs effective field theory

In the previous section, we have discussed the EW phase transition in the THDM as an example. In the literatures, in order to obtain the model independent results of the dynamics of EW phase transition, the standard model effective field theory (SMEFT) is often used. In the SMEFT with a dimension six operator $|\Phi|^6/\Lambda^2$ in the Higgs potential, the sphaleron decoupling condition requires $\Lambda < 900\,\mathrm{GeV}$ [76, 88–92, 176]. From this result, we can naively expect that the mass of new particles should be smaller than 900 GeV to realize the strong first-order EW phase transition. On the other hand, we have shown that the strong first-order EW phase transition may be realized even if the masses of new scalar fields are above 1 TeV in the THDM. The origin of the discrepancy is non-decoupling effects. The SMEFT can be used when we discuss model independent properties of the decoupling new physics. On the contrary, in several extended Higgs models, large quantum corrections to Higgs couplings can be realized by heavy new particles . This effect is so-called the non-decoupling effect, which is important to realize the strongly first-order EW phase transition. Unfortunately, the SMEFT may not be appropriate when we discuss new physics models with the non-decoupling effects. This fact is confirmed by several theorists [9]. It indicates that we should consider a new EFT framework to discuss physics related to the non-decoupling effects. In this section, we discuss a candidate of the new EFT. Also, we discuss the dynamics of the EW phase transition by using the new EFT.

5.1 Definition of the nearly aligned Higgs EFT

We define a new EFT framework which can describe the non-decoupling effects from new physics. We call this EFT as the "nearly aligned Higgs effective field theory (naHEFT)" [179]. The naHEFT is an extension of the Higgs EFT. This EFT can describe not only the large quantum corrections in the Higgs potential but also those in Higgs couplings to gauge bosons and fermions. The effective Lagrangian in the naHEFT is expressed by [179]

$$\mathcal{L}_{\mathrm{naHEFT}} = \mathcal{L}_{\mathrm{SM}} + \mathcal{L}_{\mathrm{BSM}}, \tag{5.1.1}$$

where $\mathcal{L}_{\rm SM}$ is the SM Lagrangian, and $\mathcal{L}_{\rm BSM}$ is the BSM part which is defined as

$$\begin{aligned}\mathcal{L}_{\rm BSM} = \xi\Bigg[&-\frac{\kappa_0}{4}\left[\mathcal{M}^2(h)\right]^2 \ln\frac{\mathcal{M}^2(h)}{\mu^2} \\ &+ \frac{v^2}{2}\mathcal{F}(h)\,{\rm Tr}\left[D_\mu U^\dagger D^\mu U\right] + \frac{1}{2}\mathcal{K}(h)\left(\partial_\mu h\right)\left(\partial^\mu h\right) \\ &- v\left(\bar{q}_L^i U\left[\mathcal{Y}_q^{ij}(h) + \hat{\mathcal{Y}}_q^{ij}(h)\tau^3\right]q_R^j + {\rm h.c.}\right) \\ &- v\left(\bar{l}_L^i U\left[\mathcal{Y}_l^{ij}(h) + \hat{\mathcal{Y}}_l^{ij}(h)\tau^3\right]l_R^j + {\rm h.c.}\right)\Bigg],\end{aligned} \tag{5.1.2}$$

with $\xi = 1/(4\pi)^2$ and $v \simeq 246\,{\rm GeV}$. κ_0 and μ^2 are real parameters. h is the discovered Higgs boson field whose mass is 125 GeV. The matrix U parameterizes the Nambu-Goldstone bosons π^a,

$$U = \exp\left(\frac{i}{v}\pi^a\tau^a\right), \tag{5.1.3}$$

where τ^a $(a = 1, 2, 3)$ is the Pauli matrices. The fields q_L^i and l_L^i are the $SU(2)_L$ doublet SM quark and lepton fields, respectively. The index i characterizes the generation. The fields q_R^i and l_R^i are defined as $q_R^i = (u_R^i\ d_R^i)^T$ and $l_R^i = (0\ e_R^i)^T$, where u_R^i, d_R^i and e_R^i are the $SU(2)_L$ singlet up-type quark fields, down-type quark fields and lepton fields, respectively. The covariant derivative of U is defined by

$$D_\mu U = \partial_\mu U + ig\mathbf{W}_\mu U - ig'U\mathbf{B}_\mu, \tag{5.1.4}$$

where $\mathbf{W}_\mu$ and $\mathbf{B}_\mu$ are defined as $\mathbf{W}_\mu = \sum_{a=1}^3 W_\mu^a\tau^a/2$ and $\mathbf{B}_\mu = B_\mu\tau^3/2$, respectively. The BSM part in the naHEFT given in Eq. (5.1.2) includes five form factors $\mathcal{M}^2(h)$, $\mathcal{F}(h)$, $\mathcal{K}(h)$, $\mathcal{Y}_q^{ij}(h)$ and $\mathcal{Y}_l^{ij}(h)$. These form factors are polynomials in terms of h, and characterize the new physics effects. Since we are interested in the dynamics of the EWPT in this thesis, we only consider the correction to the Higgs potential in Eq. (5.1.2). The effect on the EWPT from the kinetic term for the Higgs boson is discussed within the framework of the SMEFT [88, 92, 210].

The effective potential at the zero temperature in the naHEFT is defined by [179]

$$V_{\rm naHEFT}(\varphi) = V_{\rm SM}(\varphi) + V_{\rm BSM}(\varphi), \tag{5.1.5}$$

with

$$V_{\rm BSM}(\varphi) = \frac{\kappa_0}{4}\xi\left[\mathcal{M}^2(\varphi)\right]^2 \ln\frac{\mathcal{M}^2(\varphi)}{\mu^2}, \tag{5.1.6}$$

where φ is defined by $\varphi = h + v$ with $v \simeq 246\,{\rm GeV}$. $V_{\rm SM}$ is the effective potential in the SM up to the one-loop level. The form of $V_{\rm BSM}$ is inspired by results in extended Higgs models with the non-decoupling effects in the Higgs potential. In such models, the non-decoupling effects in the Higgs potential can be described by the Coleman-Weinberg potential [178]. The most important aspect of the Coleman-Weinberg potential is that it contains a logarithmic function. This property is taken into account in the naHEFT. The form factor $\mathcal{M}^2(\varphi)$ corresponds to the field dependent mass of BSM particles. For simplicity, we here assume that the form factor $\mathcal{M}^2(\varphi)$ can be parameterized by

$$\mathcal{M}^2(\varphi) = M^2 + \frac{\kappa_p}{2}\varphi^2, \tag{5.1.7}$$

where M^2 and κ_p are real parameters. Then, $V_{\rm BSM}$ has three free parameters,

$$\Lambda = \sqrt{M^2 + \frac{\kappa_p}{2}v^2}, \quad \kappa_0, \quad r = \frac{\frac{\kappa_p}{2}v^2}{\Lambda^2}. \tag{5.1.8}$$

The parameters Λ and κ_0 correspond to the mass and degree of freedom of BSM particles. The parameter r is called as "non-decouplingness". By changing the value of r, the naHEFT can describe not only the decoupling new physics but also the non-decoupling new physics. When the non-decouplingness r is changed in the region $0 \leq r \leq 1$, the form factor $\mathcal{M}^2(\varphi)$ is expressed by

$$\mathcal{M}^2(\varphi) \simeq \begin{cases} (1-r)\Lambda^2 & (r \simeq 0) \\ (\Lambda^2/v^2)\varphi^2 & (r \simeq 1) \end{cases}. \tag{5.1.9}$$

In the case with $r \simeq 0$, the form factor $\mathcal{M}^2(\varphi)$ does not dependn on the field φ. This situation corresponds to the decoupling case. Whereas, when $r \simeq 1$, the form factor $\mathcal{M}^2(\varphi)$ is proportional to φ^2. This case is just the non-decoupling case.

In our analysis, we impose the following renormalization conditions

$$\left.\frac{dV_{\rm naHEFT}}{d\varphi}\right|_{\varphi=v} = 0, \tag{5.1.10}$$

$$\left.\frac{d^2V_{\rm naHEFT}}{d\varphi^2}\right|_{\varphi=v} = m_h^2, \tag{5.1.11}$$

where $m_h \simeq 125\,{\rm GeV}$. By using these renormalization conditions, we can determine the parameter μ in Eq. (5.1.6). As a result, the effective potential $V_{\rm naHEFT}$ can be expressed by Λ, κ_0, r, m_h and v.

When we consider the decoupling case ($r \simeq 0$), new physics effects should be decoupled. It means that the naHEFT has the same structure as the SMEFT in the decoupling case. We here confirm the relation between the naHEFT and the SMEFT. When $M^2 \neq 0$ (corresponding to $r \neq 1$), $\ln \mathcal{M}^2(\Phi)/\mu^2$ in Eq. (5.1.6) can be decomposed as

$$\ln \frac{\mathcal{M}^2(\Phi)}{\mu^2} \;=\; \ln \frac{M^2}{\mu^2} + \ln\left(1 + x_\Phi\right), \tag{5.1.12}$$

where

$$x_\Phi \;=\; \frac{r}{1-r}\frac{|\Phi|^2}{\frac{v^2}{2}}. \tag{5.1.13}$$

We note that $x_\Phi \ll 1$ when $r \simeq 0$ and $|\Phi| \lesssim v$. If $x_\Phi \ll 1$, we can expand $\ln(1+x_\Phi)$ as

$$\ln\left(1 + x_\Phi\right) \;=\; x_\Phi - \frac{x_\Phi^2}{2} + \frac{x_\Phi^3}{3} + \mathcal{O}(x_\Phi^4). \tag{5.1.14}$$

Substituting the right-handed side of Eq. (5.1.14) into the original effective potential given in Eq. (5.1.6), we can obtain higher dimensional operators in the effective potential.

If we truncate $\ln(1+x_\Phi)$ up to $\mathcal{O}(x_\Phi)$, $V_{\rm BSM}$ given in Eq. (5.1.6) can be expressed by the SMEFT form with a mass dimension six operator. By imposing the conditions Eqs. (5.1.10) and (5.1.11), the new physics contribution $V_{\rm BSM}$ is expressed as

$$V_{\rm BSM}(\Phi) \;=\; \frac{1}{f^2}\left(|\Phi|^2 - \frac{v^2}{2}\right)^3, \tag{5.1.15}$$

where the scale f is given as

$$\frac{1}{f^2} = \frac{2}{3}\xi\,\kappa_0\,\frac{\Lambda^4}{v^6}\frac{r^3}{1-r}\,. \tag{5.1.16}$$

The decoupling limit corresponds to $r \to 0$, which leads to $f \to \infty$.

Whereas, if we truncate $\ln(1+x_\Phi)$ up to $\mathcal{O}(x_\Phi^2)$, our effective potential is expressed as the SMEFT form up to mass dimension eight operators. By using Eqs. (5.1.10) and (5.1.11) again, we obtain

$$V_{\rm BSM}(\Phi) = \frac{1}{f_6^2}\left(|\Phi|^2 - \frac{v^2}{2}\right)^3 - \frac{1}{f_8^4}\left(|\Phi|^2 - \frac{v^2}{2}\right)^4, \tag{5.1.17}$$

where f_6 and f_8 are given as

$$\frac{1}{f_6^2} = \frac{1}{f^2}\frac{1-2r}{1-r}\,, \tag{5.1.18}$$

$$\frac{1}{f_8^4} = \frac{1}{2f^2v^2}\frac{r}{1-r}\,. \tag{5.1.19}$$

The decoupling limit corresponds to $r \to 0$, which leads to $f_{6,8} \to \infty$.

In the same way, we can obtain the SMEFT form up to mass dimension ten operators by truncating $\ln(1+x_\Phi)$ up to $\mathcal{O}(x_\Phi^3)$. We find

$$V_{\rm BSM}(\Phi) = \frac{1}{F_6^2}\left(|\Phi|^2 - \frac{v^2}{2}\right)^3 - \frac{1}{F_8^4}\left(|\Phi|^2 - \frac{v^2}{2}\right)^4 + \frac{1}{F_{10}^6}\left(|\Phi|^2 - \frac{v^2}{2}\right)^5, \tag{5.1.20}$$

where F_6, F_8, and F_{10} are given as

$$\frac{1}{F_6^2} = \frac{1}{f^2}\frac{3r^2-3r+1}{(1-r)^2}\,, \tag{5.1.21}$$

$$\frac{1}{F_8^4} = \frac{1}{2f^2v^2}\frac{r(1-3r)}{(1-r)^2}\,, \tag{5.1.22}$$

$$\frac{1}{F_{10}^6} = \frac{2}{5f^2v^4}\left(\frac{r}{1-r}\right)^2. \tag{5.1.23}$$

We note that the SMEFT approximations (5.1.15), (5.1.17), and (5.1.20) fail when the case with $|x_\Phi| \simeq 1$, which corresponds to the non-decoupling case.

The hhh coupling in the naHEFT can be expressed by

$$\lambda_{hhh}^{\rm naHEFT} \equiv \frac{3m_h^2}{v}\kappa_3, \tag{5.1.24}$$

where κ_3 is given by

$$\kappa_3 = 1 + \Delta\kappa_3, \tag{5.1.25}$$

$$\Delta\kappa_3 = \frac{4}{3}\xi\kappa_0\frac{\Lambda^4}{v^2m_h^2}r^3. \tag{5.1.26}$$

The deviation in the hhh coupling $\Delta\kappa_3$ comes from the new physics effect. We here only consider the new particle effect on the hhh coupling via the corrections of the effective potential. The hhh coupling can be deviated from the SM prediction by the corrections to the kinetic term of the Higgs field, which corresponds to the third term in Eq. (5.1.2). However, such effects are relatively smaller than the effects from the quantum corrections in the effective potential when we consider the non-decoupling situation [179]. In the following, we neglect the deviation in the hhh coupling from the corrections in the kinetic term of the Higgs field.

5.2 The nearly aligned Higgs EFT at finite temperatures

In order to discuss the EWPT in the naHEFT, we should extend the effective potential at the zero temperature Eq. (5.1.5) to that at finite temperatures. We here discuss the thermal corrections in the naHEFT.

New physics corrections in the effective potential in the naHEFT given in Eq. (5.1.6) can be expressed as

$$V_{\rm BSM}(\varphi) = \frac{\kappa_0}{2}\int \frac{d^4k_E}{(2\pi)^4}\ln\left[k_E^2+\mathcal{M}^2(\varphi)\right], \tag{5.2.1}$$

where k_E is the Euclidian momentum. We note that the ultraviolet part and the constant term are neglected because the two parts are irrelevant in the following discussion. The thermal corrections from new particles can be introduced by performing the following replacement [203, 211]

$$\int \frac{d^4k_E}{(2\pi)^4}\ln\left[k_E^2+\mathcal{M}^2(\varphi)\right] \to T\sum_{n=-\infty}^{\infty}\int\frac{d^3\vec{k}}{(2\pi)^4}\ln\left[\vec{k}^{\,2}+w_n^2+\mathcal{M}^2(\varphi)\right], \tag{5.2.2}$$

where T is the temperature, and w_n is Matsubara frequency for integrated new particle which is given by

$$w_n = \begin{cases} 2n\pi T & (\kappa_0>0) \\ (2n+1)\pi T & (\kappa_0<0) \end{cases}. \tag{5.2.3}$$

Hence, the thermal corrections from new particles is expressed by

$$V_{\rm BSM}(\varphi,T) = \frac{\kappa_0}{2}T\sum_{n=-\infty}^{\infty}\int\frac{d^3\vec{k}}{(2\pi)^4}\ln\left[\vec{k}^{\,2}+w_n^2+\mathcal{M}^2(\varphi)\right]. \tag{5.2.4}$$

Then, the effective potential at finite temperatures in the naHEFT is defined as [212]

$$V_{\rm naHEFT}(\varphi,T) = V_{\rm SM}(\varphi,T)+V_{\rm BSM}(\varphi)+\Delta V_{{\rm BSM},T}(\varphi,T), \tag{5.2.5}$$

where $V_{\rm SM}(\varphi,T)$ is the effective potential at finite temperatures in the SM. The thermal correction from BSM particles $\Delta V_{{\rm BSM},T}(\varphi,T)$ is given by

$$\Delta V_{{\rm BSM},T}(\varphi,T) = 8\xi T^4\kappa_0 J_{\rm BSM}\left(\frac{\mathcal{M}^2(\varphi)}{T^2}\right), \tag{5.2.6}$$

where

$$J_{\rm BSM}\left(\frac{\mathcal{M}^2(\varphi)}{T^2}\right) = \int_0^\infty dk k^2\ln\left[1-{\rm sign}(\kappa_0)e^{-\sqrt{k^2+\frac{\mathcal{M}^2(\varphi)}{T^2}}}\right], \tag{5.2.7}$$

with

$${\rm sign}\,(\kappa_0) = \begin{cases} 1 & (\kappa_0>0) \\ -1 & (\kappa_0<0) \end{cases}. \tag{5.2.8}$$

When we consider the case with $\kappa_0>0$, the infrared divergence appears in the thermal correction to the effective potential from the zero mode [203]. In order to avoid the infrared divergence,

we should consider the thermal mass correction to BSM particles. In our analysis, we utilize the prescription discussed by Parwani [204]. In this prescription, we should replace the form factor $\mathcal{M}^2$ as following,

$$\mathcal{M}^2(\varphi) \quad \to \quad \widehat{\mathcal{M}^2}(\varphi, T) = \mathcal{M}^2(\varphi) + \Pi_{\rm BSM}(T), \tag{5.2.9}$$

where $\Pi_{\rm BSM}(T)$ is the thermal correction to the mass of BSM particles. In order to determine $\Pi_{\rm BSM}(T)$ precisely, we should specify a model. In this thesis, we take

$$\Pi_{\rm BSM}(T) = \frac{c}{6}T^2\Theta(\kappa_0), \tag{5.2.10}$$

where

$$\Theta\left(\kappa_0\right) = \begin{cases} 1 & (\kappa_0 > 0) \\ 0 & (\kappa_0 < 0) \end{cases} . \tag{5.2.11}$$

Since the zero mode does not exist in thermal corrections by fermions, we take $\Pi_{\rm BSM}(T) = 0$ when κ_0 is negative. Since the constant c is a free parameter, we take $c = \kappa_p$. This choice is based on an analogy with the $O(N)$ scalar singlet model. The detailed discussion is given in Appendix A.

We note that thermal corrections from BSM particles in the decoupling case is suppressed. In the case with $\kappa_0 > 0$ and $r \simeq 0$, $J_{\rm BSM}$ has the Boltzmann suppression as

$$J_{\rm BSM}\left(\frac{\mathcal{M}^2(\varphi)}{T^2}\right)\Big|_{r\simeq 0} \propto \exp\left[-\frac{\mathcal{M}^2(\varphi)}{T^2}\right] \simeq \exp\left[-\frac{\Lambda^2}{T^2}\right]. \tag{5.2.12}$$

This fact means that thermal corrections from bosonic BSM particles with $r \simeq 0$ have the Boltzmann suppression. As a result, sizable thermal corrections from BSM particles cannot be realized within the framework of the SMEFT in a self-consistent method. In the non-decoupling case ($r \simeq 1$), the form factor $\mathcal{M}^2(\varphi)$ can be zero around the origin $\varphi \simeq 0$ as shown in Eq. (5.1.9). Thus, the Boltzmann suppression does not appear in $J_{\rm BSM}$ around the origin $\varphi \simeq 0$. Therefore, thermal corrections from BSM particles can be significantly large in the non-decoupling case. In this case, the coefficient of the cubic term φ^3 in the effective potential can be enhanced by $\Delta V_{{\rm BSM},T}$. Actually, by using the high temperature expansion, we can obtain

$$\Delta V_{{\rm BSM},T}(\varphi, T)|_{\kappa_0>0,\, r\simeq 1} \ni -E_{\rm BSM}T\varphi^3, \tag{5.2.13}$$

where

$$E_{\rm BSM} = \frac{4\pi}{3}\xi\kappa_0\frac{\Lambda^3}{v^3}. \tag{5.2.14}$$

This result implies that the naHEFT can appropriately describe the strongly first-order EW phase transition in models with the non-decoupling effects.

By combining Eqs. (5.1.26) and (5.2.14) with the condition $r \simeq 1$, we can obtain

$$E_{\rm BSM} \propto (\Delta\kappa_3)^{3/4}. \tag{5.2.15}$$

This relation indicates that the large deviation in the hhh coupling is important to realize the strongly first-order EWPT. The relation between the deviation in the hhh coupling and the strongly first-order EWPT has been discussed in the literatures [50, 89].

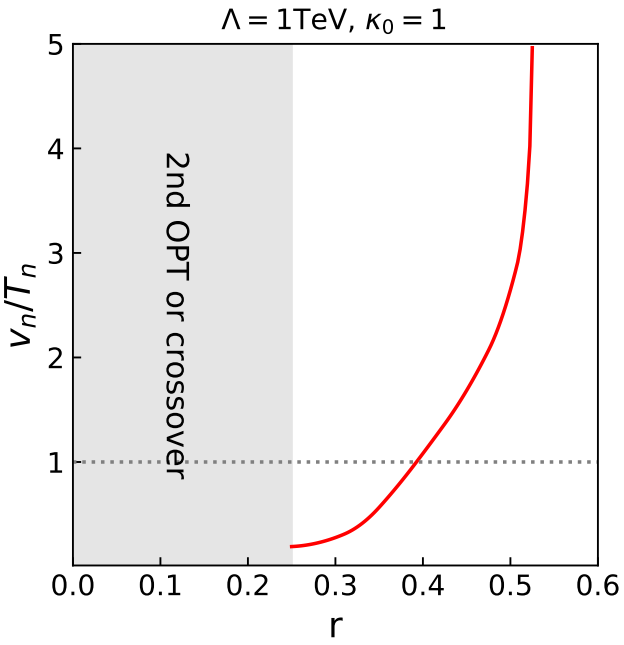

Figure 5.1: The relation between the strength of the phase transition v_n/T_n and the non-decouplingness r in the naHEFT. We take $\Lambda = 1\,\text{TeV}$ and $\kappa_0 = 1$.

5.3 EW phase transition in the naHEFT

We here investigate the parameter region where the strongly first-order EWPT can be realized within the framework of the naHEFT. In this thesis, we focus on the case with $\kappa_0 > 0$ because we can obtain the large coefficient of φ^3 term, which plays an important role to realize the strongly first-order EWPT. In addition, we consider the parameter region $0 \leq r \leq 1$. We use the public package *CosmoTransitions* to calculate the nucleation rate for the vacuum bubbles [193].

In Fig. 5.1, the relation between v_n/T_n and the non-decouplingness r is shown. We here take $\Lambda = 1\,\text{TeV}$ and $\kappa_0 = 1$ as an example. As explained, the strongly first-order EWPT can be realized when $v_n/T_n \geq \zeta_{\text{sph}}(T_n)$. We here take $\zeta_{\text{sph}}(T_n) = 1$ for simplicity. As we expected, the strongly first-order EWPT can be realized when the value of r is relatively large. For instance, the strongly first-order EWPT is realized if the non-decouplingness r is larger than 0.39 in the case with $\Lambda = 1\,\text{TeV}$ and $\kappa_0 = 1$. Even if the mass of BSM particles is at the TeV scale, T_n and v_n are at the electroweak scale, not the TeV scale. In the case with $r = 0.39$, the values of T_n and v_n are 126 GeV and 133 GeV, respectively. We note that v_n/T_n rapidly blows up when the value of r is relatively large as the temperature for starting the EWPT gets close to zero. The gray region in Fig. 5.1 corresponds to the region in which the first-order EWPT cannot be realized. We find that the non-decouplingness r should be larger than $\simeq 0.25$ to realize the first-order EWPT when $\Lambda = 1\,\text{TeV}$ and $\kappa_0 = 1$.

In Fig. 5.2, the parameter region for the strongly first-order EWPT is shown. We here take $\kappa_0 = 1$ and $\kappa_0 = 4$. In the white region, the strongly first-order EWPT can be realized. The blue region is constrained by the vacuum stability bound. We have confirmed that our results in the naHEFT are consistent with results in renormalizable extended Higgs models [68, 69]. The contours of $\kappa_p = 4\pi$ and 8π are also shown. If we consider the SM with additional singlet scalar fields as the UV theory [68, 69], the perturbative unitarity bound is given by $\kappa_p < 8\pi/\sqrt{\kappa_0}$ with

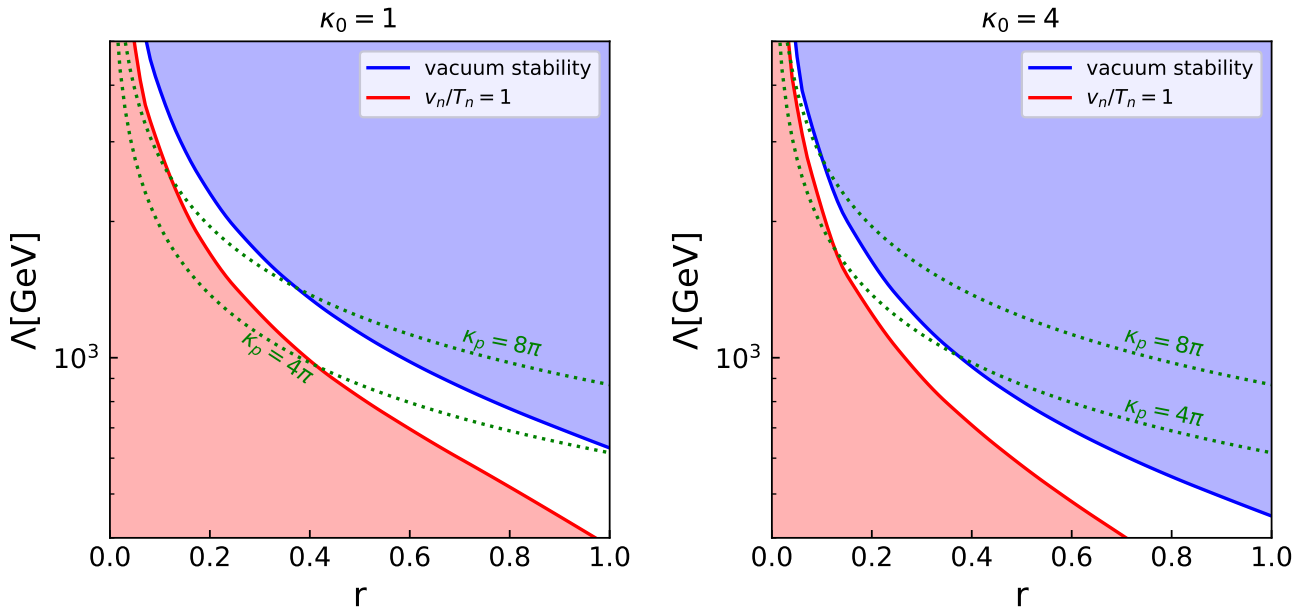

Figure 5.2: Parameter region where the strongly first-order EW phase transition can be realized. The left (right) figure corresponds to the case with $\kappa_0 = 1$ ($\kappa_0 = 4$). In the red region, the strongly first-order EW phase transition cannot be realized. The vacuum stability cannot be satisfied in the blue region. The contours of $\kappa_p = 4\pi$ and 8π are also shown.

$O(1)$ ambiguities coming from the prescription of the unitarity bound. By combining the unitarity bound and the sphaleron decoupling condition $v_n/T_n > 1$, we can obtain the upper bound on the value of Λ. In the case with $\kappa_0 = 4$, the upper bound is about 2 TeV. This fact is well consistent with the results in the THDMs discussed in the previous chapter.

5.4 Validity of finite number truncation of higher dimensional operators

We here discuss the validity of the prescription with the finite number truncation of higher dimensional operators. As we have shown, the approximation with the finite number truncation of higher dimensional operators does not work well when $|x_\Phi| \sim 1$ which corresponds to the non-decoupling case in general. We estimate the validity of the finite number truncation in the parameter space where the strongly first-order EWPT can be realized.

In Fig. 5.3, we compare the prediction on v_n/T_n in our EFT with the results estimated by the effective potential truncated up to dimension six (5.1.15), dimension eight (5.1.17) and dimension ten (5.1.20). In order to compare our EFT analysis with the SMEFT analysis equally, we neglect the finite temperature corrections from new physics in this analysis. The red, blue, blue dashed, and blue dotted lines correspond to the results in our EFT, the EFT truncated up to mass dimension six, eight and ten, respectively. If we consider the dimension six effective potential (5.1.15), we find that $v_n/T_n > 1$ requires $r \gtrsim 0.35$ when $\Lambda = 1\,\text{TeV}$ and $\kappa_0 = 1$. This requirement corresponds to $f \lesssim 890\,\text{GeV}$, which is consistent with the results in the literatures [76, 89–92, 176].

However, we note that the dimension six approximation seems to fail because of the large discrepancy in the prediction of v_n/T_n between our EFT and the the dimension six approximation.

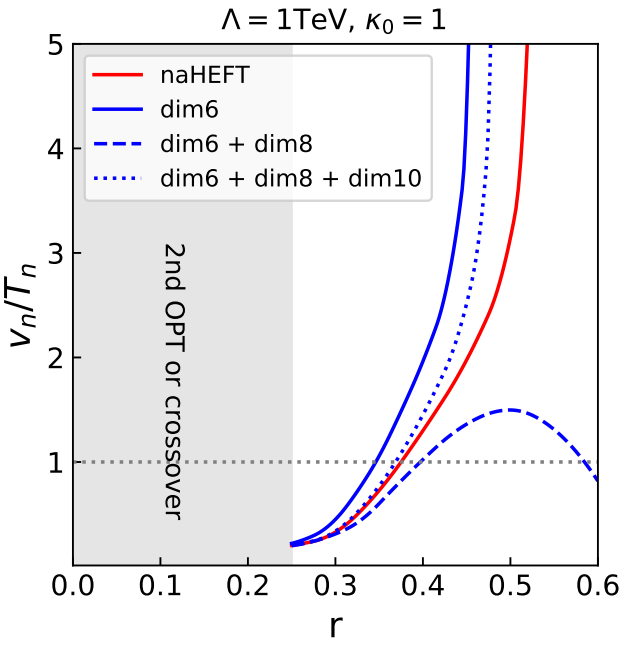

Figure 5.3: Predictions on v_n/T_n estimated by our EFT without finite temperature corrections from new physics (red), the effective potential approximated up to the dimension six (blue), eight (dashed blue), and ten (dotted blue) operators. We here take $\Lambda = 1\,\text{TeV}$ and $\kappa_0 = 1$ as an example.

In the case with $r = 0.35$, $\Lambda = 1\,\text{TeV}$ and $\kappa_0 = 1$, the discrepancy is about 44%. In order to improve the discrepancy, we need to include higher mass dimension operators consisted of up to mass dimension six operators. For instance, when we consider the region $0.25 \lesssim r \lesssim 0.5$, we can improve the EFT prediction on v_n/T_n by adding higher mass dimension operators appropriately. The importance of higher dimensional operators for studying the strongly first-order EWPT has been also emphasized in Refs. [80, 84, 92, 213, 214]. However, the improvement with finite number of the higher dimensional operators does not work when $r \gtrsim 0.5$ because the Taylor expansion (5.1.14) is ill-defined due to the large x_Φ. Therefore, in order to discuss new physics with $r \gtrsim 0.5$, we have to use our EFT formalism instead of the EFT formalism with the finite truncation of higher dimensional operators.

5.5 Predictions on gravitational waves from the strongly first-order EWPT

We next estimate the GW spectrum from the strongly first-order EWPT, which is one of the important signatures in our scenario. The GW spectrum from the strongly first-order EWPT can be characterized by two parameters, α and β/H. The parameters α and β/H are defined in Eqs. (3.4.19) and (3.4.21).

In Fig. 5.4, we show the prediction on values of α and β/H with different values of Λ and κ_0. The green, blue, and red lines correspond to the cases with $\kappa_0 = 1, 4$, and 20, respectively. The numbers in these figures are the values of Λ. We here set $r = 1$ and 0.5 in the left and right figures, respectively. The maximum value of Λ is determined by the completion condition of the phase transition given in Eq. (4.1.13). On the other hand, the minimum value of Λ is fixed by the

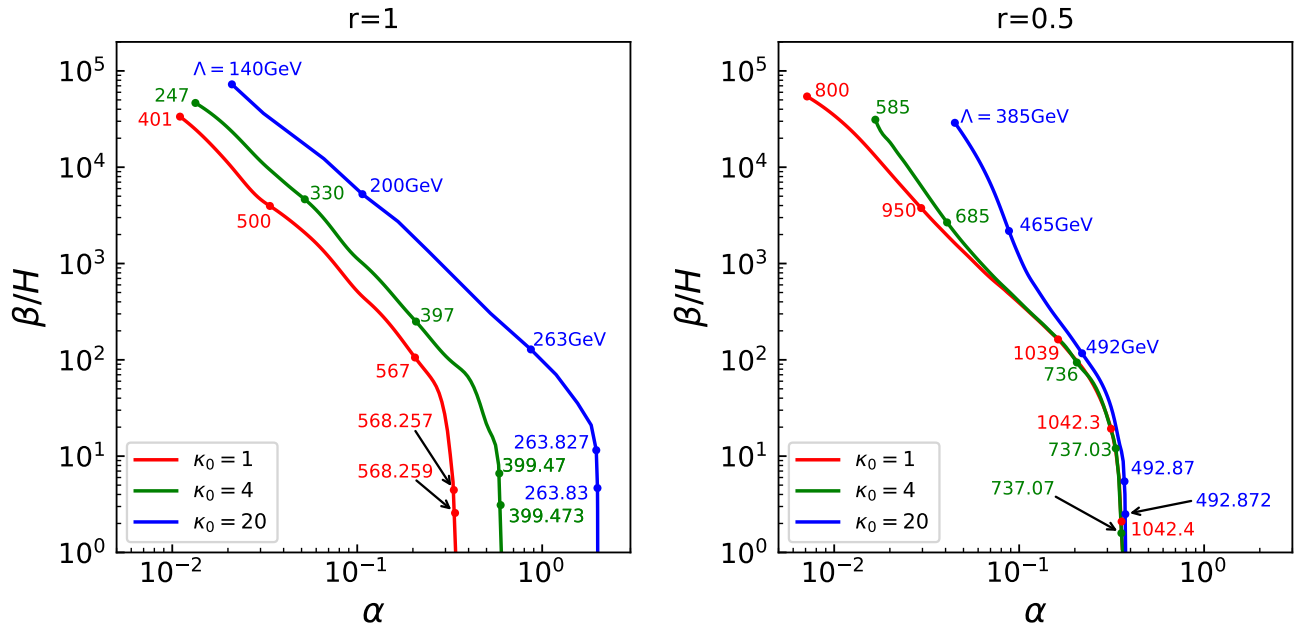

Figure 5.4: α and β/H in our EFT. We take $r = 1$ and 0.5 in the left and right figures, respectively. The red, green and blue lines correspond to $\kappa_0 = 1, 4$, and 20 cases. The numbers in these figures are the value of Λ.

sphaleron decoupling condition $v_n/T_n > 1$ or $\Lambda \geq v$. We find that the large Λ predicts the large α and small β/H. This is because, in the case with sizable r (corresponding to the non-decoupling case), the large Λ induces the large v_n/T_n.

We show the GW spectra for some benchmark scenarios in Fig. 5.5. The colored lines are the predicted GW spectra, while the black lines are the sensitivity curves of the LISA [74], DECIGO [75], TianQin [209], Taiji [208] and BBO [207][1]. In the top-left figure, we show the r-dependence in the GW spectra. Here we take $\Lambda = 1\,\text{TeV}$ and $\kappa_0 = 1$. The red, blue, green, and purple lines correspond to the results for $r = 0.525$, 0.52, 0.48, and 0.44, respectively. We find that the large r makes the amplitude and the peak frequency larger and lower. This is because the large r makes the first-order phase transition stronger, and results in the large α and small β/H. We also show the dependences of Λ and κ_0 on the GW spectra in the top-right and the bottom figures, respectively. We find that the large Λ and κ_0 also make the height and the peak frequency of the GW spectrum higher and lower. This is due to the same reason as the large r case.

5.6 Discussions and conclusions

Finally, we discuss the predictions of our scenario by combining all results we have obtained so far. The final result is summarized in Fig. 5.6, in which we add the information of future GW observations and the deviation in the hhh coupling to Fig. 5.2. The green and purple regions correspond to the parameter regions where the predicted GW spectrum is above the sensitivity curves of LISA and DECIGO shown in Fig. 5.5. We also show the deviation in the hhh coupling ($\Delta\kappa_3 = \kappa_3 - 1$) by the black lines, which correspond to $\Delta\kappa_3 = 0.2, 0.5$ and 1. In addition to the GW

[1]Performing the detailed analysis of the sensitivity, one can find the factor improved effective sensitivity comparing than ones shown in Fig. 5.5 [82].

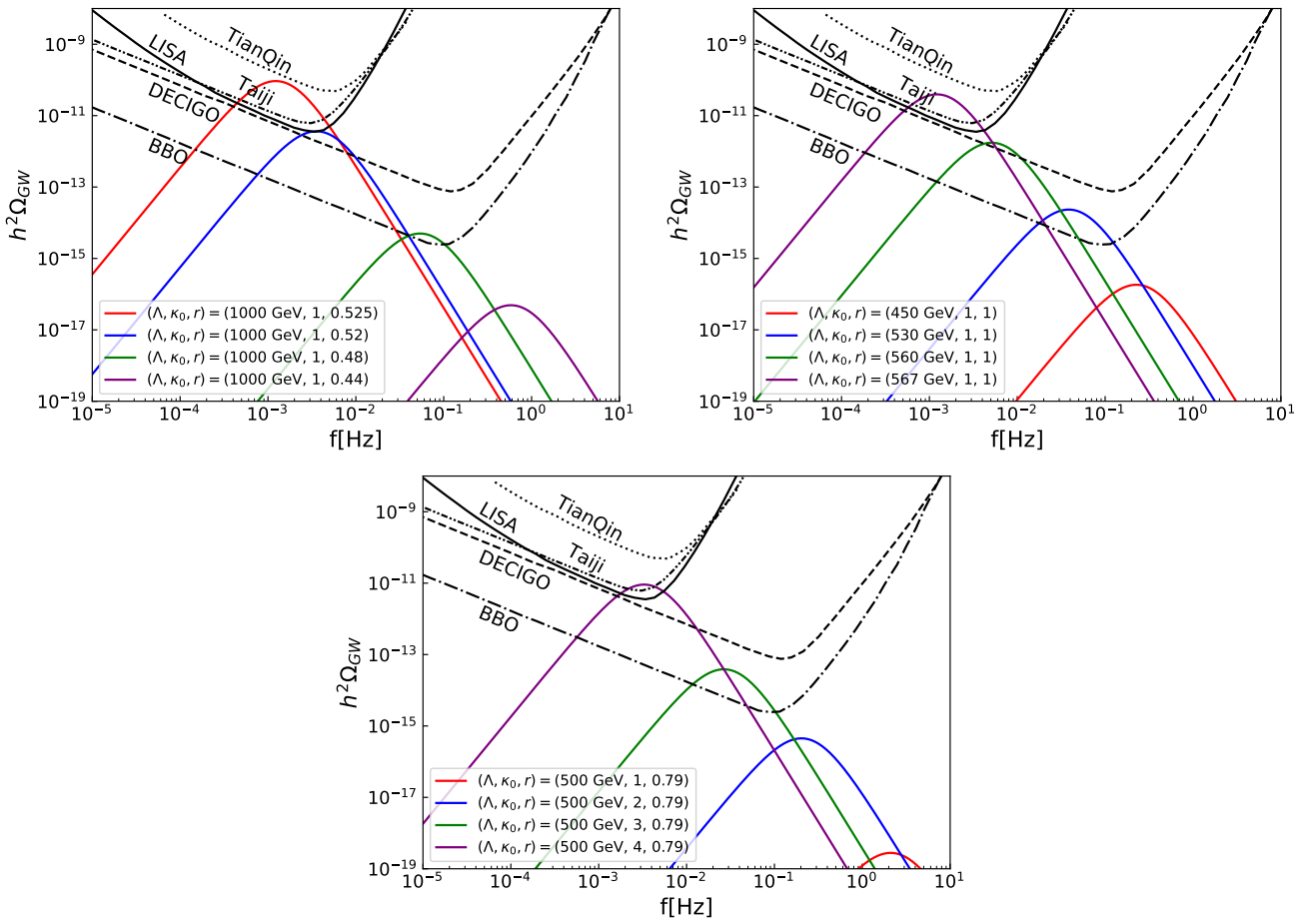

Figure 5.5: The GW spectra for some benchmark values.

observations, the hhh coupling measurements at future colliders are also important to investigate the parameter region with the strongly first-order EWPT. As we can see, the parameter region with strongly first-order EWPT predicts $\mathcal{O}(10\,\%) \sim \mathcal{O}(100\,\%)$ deviation in the hhh coupling from the SM prediction. Such large deviation is expected to be tested by future collider experiments. For example, the HL-LHC can reach 50% accuracy [70], and the lepton colliders such as the ILC with $\sqrt{s} \simeq 1\,\text{TeV}$ is expected to achieve a precision of some tens of percent [71]. Therefore, we can expect that the strongly first-order EWPT can be tested by the ILC and HL-LHC.

In summary, we find that the scenarios in which the strongly first-order EWPT can be realized by the non-decoupling quantum effects can be widely tested by the future GW interferometers and the precise measurement of the hhh coupling at future colliders. This fact has been pointed out in many concrete renormalizable model studies so far (See Refs. [68, 69] for example). Our EFT analyses are consistent with the results obtained in these model-dependent studies.

5.7 Summary

We have provided an effective field theoretical framework for the strongly first-order EWPT. We have employed an extension of the Higgs EFT in which the Higgs potential is parameterized by a Coleman-Weinberg like form. Our EFT can describes a class of new physics models in which i) the mixing between new scalar particles and the SM Higgs boson is much suppressed (alignment

limit) and ii) the sizable non-decoupling quantum effect appears. We have formulated the finite temperature corrections to the effective potential in the EFT, and studied the EWPT by using the EFT framework.

We have found that the non-decoupling effect plays an essential role in realizing the strongly first-order EWPT. This fact is consistent with the results discussed in many concrete models studies. The importance of the non-decoupling effect means that the conventional EFT description with the finite number truncation of the higher-dimensional operators is not appropriate for the study on the strongly first-order EWPT. Comparing our EFT results with the those estimated by the effective potential with finite number truncation of higher dimensional operators, we have numerically shown that the approximation of the finite number truncation does not work well in the parameter region with the strongly first-order EWPT.

Applying our EFT formalism, we have estimated the spectra of the stochastic GWs produced by the strongly first-order EWPT. We have found that the non-decoupling effect results in the GW spectrum which can be detected at future GW interferometers like LISA and DECIGO. We also emphasized that the deviation in the hhh coupling is also an important signature of our scenario. We have shown that $\mathcal{O}(10\,\%) \sim \mathcal{O}(100\,\%)$ deviation of the hhh coupling is predicted in the parameter space where the strongly first-order EWPT is realized. This result means that the future hhh coupling measurements and the GW observations are important probes for scenarios with the strongly first-order EWPT. Our results can be generally applied to the class of new physics models in which the strongly first-order EWPT is realized by non-decoupling quantum effects.

We finally emphasize the importance of the study on non-decoupling physics. The non-decoupling effects are essential origin of the strongly first-order EWPT, and provide us rich phenomenology such as the large deviation in the hhh coupling. Therefore, it is important to study these non-decoupling new physics in a complemental way. Our EFT description is a promising candidate of the simplest and most systematic descriptions for this EFT approach. In the next chapter, we discuss the further phenomenological analysis based on the naHEFT.

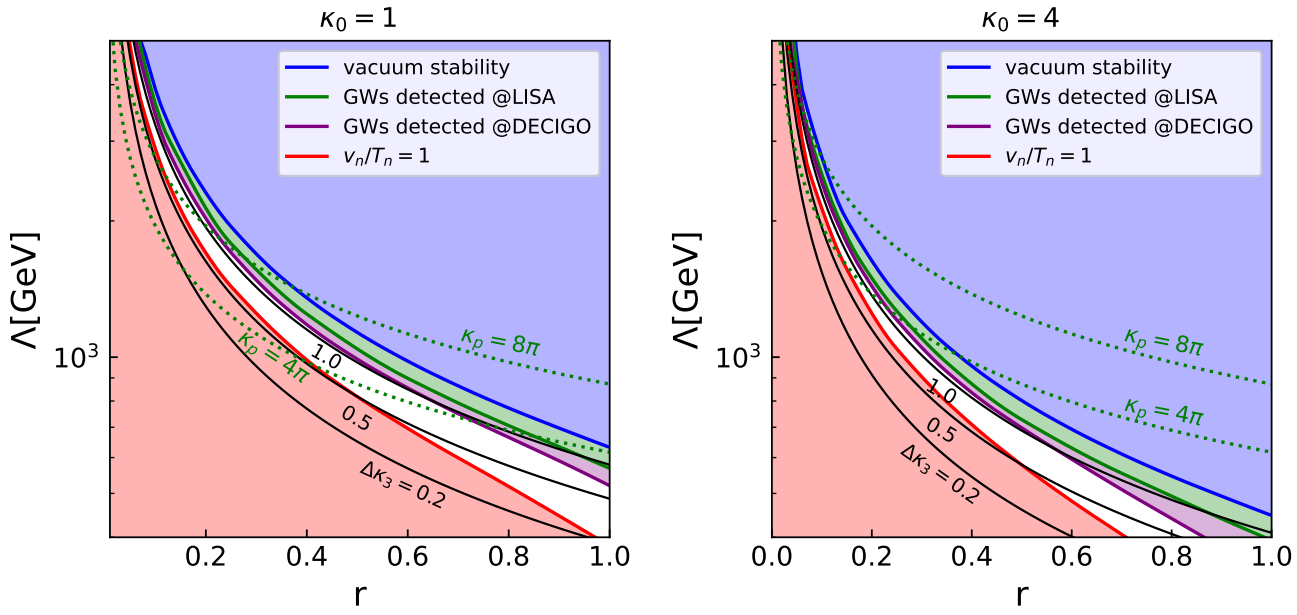

Figure 5.6: Parameter space in which the GW will be detected at LISA (green) and DECIGO (purple). The color notation of the red and blue regions are same with Fig. 5.2. We take $\kappa_0 = 1$ and 4 in the left and right figure, respectively. The black lines are contours of $\Delta\kappa_3 = \kappa_3 - 1 = 0.2$, 0.5 and 1.

Chapter 6

Primordial black holes and the first-order phase transition

In this section, we discuss a new possibility to test the strongly first-order EWPT. The possibility is the measurement of primordial black holes (PBHs). PBHs may be produced at the early Universe before the star formation [111–113]. In order to realize the PBH formation mechanism, a sufficiently large energy density fluctuation is required. The first-order phase transition at the early Universe may realize the large density fluctuation. The first-order phase transition proceeds by the vacuum bubble nucleation. In general, the vacuum energy density in the vacuum bubbles is smaller than that in the outside the vacuum bubbles because of the difference of the vacuum energy density. Thus, the large energy density fluctuation may be produced as the first-order phase transition proceeds [114, 115].

6.1 Review of PBHs

If a large density fluctuation is realized at the early Universe, PBHs may be formed before the star formation [111–113]. It means that we may know what happened in the early Universe by using PBH observations.

We here give a brief review for PBHs. The following discussion is based on the literature [215]. In order to form a PBH by collapsing an overdensity region in the early Universe, the size of the overdensity region $R_{\rm over}$ should be larger than the Jeans scale R_J [113]. This requirement is so called the Jeans criterion. In order for the overdense region to avoid the separation from the rest of the Universe, it is necessary to satisfy $R_{\rm over} \lesssim R_{\rm PH}$, where $R_{\rm PH}$ is a particle Horizon. Therefore, the PBH formation requires

$$R_J \lesssim R_{\rm over} \lesssim R_{\rm PH}. \tag{6.1.1}$$

The particle Horizon and the Jeans scale is given by

$$R_{\rm PH} \simeq \frac{c}{\sqrt{8\pi G\rho_{\rm over}}}, \tag{6.1.2}$$

$$R_J \simeq \frac{wc}{\sqrt{8\pi G\rho_{\rm over}}} = wR_{\rm PH}, \tag{6.1.3}$$

where $\rho_{\rm over}$ is the energy density of the overdense region. The constant G is the Newton constant. We here assume that the equation of state is given by $p = w\rho c^2$. The condition (6.1.1) can be

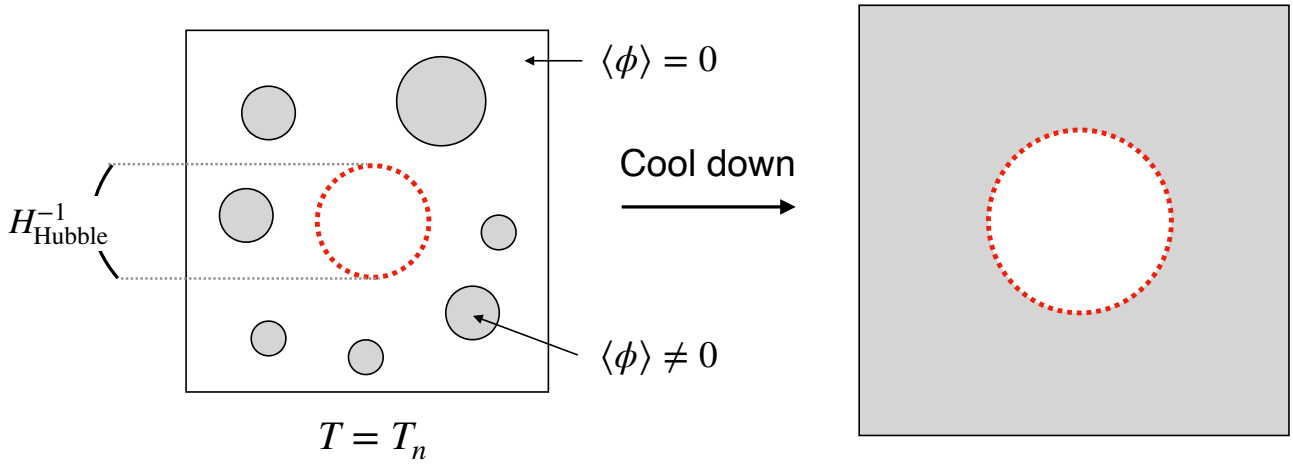

Figure 6.1: Conceptual figure for the origin of the large energy density fluctuation between the symmetric phase and the broken phase. In the gray region, the symmetry is broken. In the white region, the symmetry breaking does not occur.

expressed in terms of energy density fluctuations as [113]

$$w \simeq \delta_c \lesssim \delta \lesssim \delta_{\rm max} \simeq 1, \tag{6.1.4}$$

where δ_c and $\delta_{\rm max}$ are the threshold value and the maximum value to realize the PBH formation. The energy density fluctuation δ is defined by

$$\delta \equiv \frac{\rho_{\rm over} - \rho_{\rm back}}{\rho_{\rm back}}, \tag{6.1.5}$$

where $\rho_{\rm over}$ and $\rho_{\rm back}$ are the density in the overdensity region and the average energy density in the Universe, respectively. The condition for the PBH formation (6.1.4) is called as Carr's condition [113]. If we consider the PBH formation at the radiation dominant Universe ($w = 1/3$), the following condition should be satisfied

$$\delta > \delta_c = \frac{1}{3}. \tag{6.1.6}$$

The result given in Eq. (6.1.6) is based on the simple analytical calculation. More precise analytical calculations are discussed by Harada et al. [215]. The numerical evaluation of the threshold for δ is analyzed in Refs. [216–218]. In this thesis, we use the following condition as the criteria for the PBH formation

$$\delta > 0.45. \tag{6.1.7}$$

If this condition is satisfied, the overdensity region can collapse into PBHs.

6.2 PBH formation by the first-order phase transition

There are several ways to produce PBHs as a remnant of the first-order phase transition [219]. In this thesis, we focus on the the PBH formation mechanism discussed by Liu et al. [120]. According

to Ref. [120], the large density fluctuation can be generated by delaying the nucleation of vacuum bubbles. Since the bubble nucleation is probabilistic, there is a possibility that the symmetry breaking is delayed in a whole Hubble volume.

In Fig. 6.1, the delay of the first-order phase transition is shown. In the gray region, the symmetry is already broken. On the other hand, in the white region, the symmetry is not broken. Each patch corresponds to the Hubble volumes. In the red region, the first-order phase transition is not completed. If this situation is realized, the large energy density fluctuation can be realized between the outside and the inside of the red region. The vacuum energy density in the unbroken symmetry region is larger than that in the broken symmetry region because the difference of the vacuum energy density is related to the difference of the height of the Higgs potential. This energy density difference leads to the energy density fluctuation between the inside and outside of the Hubble volume (red region) in which the symmetry breaking is delayed. We here define the energy density fluctuation as

$$\delta \equiv \frac{\rho_{\rm in} - \rho_{\rm out}}{\rho_{\rm out}}, \tag{6.2.1}$$

where $\rho_{\rm in}$ and $\rho_{\rm out}$ is the total energy density inside and outside the Hubble volume, respectively. When the energy density fluctuation δ satisfy the condition given in Eq. (6.1.7), the inside of the Hubble volume can gravitationally collapse into a PBH. Therefore, the mass of PBHs is roughly determined by the Hubble horizon mass at the time when the PBHs are produced. For the first-order EWPT, the mass of PBHs is about $10^{-5}M_\odot$ ($M_\odot$ is the solar mass). Hence, the fraction of the PBHs $f_{\rm PBH}$ produced by the first-order EWPT can be probed by current and future microlensing observations such as Subaru HSC, OGLE, PRIME and Roman Space Telescope. The fraction $f_{\rm PBH}$ can be determined by the phase transition parameters α and β/H in Eqs. (3.4.19) and (3.4.21).

In order to realize the PBH production mechanism we focused on, the delay of the first-order phase transition is important. Thus, we should calculate the ratio of the symmetry unbroken region and the symmetry broken region. The fraction of the false vacuum in the whole Universe is given by [220]

$$F(t) = \exp\left[-\frac{4\pi}{3}\int_{t_i}^{t} dt'\Gamma(t')a^3(t)r^3(t,t')\right], \tag{6.2.2}$$

where t_i is the time when a first vacuum bubble is produced in the Universe, $a(t)$ is the scale factor, and $r(t,t')$ is the comoving radius of the true vacuum from t' to t. The comoving radius $r(t,t')$ is defined by [79]

$$r(t,t') \equiv r_0(t') + \int_{t'}^{t} \frac{v_w}{a(\tilde{t})} d\tilde{t}, \tag{6.2.3}$$

where $r_0(t')$ is the initial radius of the vacuum bubbles. If the first-order phase transition is supercooling, the phase transition is completed by the vacuum bubble expansion instead of the bubble nucleation. For example, for the first-order EWPT in the SM with $m_h = 60\,\text{GeV}$ and $m_t = 120\,\text{GeV}$, 10% of space in the Universe is converted into the broken phase by the vacuum bubble nucleation. The other region is also converted into the broken phase by the vacuum bubble expansion [221]. Therefore, the initial radius $r_0(t')$ can be negligible when we consider the supercooled first-order phase transition. In our analysis, we neglect the contribution from $r_0(t')$. In addition, we assume that the velocity of vacuum bubbles v_w is closed to the light speed ($v_w \simeq 1$).

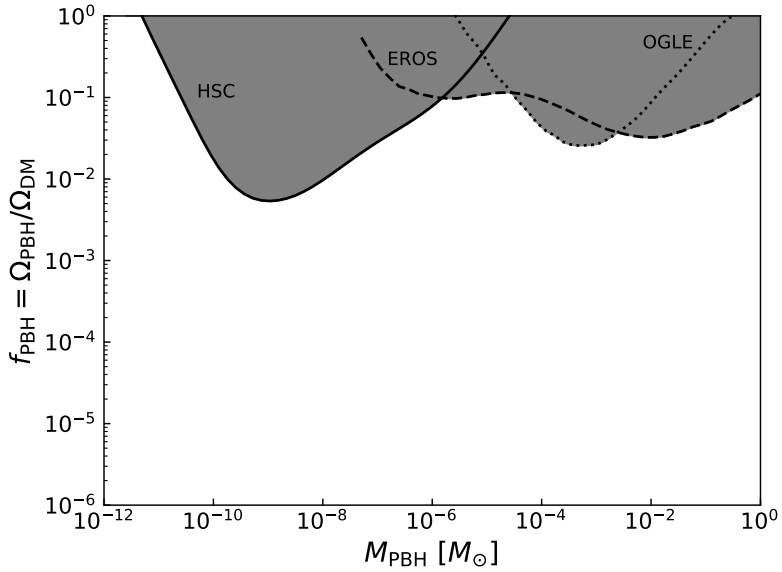

Figure 6.2: Current constraints on the fraction $f_{\rm PBH}$ by microlensing observations. The constraints from Subaru HSC [223], OGLE [224] and EROS [225] are shown.

Then, the energy density for the vacuum bubbles ρ_w can be regarded as part of the radiation energy density. Thus, the total radiation energy density ρ_R is given by

$$\rho_R = \rho_{\rm rad} + \rho_w. \tag{6.2.4}$$

The evolution of ρ_R is determined by

$$\frac{d\rho_R}{dt} + 4\rho_R H = -\frac{d\rho_V}{dt}, \tag{6.2.5}$$

where ρ_V is the vacuum energy density, which is given by

$$\rho_V = F(t)\Delta V_{\rm eff}. \tag{6.2.6}$$

The evolution of the Hubble parameter H is described by the Friedmann equation [222],

$$H^2 = \frac{\rho_R + \rho_V}{3}, \tag{6.2.7}$$

where we take the unit with $M_{p\ell} = 1$. Since the potential energy density difference $\Delta V_{\rm eff}$ is related to the parameter α, the energy densities of radiation and vacuum at the time t_i are given by

$$\rho_R(t_i) = \frac{1}{1+\alpha}\rho_{\rm tot}(t_i), \quad \rho_V(t_i) = \frac{\alpha}{1+\alpha}\rho_{\rm tot}(t_i), \tag{6.2.8}$$

where $\rho_{\rm tot}(t_i) = \rho_R(t_i) + \rho_V(t_i)$. These values are used as the initial conditions in solving Eqs. (6.2.5) and (6.2.7).

From Eqs. (6.2.2), (6.2.5) and (6.2.7), we can determine the time evolutions of $a(t)$, $\rho_R(t)$ and $\rho_V(t)$. Then, we can evaluate the probability that Hubble volumes collapse into PBHs. The probability is given by

$$P(t_n) = \exp\left[-\frac{4\pi}{3}\int_{t_i}^{t_n} \frac{a^3(t)}{a^3(t_{\rm PBH})}\frac{1}{H^3(t_{\rm PBH})}\Gamma(t)dt\right], \tag{6.2.9}$$

where $t_{\rm PBH}$ is the time when the PBHs are produced, which can be determined by the condition (6.1.7). If the condition (6.1.7) is satisfied, the symmetry unbroken Hubble volume (red region in Fig. 6.1) can collapse into a PBH. The mass of the PBHs $M_{\rm PBH}$ is roughly given by

$$M_{\rm PBH} \sim \frac{4\pi}{3} H^{-3}(t_{\rm PBH})\rho_{\rm tot}(t_{\rm PBH}) = 4\pi H^{-1}(t_{\rm PBH}). \tag{6.2.10}$$

Since the PBH production time $t_{\rm PBH}$ is related to a time when the first-order phase transition occurs, $M_{\rm PBH}$ is also related to the time.

If PBHs are produced by the first-order EWPT, the PBH mass is given by

$$M^{\rm EW}_{\rm PBH} \sim 10^{-5} M_\odot, \tag{6.2.11}$$

where $M_\odot$ is the solar mass. The fraction of the PBHs in dark matter density $f_{\rm PBH}$ can be observed by PBH observations. For the EWPT, the fraction $f^{\rm EW}_{\rm PBH}$ is given by

$$f^{\rm EW}_{\rm PBH} \equiv \frac{\Omega^{\rm EW}_{\rm PBH}}{\Omega_{\rm CDM}} \sim 1.49 \times 10^{11} \left(\frac{0.25}{\Omega_{\rm CDM}}\right) \left(\frac{T_{\rm PBH}}{100\,{\rm GeV}}\right) P(t_{\rm PBH}), \tag{6.2.12}$$

where $\Omega_{\rm CDM}$ is the current energy density of cold dark matter normalized by the total energy density, and $T_{\rm PBH}$ is temperature when the PBHs are produced.

In Fig. 6.2, the current constraint on the PBH fraction is shown. We note that the fraction around the mass region of $10^{-5} M_\odot$ is already constrained by current microlensing observations such as Subaru HSC and OGLE. It means that the first-order EWPT can be tested by using results at microlensing observations. For future microlensing experiments, such as Roman Space Telescope and PRIME, may be able to test the parameter region with $f_{\rm PBH} > 10^{-4}$ [226].

6.3 PBH formation via the first-order phase transition in the naHEFT

We here discuss the PBH formation in the naHEFT.

In Fig. 6.3, model independent results of the PBH fraction $f_{\rm PBH}$ are shown in the $(\alpha, \beta/H)$ plane. This result was first discussed in Ref. [87]. The brown, green, orange, blue and red solid lines correspond to the contours for $f_{\rm PBH} = 10^{-8}$, 10^{-6}, 10^{-4}, 10^{-2}, 1, respectively. We find that the PBH fraction $f_{\rm PBH}$ is sensitive to the value of β/H. According to Fig. 6.3, the large PBH fraction can be realized in the case with large α and β/H. It indicates that the strongly first-order EWPT is preferred to produce large amounts of PBHs. In the white region above the brown line, the PBH abundance becomes too small to detect future PBH observations or the PBHs cannot be produced from the first-order EWPT. In the white region below the red line, PBHs are overproduced ($f_{\rm PBH} > 1$). It means that we can discuss constraints on the Higgs sector by assuming the condition $f_{\rm PBH} \leq 1$. Current microlensing experiments, such as Subaru HSC and OGLE, can explore the parameter region between the red and blue lines with $10^{-2} < f_{\rm PBH} < 1$. The parameter region between the red and orange lines with $10^{-4} < f_{\rm PBH} < 1$ may be tested by future microlensing observations such as PRIME and Roman Space Telescope.

In Fig. 6.4, the parameters α and β/H are shown in the naHEFT. The non-decouplingness r is assumed as r =1 and 0.5 in the left and right panels, respectively. The red, green and blue lines correspond to the predictions on the parameters α and β/H in the case with $\kappa_0 = 1$, 4 and 20, respectively. Points on these lines in Fig. 6.4 represent the value of Λ. Purple dotted and solid

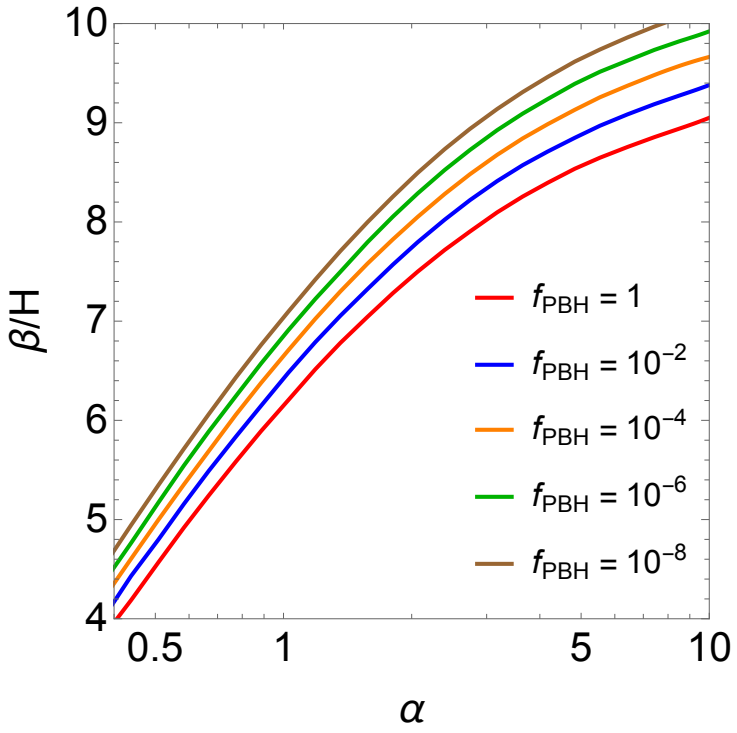

Figure 6.3: Contours for the PBH abundance are shown in the α and β/H plane. Red, blue, orange, green and brown lines correspond to the contours with $f_{\rm PBH} = 1, 10^{-2}, 10^{-4}, 10^{-6}$ and 10^{-8}, respectively. The region $10^{-4} < f_{\rm PBH} < 1$, between red and orange lines, can be explored by PBH observations, such as PRIME and Roman Space Telescope. In the white region above the brown line, the abundance of the PBH cannot be produced or otherwise is too small. In the white region below the red line, PBHs are overproduced ($f_{\rm PBH} > 1$). This result was first discussed in Ref. [87].

lines are the contours of $f_{\rm PBH} = 10^{-4}$ and 1, respectively. These purple lines are already shown in Fig. 6.3. According to Fig. 6.4, the PBH fraction is sensitive to the value of Λ in the naHEFT. As we expected, by using the overproduction condition $f_{\rm PBH} \leq 1$, we can obtain constraints on Λ in each κ_0. For instance, in the case with $\kappa_0 = 4$ and $r = 1$, we can obtain $\Lambda < 399.471\,\text{GeV}$ by using the condition $f_{\rm PBH} \leq 1$.

We here comment on the behaviors of the lines in right panel of Fig. 6.4, which are degenerate in the case with large Λ values. The behavior is ascribed to the Boltzmann suppression with respect to finite temperature effects: $\Delta V_{{\rm BSM},T}(0,T) \propto \exp\left[-\Lambda^2(1-r)/T^2\right]$. For small r and large Λ, the effective potential is mainly determined by the zero temperature BSM effects. Then, the difference between the origin ($\varphi = 0$) and the bottom ($\varphi = v$) of the effective potential, which is related to the phase transition parameters. The potential difference $\Delta V_{\rm eff}$ at the zero temperature is roughly given by

$$\Delta V_{\rm eff}(T=0) \simeq \frac{m_h^2 v^2}{8} - \frac{\xi}{4}\kappa_0 \Lambda^4 \left[(1-r)\ln(1-r) - \frac{r}{2}\right]. \tag{6.3.1}$$

In Fig. 6.5, the relation between the potential difference $\Delta V_{\rm eff}$ and the parameter α is shown in the naHEFT with $r = 0.5$. The red and green lines are the potential differences in the cases with $\kappa_0 = 1$ and $\kappa_0 = 4$, respectively. The value of the potential barrier is normalized by the vacuum

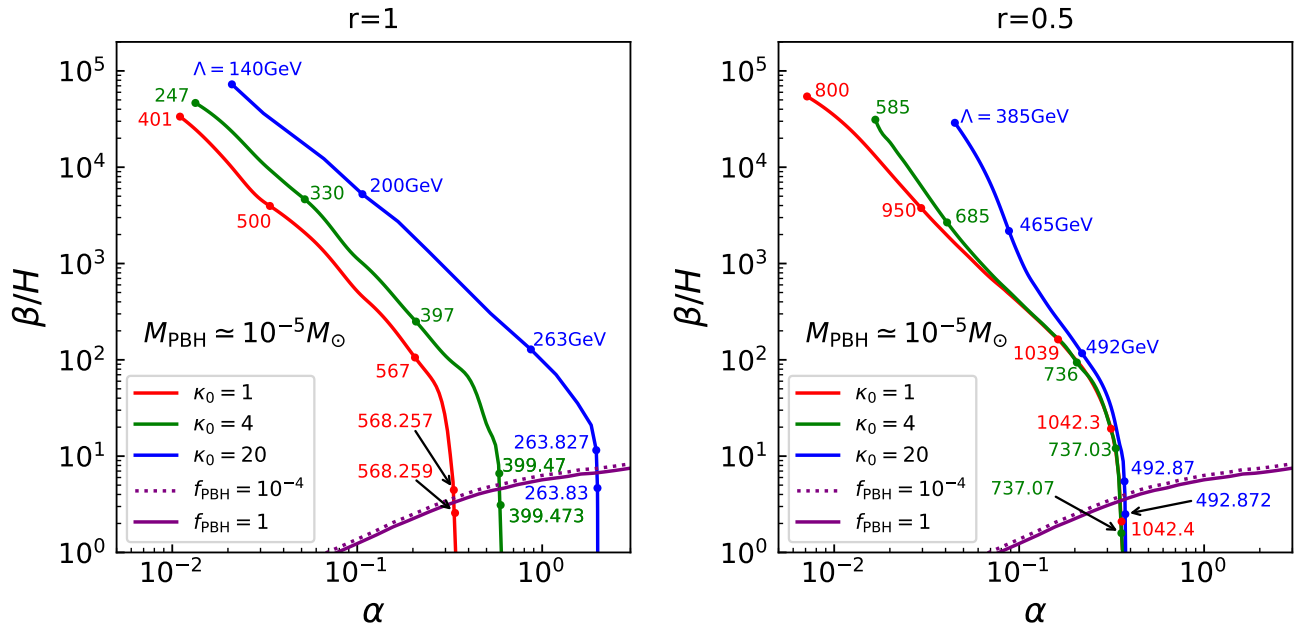

Figure 6.4: Parameters α and β/H with respect to κ_0, Λ and r. Left (right) figure represents α and β/H in the naHEFT with $r = 1$ (0.5). The red, green and blue lines are $\kappa_0 = 1$, 4 and 20, respectively. The points on these lines correspond to the Λ value. Purple dotted and solid lines respectively are $f_{\rm PBH} = 10^{-4}$ and 1.

expectation value. Each point indicates the values of Λ. This figure indicates that α is determined by the effective potential at the zero temperature as the value of Λ gets large in the decoupling case ($r \neq 1$). For instance, in the cases with (κ_0, Λ [GeV], r) = (1, 1039, 0.5), (4, 736, 0.5) and (20, 492, 0.5), the values of $\Delta V_{\rm eff}$ are almost the same. These three points are depicted in the right panel of Fig. 6.4. Actually, these points get close to each other.

In Fig. 6.6, predictions on masses of the PBHs are shown. We take $\kappa_0 = 5$ and $r = 1$ in Fig. 6.6. As we have confirmed in Fig. 6.4, the PBH fraction $f_{\rm PBH}$ is sensitive to the parameters in the naHEFT. Since $t_{\rm PBH}$ is almost the same, the PBH mass is hardly changed even if we take different values of Λ.

Why does the large PBH fraction favor the small β/H? In the following, we give a qualitative answer for the question. For simplicity, we use the high temperature expansion for the effective potential [227]

$$V_{\rm eff}(\phi, T) \simeq D(T^2 - T_0^2)\phi^2 - ET\phi^3 + \frac{\lambda_T}{4}\phi^4. \tag{6.3.2}$$

At the critical temperature, there is the potential barrier between the true vacuum and the false vacuum. We define the configuration at the maximum point of the barrier as ϕ_M. The configuration ϕ_M can be expressed by

$$\phi_M = \frac{ET_c}{\lambda_T} = \frac{\phi_c}{2}. \tag{6.3.3}$$

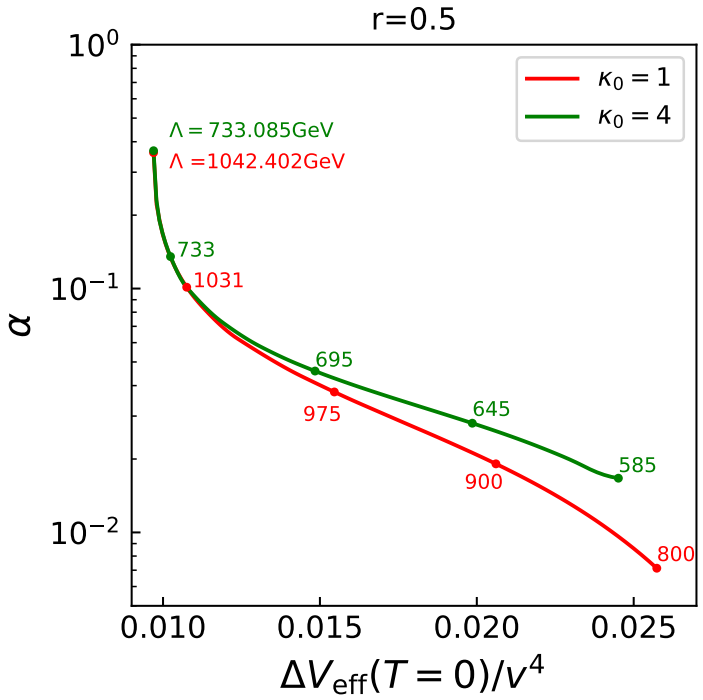

Figure 6.5: Relation between the parameter α and the potential difference at zero temperature. Each point corresponds to the value of Λ. The value of the potential barrier is normalized by the vacuum expectation value.

Then, the potential barrier between $\phi = 0$ and $\phi = \phi_M$ can be expressed by

$$\begin{aligned}\Delta V(\phi_M, T_c) &\equiv V(\phi = \phi_M, T_c) - V(\phi = 0, T_c) \\ &\simeq \frac{E}{32} T_0^4 \left(\frac{\lambda D}{\lambda D - E^2}\right)^2 \left(\frac{\phi_c}{T_c}\right)^3 . \end{aligned} \tag{6.3.4}$$

The above approximate equation indicates that the potential barrier $\Delta V(\phi_M, T_c)$ can be large when the strongly first-order EWPT can be realized ($\phi_c/T_c > 1$). In order to realize the PBH production via the mechanism we focused on, the first-order EWPT should be delayed. The delay of the first-order phase transition can be realized when the potential barrier is large because of the suppression of the tunneling rate. Therefore, the first-order EWPT can be delayed when the phase transition is strong. It means that the fraction $f_{\rm PBH}$ can be large when the strongly first-order EWPT occurs.

On the other hand, the relation between the parameter β/H and ϕ_c/T_c is given by [228]

$$\frac{\beta}{H} \simeq \frac{36 \cdot 2^{1/4}}{\pi^{1/2} \lambda_T^{3/4}} \left(D - \frac{E^2}{\lambda_T}\right) \left(\frac{S_3(T_c)}{T_c}\right)^{\frac{5}{2}} \left(\frac{\phi_c}{T_c}\right)^{-5/2} . \tag{6.3.5}$$

Thus, small β/H is favored to realize the strongly first-order EWPT. By combining Eq. (6.3.4) and Eq. (6.3.5), we can expect that the large $f_{\rm PBH}$ can be realized when the parameter β/H is small. This is the reason why the large PBH fraction requires small β/H.

Fig. 6.7 represents the region of strongly first-order EWPT in the naHEFT with $\kappa_0 = 1$, 4, 8 and 16 in the r-Λ plane. For example, assuming the $O(N)$ singlet scalar field theory as the UV

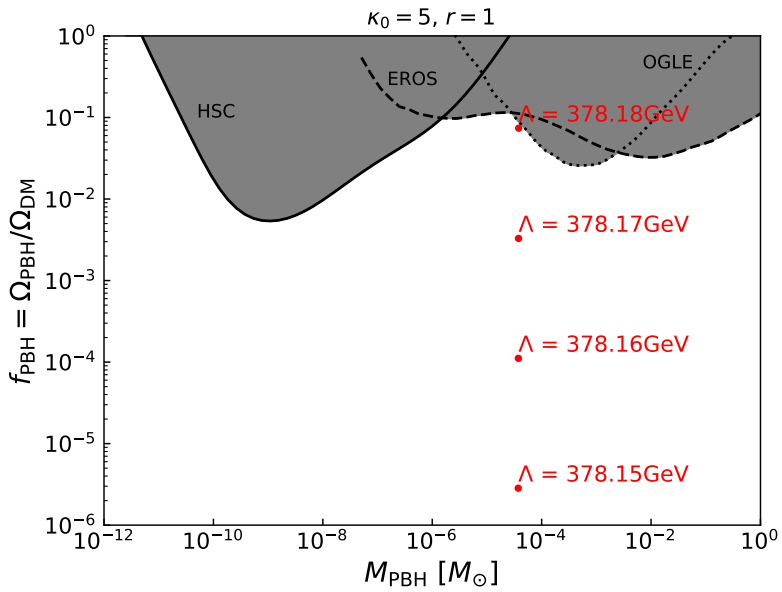

Figure 6.6: Predictions on the PBH mass in the naHEFT. We take $\kappa_0 = 5$ and $r = 1$. The constraints from Subaru HSC [223], OGLE [224] and EROS [225] are also shown.

theory, the parameter region with $r < 0.3$ is prohibited by the perturbative unitarity bound [69]. Thus, we do not take into account the parameter region with $r < 0.3$ in the following numerical analysis. The black dotted lines correspond to the contours of $\Delta\lambda_{hhh}/\lambda_{hhh}^{\rm SM} = 20$, 50, 100 and 200 % from the bottom, respectively. In the red region, the PBH fraction $f_{\rm PBH}$ can be larger than 10^{-4}. Therefore, the red region can be tested using PBH observations. In this region, we can also use GW observations to test the EWPT. In the blue (orange) parameter region, the first-order EWPT can be tested by using GW observations at both LISA and DECIGO (only at DECIGO). In the green region, although GWs cannot be detected at LISA nor DECIGO, the first-order EWPT can still be tested by the precise measurement of the hhh coupling at future collider experiments. In the top right white region above the red solid line of these panels, the EWPT has not been completed at the current Universe, in which $\Gamma/H^4 < 1$. In the bottom left white region below the colored region of this figure, the strongly first-order EWPT cannot be realized because of $v_n/T_n < 1$. As the value of r gets small, the parameter region with the large Λ value is preferred to realize the strongly first-order EWPT.

Fig. 6.8 represents the parameter region where the strongly first-order EWPT can be realized in the naHEFT with $r = 0.3$, 0.5, 0.8 and 1 in the κ_0 –Λ plane. The colored regions and black dotted contours have the same definitions in Fig. 6.7. For large κ_0 value, the strongly first-order EWPT can be realized by small Λ value. According to Figs. 6.7 and 6.8, the naHEFT with the first-order EWPT can be complementarily tested by collider experiments, GW and PBH observations. These results do not depend on the model details. Therefore, we can expect that extended Higgs models with the strongly first-order EWPT may be tested by collider experiments, GW and PBH observations.

Finally, we show the parameter region where the PBHs can be formed by the first-order EWPT in Fig. 6.9. The solid and dashed red lines in this figure correspond to the same as the red region of Fig. 6.8 for $r = 1$ and 0.3, respectively. In the red region, the PBH fraction may be sizable with $f_{\rm PBH} > 10^{-4}$ for $0.3 < r < 1$. The PBH observation may be able to be used to explore the strongly

first-order EWPT in such a wide parameter region.

6.4 Discussion

We give a comment on the criterion for the PBH formation. The criterion of the PBH formation given in Eq. (6.1.7) is calculated in the case where the radiative components realize a large energy density fluctuation. On the other hand, we have considered the PBH formation mechanism proposed by Liu et al. [120] in this thesis. In order to realize the mechanism, the vacuum energy plays an important to produce the large energy density fluctuation. Therefore, one may doubt whether it is really correct to use the condition (6.1.7). We expect that the analysis of the PBH formation by domain walls will be helpful in resolving this question. The PBH formation via gravitationally collapsing the domain walls is numerically analyzed by Liu, Guo and Cai [229]. The authors have shown that PBHs can be formed when the energy contract between the inside and the outside of the domain walls is sufficiently large. The important point is that the dominant energy component of the domain walls is the vacuum energy. The vacuum energy plays an important role to realize the PBH formation mechanism we focused on in this thesis. Thus, the results in Ref. [229] indicate that the PBH formation mechanism can work well. In the future, however, the mechanism should be verified precisely.

In our analysis, we assume that the Hubble volume collapsing to a PBH has a spherical symmetry. If the shape of the Hubble volume is deformed from the sphere, the criterion (6.1.7) may be changed. The PBH formation with a spheroidal over density region is numerically analyzed [230]. In Ref. [230], it was shown that the criterion for the PBH formation is not changed even if the shape of the overdensity region is not spherical. Therefore, we can expect that the PBH formation mechanism discussed in this thesis works well. Detailed analysis is a future work.

6.5 Summary

In this chapter, we have discussed the relation between the first-order EWPT and PBHs. In order to obtain model independent results, we have used the naHEFT, which is appropriate when we discuss extended Higgs models with the strongly first-order EWPT. We have shown that the first-order EWPT can be tested by PBH observations such as Subaru HSC, OGLE, PRIME and Roman. The wide parameter region with the first-order EWPT may be tested by PBH observations. We have also discussed complementarity of PBH observations, future GW observations and collider experiments to test the first-order EWPT.

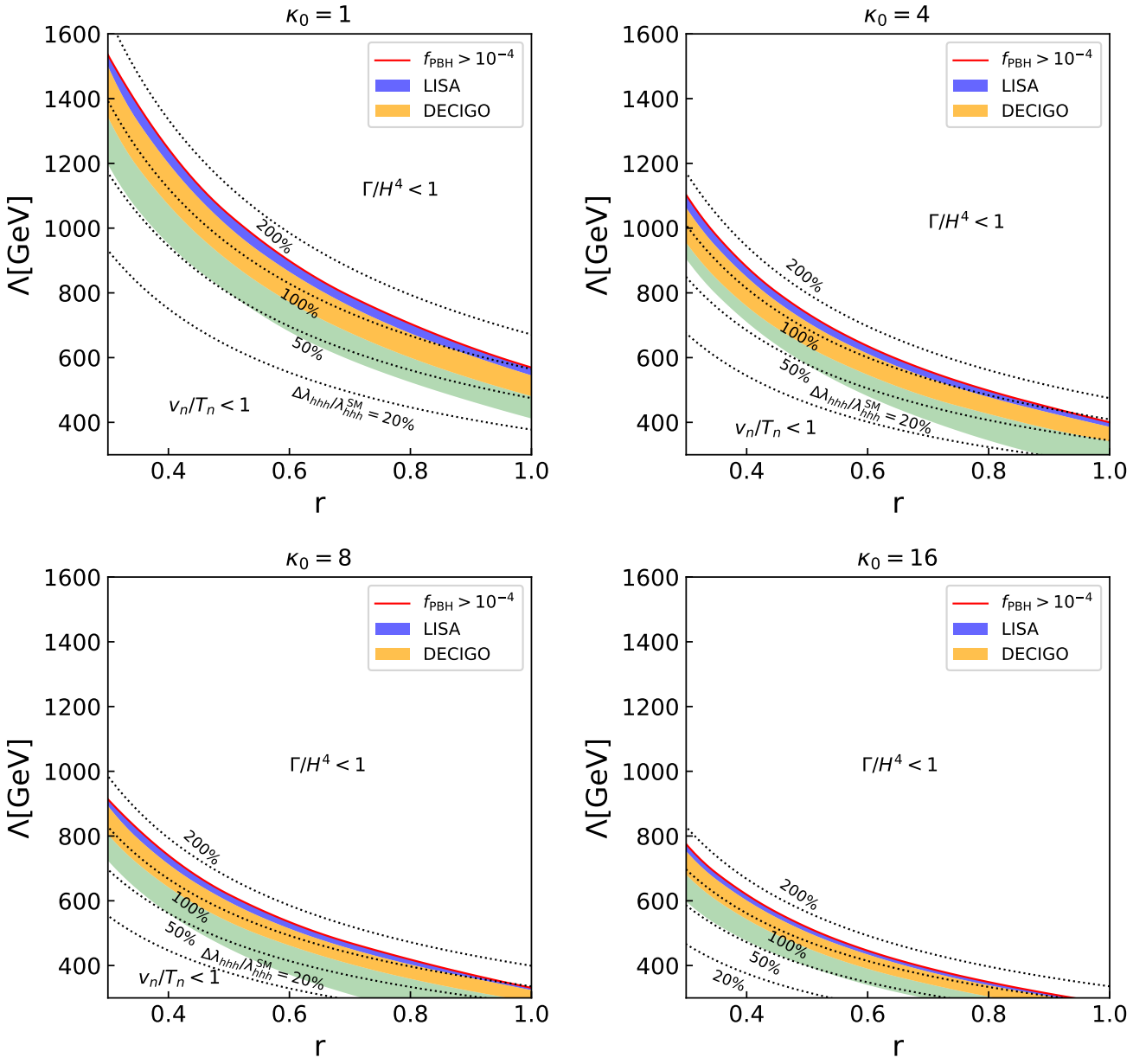

Figure 6.7: Regions of strongly first-order EWPT, where $v_n/T_n \geq 1$, are shown as colored regions in the r-Λ plane for $\kappa_0 = 1$, 4, 8 and 16. In the red region, $f_{\rm PBH}$ can be larger than 10^{-4}. The EWPT has not been finished at the current Universe in top right white regions above the red one: $\Gamma/H^4 < 1$. The orange regions represent that the detectable GW at DECIGO experiment can be produced. The GW spectrum for the blue and red regions can be observed by both LISA and DECIGO experiments. The black dotted lines are the deviation in the hhh coupling from the SM prediction value $\Delta\lambda_{hhh}/\lambda^{\rm SM}_{hhh} = 20$, 50, 100 and 200 % from the bottom, respectively.

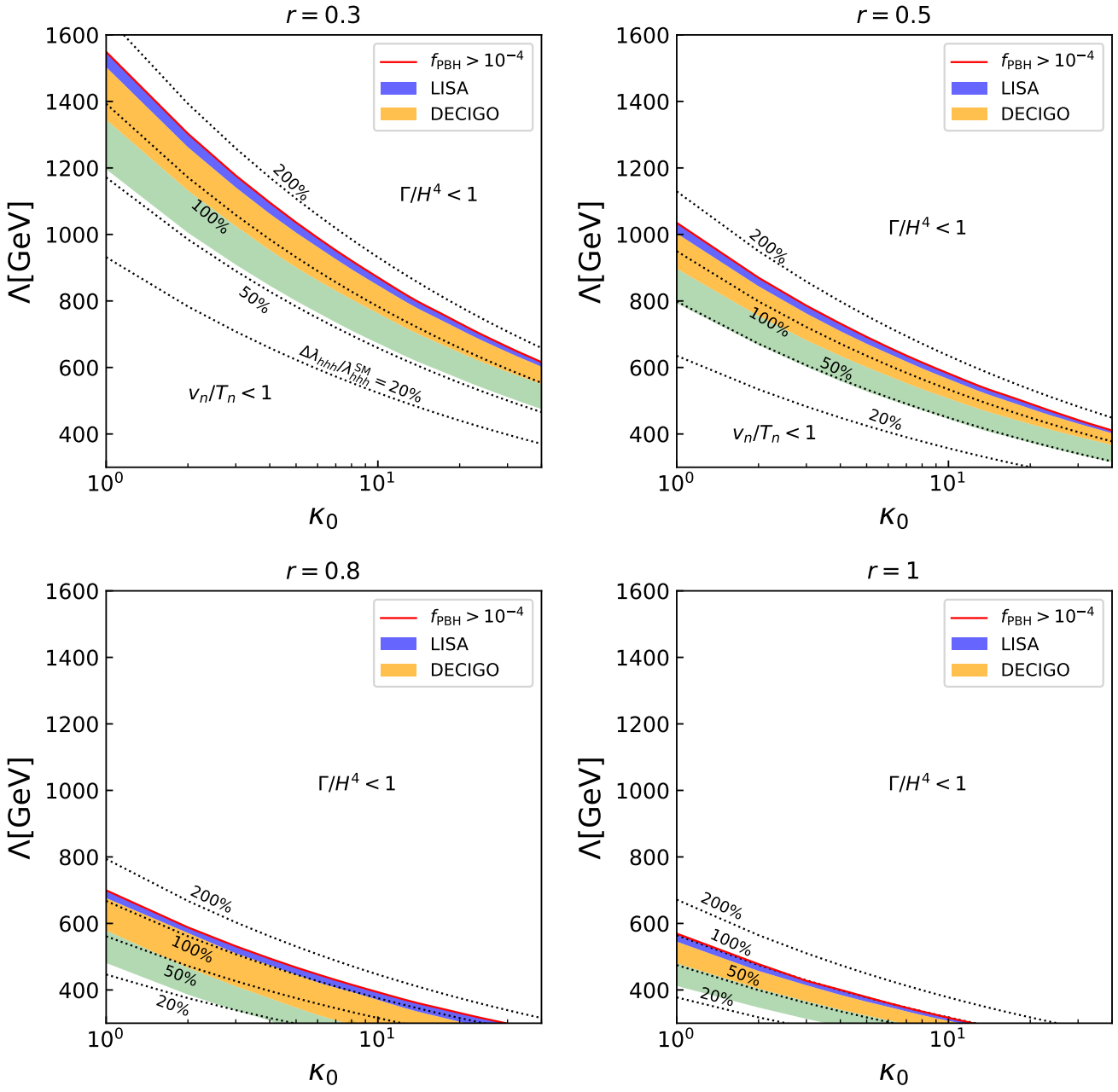

Figure 6.8: Regions of strongly first-order EWPT, where $v_n/T_n \geq 1$, are shown as colored regions in the κ_0-Λ plane for $r = 0.3$, 0.5, 0.8 and 1. Otherwise the same as Fig. 6.7.

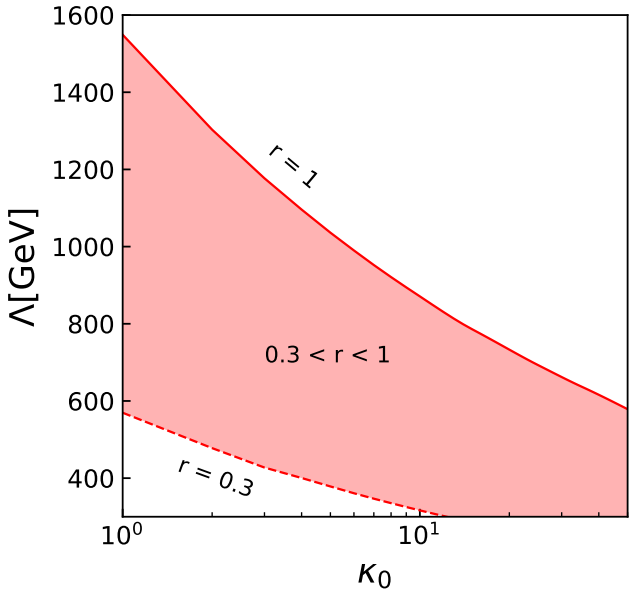

Figure 6.9: The parameter region where PBHs from strongly first-order EWPT may be able to be detected in the κ_0-Λ plane ($f_{\rm PBH} > 10^{-4}$).

Chapter 7

Grand summary

In this chapter, we summarize the contents in this thesis.

In Chapter 2, we have reviewed the SM in particle physics. In the SM, the interactions between elementary particles are determined by the gauge principle. Particles in the SM get their masses via the Higgs mechanism. The predictions on the SM is consistent with the results in the LHC. On the other hand, the SM cannot explain several cosmological observations such as the BAU. In order to explain those cosmological observation facts, extensions of the Higgs sectors have been discussed. If the Higgs sector is extended, dynamics of the EWPT can be changed.

In Chapter 3, we have given a review for extended Higgs models and the details of the first-order EWPT. As examples for renormalizable extended Higgs models, we have focused on the THDMs and $O(N)$ scalar singlet model. In general, extended Higgs models predict existence of heavy new particles. Effects on low energy observations from the new particles can be described by the EFT framework. In this chapter, we have reviewed the SMEFT and the Higgs EFT. We have shown that extensions of the Higgs EFT can describe extended Higgs models with the non-decoupling effects. The non-decoupling effects are important to realize the strongly first-order EWPT, which satisfy the sphaleron decoupling condition given in Eq. (3.4.18). If the strongly first-order EWPT occurs at the early Universe, characteristic GW spectrum can be produced. It means that we can test the strongly first-order EWPT via the GW observations like the LISA and DECIGO.

In Chapter 4, we have discussed the EWPT in the THDMs. To obtain the precise sphaleron decoupling condition, we have numerically calculated the sphaleron energy in the THDMs. By using the improved sphaleron decoupling condition, the parameter regions with the strongly first-order EWPT have been shown. Lower bounds and upper bounds on additional scalar bosons can be determined by using the sphaleron decoupling condition and the unitarity bounds. We have shown that mass upper bounds of additional scalar bosons can be determined by combining the sphaleron decoupling condition and the unitarity bound. The mass upper bounds are about $1.6 - 2\,\mathrm{TeV}$. The bounds implies that the scenario of the EWBG cannot be realized if we cannot discover new scalar bosons whose mass are lighter than $2\,\mathrm{TeV}$. We have also shown that the typical mass scale of new scalar bosons can be determined by using GW observations and the precise measurement of the hhh coupling. It means that we can obtain the information of heavy new particles by the combination of GW observations and hhh coupling measurement even if heavy new particles cannot be detected at collider experiments.

In Chapter 5, we have discussed phenomenology in the naHEFT. The naHEFT can describe extended Higgs models with the non-decoupling effects. We have shown that the naHEFT is appropriate to discuss models with the strongly first-order EWPT. The comparison between the SMEFT and the naHEFT has been also discussed. We have shown that the SMEFT may not be a

good framework when we discuss the strongly first-order EWPT. The predictions on special GW spectra have been also calculated.

In Chapter 6, the relation between the first-order EWPT and PBHs has been discussed. In this thesis, we have focused on the PBH formation mechanism proposed by Liu et al. [120]. In order to obtain model independent results, we have utilized the effective potential in the naHEFT. We have shown that the strongly first-order EWPT can be tested by PBH observations. Especially, PBHs produced by the first-order EWPT can be observed by current and future microlensing observations such as the Subaru HSC, OGLE, PRIME and Roman Space Telescope. Complementarity of PBH observations, future GW observations and collider experiments to test the first-order EWPT has been shown in Figs. 6.7 and 6.8. As shown in Fig. 6.9, wide parameter regions with the strongly first-order EWPT can be explored by PBH observations.

Appendix A

Thermal masses in extended Higgs models

In this appendix, we discuss thermal corrections to masses in the THDMs and $O(N)$ scalar singlet model.

A.1 Thermal masses in the THDMs

In the THDMs, the order parameters ϕ_i $(i = 1, 2)$ are defined by

$$\Phi_i = \frac{1}{\sqrt{2}} \begin{pmatrix} 0 \\ \phi_i \end{pmatrix}. \tag{A.1.1}$$

Then, mass matrices for the Higgs bosons in the THDMs are given by

$$\mathcal{M}_h^2(\phi_1, \phi_2) = \frac{1}{2} \begin{pmatrix} 2m_1^2 + 3\lambda_1\phi_1^2 + (\lambda_3 + \lambda_4 + \lambda_5)\phi_2^2 & -2m_{12}^2 + 2(\lambda_3 + \lambda_4 + \lambda_5)\phi_1\phi_2 \\ -2m_{12}^2 + 2(\lambda_3 + \lambda_4 + \lambda_5)\phi_1\phi_2 & 2m_2^2 + 3\lambda_2\phi_2^2 + (\lambda_3 + \lambda_4 + \lambda_5)\phi_1^2 \end{pmatrix}, \tag{A.1.2}$$

$$\mathcal{M}_z^2(\phi_1, \phi_2) = \frac{1}{2} \begin{pmatrix} 2m_1^2 + \lambda_1\phi_1^2 + (\lambda_3 + \lambda_4 - \lambda_5)\phi_2^2 & -2m_{12}^2 + 2\lambda_5\phi_1\phi_2 \\ -2m_{12}^2 + 2\lambda_5\phi_1\phi_2 & 2m_2^2 + \lambda_2\phi_2^2 + (\lambda_3 + \lambda_4 - \lambda_5)\phi_1^2 \end{pmatrix}, \tag{A.1.3}$$

$$\mathcal{M}_\pm^2(\phi_1, \phi_2) = \frac{1}{2} \begin{pmatrix} 2m_1^2 + \lambda_1\phi_1^2 + \lambda_3\phi_2^2 & -2m_{12}^2 + 2(\lambda_4 + \lambda_5)\phi_1\phi_2 \\ -2m_{12}^2 + 2(\lambda_4 + \lambda_5)\phi_1\phi_2 & 2m_2^2 + \lambda_2\phi_2^2 + \lambda_3\phi_1^2 \end{pmatrix}. \tag{A.1.4}$$

The field dependent masses for the Higgs and Nambu-Goldstone bosons are given by

$$m_{h,H}^2(\phi_1, \phi_2) = \text{Eigenvalue}[\mathcal{M}_h^2(\phi_1, \phi_2)], \tag{A.1.5}$$

$$m_{G,A}^2(\phi_1, \phi_2) = \text{Eigenvalue}[\mathcal{M}_z^2(\phi_1, \phi_2)], \tag{A.1.6}$$

$$m_{G^\pm,H^\pm}^2(\phi_1, \phi_2) = \text{Eigenvalue}[\mathcal{M}_\pm^2(\phi_1, \phi_2)]. \tag{A.1.7}$$

When we consider the thermal corrections to the masses of the Higgs and Nambu-Goldstone bosons, the mass matrices can be expressed by

$$\widehat{\mathcal{M}_h^2}(\phi_1, \phi_2, T) = \mathcal{M}_h^2(\phi_1, \phi_2) + \begin{pmatrix} c_1 & 0 \\ 0 & c_2 \end{pmatrix} T^2, \tag{A.1.8}$$

$$\widehat{\mathcal{M}_z^2}(\phi_1, \phi_2, T) = \mathcal{M}_h^2(\phi_1, \phi_2) + \begin{pmatrix} c_1 & 0 \\ 0 & c_2 \end{pmatrix} T^2, \tag{A.1.9}$$

$$\widehat{\mathcal{M}_\pm^2}(\phi_1, \phi_2, T) = \mathcal{M}_\pm^2(\phi_1, \phi_2) + \begin{pmatrix} c_1 & 0 \\ 0 & c_2 \end{pmatrix} T^2, \tag{A.1.10}$$

where c_i is given by

$$c_1 = \frac{3}{16}g^2 + \frac{1}{16}g'^2 + \frac{\lambda_1}{4} + \frac{\lambda_3}{6} + \frac{\lambda_4}{12}, \tag{A.1.11}$$

$$c_2 = \frac{3}{16}g^2 + \frac{1}{16}g'^2 + \frac{\lambda_2}{4} + \frac{\lambda_3}{6} + \frac{\lambda_4}{12} + \frac{y_t^2}{4} + \frac{y_b^2}{4}. \tag{A.1.12}$$

For weak gauge bosons, thermal mass corrections depend on the component of the gauge boson. The weak gauge bosons with the transverse component does not receive thermal mass corrections. Therefore, we can obtain

$$\widehat{\mathcal{M}}^2_{W_T}(\phi, T) = \mathcal{M}^2_{W_T}(\phi), \tag{A.1.13}$$

$$\widehat{\mathcal{M}}^2_{Z_T}(\phi, T) = \mathcal{M}^2_{Z_T}(\phi). \tag{A.1.14}$$

On the other hand, the weak gauge bosons with the longitudinal component receive thermal mass corrections. The thermal masses are given by

$$\widehat{\mathcal{M}}^2_{W_L}(\phi, T) = \mathcal{M}^2_{W_L}(\phi) + \Pi_W(T), \tag{A.1.15}$$

$$\widehat{\mathcal{M}}^2_{Z_L}(\phi, T) = \frac{1}{2}\left[\frac{g^2+g'^2}{4}\phi^2 + \Pi_W(T) + \Pi_B(T) + \sqrt{\left(\frac{g^2-g'^2}{4}\phi^2 + \Pi_W(T) - \Pi_B(T)\right)^2 + \frac{g^2g'^2}{4}\phi^4}\right], \tag{A.1.16}$$

$$\widehat{\mathcal{M}}^2_{A_L}(\phi, T) = \frac{1}{2}\left[\frac{g^2+g'^2}{4}\phi^2 + \Pi_W(T) + \Pi_B(T) - \sqrt{\left(\frac{g^2-g'^2}{4}\phi^2 + \Pi_W(T) - \Pi_B(T)\right)^2 + \frac{g^2g'^2}{4}\phi^4},\right] \tag{A.1.17}$$

where $\phi^2 = \phi_1^2 + \phi_2^2$. Thermal corrections $\Pi_W(T)$ and $\Pi_B(T)$ in the SM and the THDMs are given by

$$\Pi_W(T) = \begin{cases} \frac{11}{6}g^2T^2 & \text{(SM)} \\ 2g^2T^2 & \text{(THDMs)} \end{cases}, \tag{A.1.18}$$

$$\Pi_B(T) = \begin{cases} \frac{11}{6}g'^2T^2 & \text{(SM)} \\ 2g'^2T^2 & \text{(THDMs)} \end{cases}. \tag{A.1.19}$$

A.2 Thermal masses in the $O(N)$ scalar singlet model

Since the additional singlet scalar field cannot interact with the weak gauge bosons, the thermal masses of the weak gauge bosons are the same as those in the SM. On the contrary, scalar fields can receive thermal corrections. The thermal masses of the singlet scalar fields are given by [68]

$$\widehat{\mathcal{M}^2_S}(\phi, T) = \mu_S^2 + \frac{\lambda_{\Phi S}}{2}\phi^2 + \Pi_S(T), \tag{A.2.1}$$

where the thermal correction Π_S is expressed by

$$\Pi_S(T) = \frac{T^2}{12}\left[(N+2)\lambda_S + 2\lambda_{\Phi S}\right]. \tag{A.2.2}$$

The thermal mass correction in the naHEFT (5.2.10) with $c = \kappa_p$ corresponds to the Π_S with $\lambda_S = 0$. By changing the value of the constant c in Eq. (5.2.10), we can take into account thermal mass corrections from self-interactions of new particles.

Appendix B

Analysis for the PBH production

B.1 Fraction of the false vacua in radiation dominant Universe

In this appendix, we explain the analysis for the PBH production by the first-order phase transition. The following formulae are based on Ref. [231].

As we mentioned, the false vacua with the large vacuum energy are important to realize the PBH formation. The fraction of the false vacuum in the inside and outside of the Hubble volume is given by

$$F^0_{\rm in}(T) = \exp\left[-I^R_{\rm in}(T)\right], \tag{B.1.1}$$
$$F^0_{\rm out}(T) = \exp\left[-I^R_{\rm out}(T)\right], \tag{B.1.2}$$

where

$$I^R_{\rm out}(T) = 12\pi(m_{p\ell}\xi_g)^4 \int_T^{T_C} \frac{dT'}{T'^2}\left(\frac{S_3(T')}{2\pi T'}\right)^{3/2} \exp\left[-\frac{S_3(T')}{T'}\right]\left(\frac{1}{T}-\frac{1}{T'}\right)^3, \tag{B.1.3}$$
$$I^R_{\rm in}(T) = 12\pi(m_{p\ell}\xi_g)^4 \int_T^{T_{\rm in}} \frac{dT'}{T'^2}\left(\frac{S_3(T')}{2\pi T'}\right)^{3/2} \exp\left[-\frac{S_3(T')}{T'}\right]\left(\frac{1}{T}-\frac{1}{T'}\right)^3. \tag{B.1.4}$$

We here assume that the Hubble parameter is mainly determined by the radiation component in the Universe. At $T = T_{\rm in}$, the first-order phase transition starts in the Hubble volume we focus on.

B.2 Determination of the inside and outside Hubble parameter

By using the results in Eqs. (B.1.1) and (B.1.2), we can calculate the vacuum energy density. The vacuum energy densities inside and outside the Hubble volume are given by

$$\rho_V^{\rm in} = F^0_{\rm in}(T)\Delta V_{\rm eff}(T), \tag{B.2.1}$$
$$\rho_V^{\rm out} = F^0_{\rm out}(T)\Delta V_{\rm eff}(T). \tag{B.2.2}$$

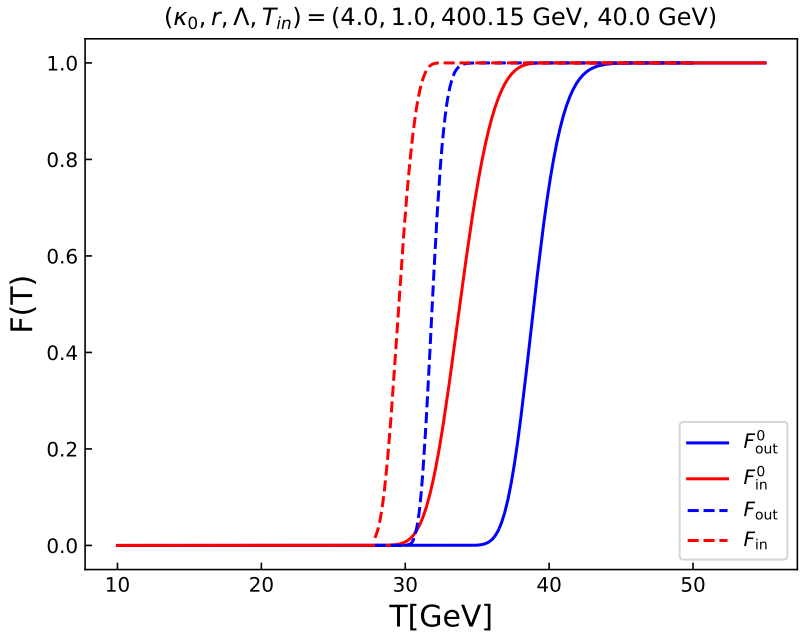

Figure B.1: Fraction of the false vacuum in the naHEFT. We take $\kappa_0 = 4$, $r = 1$, $\Lambda = 400.15\,\mathrm{GeV}$ and $T_{\mathrm{in}} = 40\,\mathrm{GeV}$. The red solid and red dashed line indicate the fraction of the false vacua in the Hubble volume, which may be able to collapse into a PBH. The blue solid and blue dashed line is the fraction of the false vacua outside the Hubble volume.

Effects on the development of the radiation energy density from the vacuum energy densities are determined by the following equations

$$\frac{d\rho_R^{\mathrm{in}}}{dT} + \frac{4\rho_R^{\mathrm{in}}}{T} = -\frac{d\rho_V^{\mathrm{in}}}{dT}, \tag{B.2.3}$$

$$\frac{d\rho_R^{\mathrm{out}}}{dT} + \frac{4\rho_R^{\mathrm{out}}}{T} = -\frac{d\rho_V^{\mathrm{out}}}{dT}. \tag{B.2.4}$$

When we solve the above differential equations, the initial conditions (6.2.8) are used.

As a result, we can obtain the Hubble parameter in the inside and the outside of the Hubble volume as

$$H_{\mathrm{in}}^2 = \frac{1}{3}\left(\rho_R^{\mathrm{in}} + \rho_V^{\mathrm{in}}\right), \tag{B.2.5}$$

$$H_{\mathrm{out}}^2 = \frac{1}{3}\left(\rho_R^{\mathrm{out}} + \rho_V^{\mathrm{out}}\right). \tag{B.2.6}$$

B.3 Fraction of the false vacua with the vacuum energy contribution

In Eqs. (B.1.3), the fraction of the false vacua has been evaluated with the assumption that the radiative component is dominant in the Universe. However, the fraction can be changed by the contribution of the vacuum energy in the false vacua. The fraction of the false vacua with the

vacuum energy contribution is expressed by

$$F_{\rm in,out}(T) = \exp[-I_{\rm in,out}(T)], \tag{B.3.1}$$

with

$$I_{\rm in}(T) = \frac{4\pi}{3}\int_T^{T_C} dT' \frac{\Gamma(T')}{H_V^{\rm in} T'^4 \sqrt{1+\chi_{\rm in}(T')^{-1}}} \left(\int_T^{T'} \frac{d\widetilde{T}}{H_V^{\rm in}\sqrt{1+\chi_{\rm in}(\widetilde{T})^{-1}}}\right)^3, \tag{B.3.2}$$

$$I_{\rm out}(T) = \frac{4\pi}{3}\int_T^{T_{\rm in}} dT' \frac{\Gamma(T')}{H_V^{\rm out} T'^4 \sqrt{1+\chi_{\rm out}(T')^{-1}}} \left(\int_T^{T'} \frac{d\widetilde{T}}{H_V^{\rm out}\sqrt{1+\chi_{\rm out}(\widetilde{T})^{-1}}}\right)^3, \tag{B.3.3}$$

where $(H_V^{\rm in,out})^2 = F_{\rm in,out}(T)\Delta V/(3M_{p\ell}^2)$ and $\chi_{\rm in,out} = \rho_V^{\rm in,out}/\rho_R^{\rm in,out}$. T_c is the critical temperature.

In Fig. B.1, the temperature dependence in the fractions of the false vacua are shown in the naHEFT. We here take $\kappa_0 = 4$, $r = 1$, $\Lambda = 400.15\,\mathrm{GeV}$ and $T_{\rm in} = 40\,\mathrm{GeV}$. The red solid and red dashed line indicate the fraction of the false vacua in the Hubble volume, which may be able to collapse into a PBH. The blue solid and blue dashed line is the fraction of the false vacua outside the Hubble volume.

Then, we can obtain the total energy density in the inside and outside of the Hubble volume, which are given by

$$\rho_{\rm in}(T) = \rho_R^{\rm in}(T) + \rho_V^{\rm in}(T) = \rho_R^{\rm in}(T) + F_{\rm in}(T)\Delta V_{\rm eff}(T), \tag{B.3.4}$$

$$\rho_{\rm out}(T) = \rho_R^{\rm out}(T) + \rho_V^{\rm out}(T) = \rho_R^{\rm out}(T) + F_{\rm out}(T)\Delta V_{\rm eff}(T). \tag{B.3.5}$$

By substituting $\rho_{\rm in}$ and $\rho_{\rm out}$ into the PBH formation criterion (6.2.1), we can determine the values of $t_{\rm PBH}$ and $T_{\rm PBH}$.

In Fig. B.2, the temperature dependence in the fluctuation of the energy density δ is shown in the naHEFT with $\kappa_0 = 4$, $r = 1$, $\Lambda = 400.15\,\mathrm{GeV}$ and $T_{\rm in} = 40\,\mathrm{GeV}$. The gray dotted line corresponds to the case with $\delta = 0.45$. As we can see, the PBH formation condition $\delta > 0.45$ is satisfied when $T_{\rm PBH} = 32.87\,\mathrm{GeV}$.

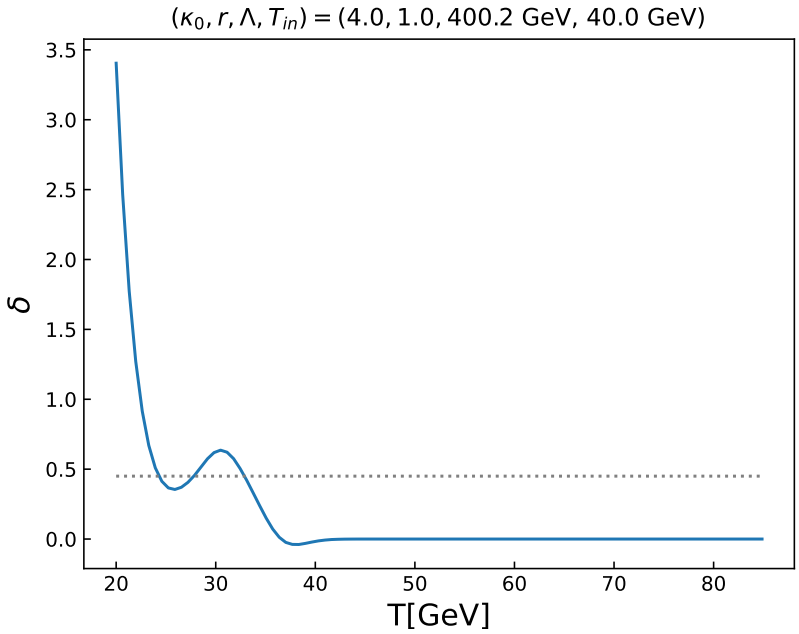

Figure B.2: Fraction of the false vacuum in the naHEFT. We take $\kappa_0 = 4$, $r = 1$, $\Lambda = 400.15\,\text{GeV}$ and $T_{\text{in}} = 40\,\text{GeV}$. The condition $\delta > 0.45$ is satisfied when $T = 32.87\,\text{GeV}$.

Bibliography

[1] Particle Data Group collaboration, *Review of Particle Physics*, *PTEP* **2022** (2022) 083C01.

[2] P. W. Higgs, *Spontaneous Symmetry Breakdown without Massless Bosons*, *Phys. Rev.* **145** (1966) 1156.

[3] P. W. Higgs, *Broken Symmetries and the Masses of Gauge Bosons*, *Phys. Rev. Lett.* **13** (1964) 508.

[4] P. W. Higgs, *Broken symmetries, massless particles and gauge fields*, *Phys. Lett.* **12** (1964) 132.

[5] F. Englert and R. Brout, *Broken Symmetry and the Mass of Gauge Vector Mesons*, *Phys. Rev. Lett.* **13** (1964) 321.

[6] G. S. Guralnik, C. R. Hagen and T. W. B. Kibble, *Global Conservation Laws and Massless Particles*, *Phys. Rev. Lett.* **13** (1964) 585.

[7] K. Kajantie, M. Laine, K. Rummukainen and M. E. Shaposhnikov, *Is there a hot electroweak phase transition at $m_H \gtrsim m_W$?*, *Phys. Rev. Lett.* **77** (1996) 2887 [hep-ph/9605288].

[8] M. D'Onofrio and K. Rummukainen, *Standard model cross-over on the lattice*, *Phys. Rev. D* **93** (2016) 025003 [1508.07161].

[9] S. Kanemura, Y. Okada, E. Senaha and C. P. Yuan, *Higgs coupling constants as a probe of new physics*, *Phys. Rev. D* **70** (2004) 115002 [hep-ph/0408364].

[10] A. Arhrib, M. Capdequi Peyranere, W. Hollik and S. Penaranda, *Higgs decays in the two Higgs doublet model: Large quantum effects in the decoupling regime*, *Phys. Lett. B* **579** (2004) 361 [hep-ph/0307391].

[11] E. Asakawa, D. Harada, S. Kanemura, Y. Okada and K. Tsumura, *Higgs boson pair production at a photon-photon collision in the two Higgs doublet model*, *Phys. Lett. B* **672** (2009) 354 [0809.0094].

[12] E. Asakawa, D. Harada, S. Kanemura, Y. Okada and K. Tsumura, *Higgs boson pair production in new physics models at hadron, lepton, and photon colliders*, *Phys. Rev. D* **82** (2010) 115002 [1009.4670].

[13] S. Kanemura, H. Yokoya and Y.-J. Zheng, *Complementarity in direct searches for additional Higgs bosons at the LHC and the International Linear Collider*, *Nucl. Phys. B* **886** (2014) 524 [1404.5835].

[14] S. Kanemura, K. Tsumura, K. Yagyu and H. Yokoya, *Fingerprinting nonminimal Higgs sectors*, *Phys. Rev. D* **90** (2014) 075001 [1406.3294].

[15] J. Bernon, J. F. Gunion, H. E. Haber, Y. Jiang and S. Kraml, *Scrutinizing the alignment limit in two-Higgs-doublet models: m_h=125 GeV*, *Phys. Rev. D* **92** (2015) 075004 [1507.00933].

[16] M. Krause, R. Lorenz, M. Muhlleitner, R. Santos and H. Ziesche, *Gauge-independent Renormalization of the 2-Higgs-Doublet Model*, *JHEP* **09** (2016) 143 [1605.04853].

[17] J. Bernon, J. F. Gunion, H. E. Haber, Y. Jiang and S. Kraml, *Scrutinizing the alignment limit in two-Higgs-doublet models. II. m_H=125 GeV*, *Phys. Rev. D* **93** (2016) 035027 [1511.03682].

[18] D. Chowdhury and O. Eberhardt, *Update of Global Two-Higgs-Doublet Model Fits*, *JHEP* **05** (2018) 161 [1711.02095].

[19] S. Kanemura, M. Kikuchi, K. Mawatari, K. Sakurai and K. Yagyu, *Full next-to-leading-order calculations of Higgs boson decay rates in models with non-minimal scalar sectors*, *Nucl. Phys. B* **949** (2019) 114791 [1906.10070].

[20] J. Braathen and S. Kanemura, *On two-loop corrections to the Higgs trilinear coupling in models with extended scalar sectors*, *Phys. Lett. B* **796** (2019) 38 [1903.05417].

[21] J. Braathen and S. Kanemura, *Leading two-loop corrections to the Higgs boson self-couplings in models with extended scalar sectors*, *Eur. Phys. J. C* **80** (2020) 227 [1911.11507].

[22] M. Aiko, S. Kanemura, M. Kikuchi, K. Mawatari, K. Sakurai and K. Yagyu, *Probing extended Higgs sectors by the synergy between direct searches at the LHC and precision tests at future lepton colliders*, *Nucl. Phys. B* **966** (2021) 115375 [2010.15057].

[23] S. Kanemura, M. Kikuchi and K. Yagyu, *Next-to-leading order corrections to decays of the heavier CP-even Higgs boson in the two Higgs doublet model*, *Nucl. Phys. B* **983** (2022) 115906 [2203.08337].

[24] S. Iguro, T. Kitahara, Y. Omura and H. Zhang, *Chasing the two-Higgs doublet model in the di-Higgs production*, 2211.00011.

[25] D. López-Val and T. Robens, *Δr and the W-boson mass in the singlet extension of the standard model*, *Phys. Rev. D* **90** (2014) 114018 [1406.1043].

[26] T. Robens and T. Stefaniak, *Status of the Higgs Singlet Extension of the Standard Model after LHC Run 1*, *Eur. Phys. J. C* **75** (2015) 104 [1501.02234].

[27] F. Bojarski, G. Chalons, D. Lopez-Val and T. Robens, *Heavy to light Higgs boson decays at NLO in the Singlet Extension of the Standard Model*, *JHEP* **02** (2016) 147 [1511.08120].

[28] T. Robens and T. Stefaniak, *LHC Benchmark Scenarios for the Real Higgs Singlet Extension of the Standard Model*, *Eur. Phys. J. C* **76** (2016) 268 [1601.07880].

[29] S. Kanemura, M. Kikuchi and K. Yagyu, *Radiative corrections to the Higgs boson couplings in the model with an additional real singlet scalar field*, *Nucl. Phys. B* **907** (2016) 286 [1511.06211].

[30] I. M. Lewis and M. Sullivan, *Benchmarks for Double Higgs Production in the Singlet Extended Standard Model at the LHC*, *Phys. Rev. D* **96** (2017) 035037 [1701.08774].

[31] S. Kanemura, M. Kikuchi and K. Yagyu, *One-loop corrections to the Higgs self-couplings in the singlet extension*, *Nucl. Phys. B* **917** (2017) 154 [1608.01582].

[32] S. Adhikari, I. M. Lewis and M. Sullivan, *Beyond the Standard Model effective field theory: The singlet extended Standard Model*, *Phys. Rev. D* **103** (2021) 075027 [2003.10449].

[33] M. Aoki, S. Kanemura and H. Yokoya, *Reconstruction of Inert Doublet Scalars at the International Linear Collider*, *Phys. Lett. B* **725** (2013) 302 [1303.6191].

[34] A. Arhrib, R. Benbrik, J. El Falaki and A. Jueid, *Radiative corrections to the Triple Higgs Coupling in the Inert Higgs Doublet Model*, *JHEP* **12** (2015) 007 [1507.03630].

[35] S. Kanemura, M. Kikuchi and K. Sakurai, *Testing the dark matter scenario in the inert doublet model by future precision measurements of the Higgs boson couplings*, *Phys. Rev. D* **94** (2016) 115011 [1605.08520].

[36] J. Kalinowski, W. Kotlarski, T. Robens, D. Sokolowska and A. F. Zarnecki, *Benchmarking the Inert Doublet Model for e^+e^- colliders*, *JHEP* **12** (2018) 081 [1809.07712].

[37] F. Arbabifar, S. Bahrami and M. Frank, *Neutral Higgs Bosons in the Higgs Triplet Model with nontrivial mixing*, *Phys. Rev. D* **87** (2013) 015020 [1211.6797].

[38] S. Kanemura, M. Kikuchi and K. Yagyu, *Probing exotic Higgs sectors from the precise measurement of Higgs boson couplings*, *Phys. Rev. D* **88** (2013) 015020 [1301.7303].

[39] M. Aoki, S. Kanemura, M. Kikuchi and K. Yagyu, *Radiative corrections to the Higgs boson couplings in the triplet model*, *Phys. Rev. D* **87** (2013) 015012 [1211.6029].

[40] S. Blunier, G. Cottin, M. A. Díaz and B. Koch, *Phenomenology of a Higgs triplet model at future e^+e^- colliders*, *Phys. Rev. D* **95** (2017) 075038 [1611.07896].

[41] M. Chabab, M. C. Peyranère and L. Rahili, *Probing the Higgs sector of $Y = 0$ Higgs Triplet Model at LHC*, *Eur. Phys. J. C* **78** (2018) 873 [1805.00286].

[42] A. D. Sakharov, *Violation of CP Invariance, C asymmetry, and baryon asymmetry of the universe*, *Pisma Zh. Eksp. Teor. Fiz.* **5** (1967) 32.

[43] V. A. Kuzmin, V. A. Rubakov and M. E. Shaposhnikov, *On the Anomalous Electroweak Baryon Number Nonconservation in the Early Universe*, *Phys. Lett. B* **155** (1985) 36.

[44] N. S. Manton, *Topology in the Weinberg-Salam Theory*, *Phys. Rev. D* **28** (1983) 2019.

[45] F. R. Klinkhamer and N. S. Manton, *A Saddle Point Solution in the Weinberg-Salam Theory*, *Phys. Rev. D* **30** (1984) 2212.

[46] N. Turok and J. Zadrozny, *Phase transitions in the two doublet model*, *Nucl. Phys. B* **369** (1992) 729.

[47] W. N. Cottingham and N. Hasan, *Two Higgs doublet potential at finite temperature*, *Phys. Rev. D* **51** (1995) 866.

[48] J. M. Cline and P.-A. Lemieux, *Electroweak phase transition in two Higgs doublet models*, *Phys. Rev. D* **55** (1997) 3873 [hep-ph/9609240].

[49] J. M. Moreno, D. H. Oaknin and M. Quiros, *Sphalerons in the MSSM*, *Nucl. Phys. B* **483** (1997) 267 [hep-ph/9605387].

[50] S. Kanemura, Y. Okada and E. Senaha, *Electroweak baryogenesis and quantum corrections to the triple Higgs boson coupling*, *Phys. Lett. B* **606** (2005) 361 [hep-ph/0411354].

[51] L. Fromme, S. J. Huber and M. Seniuch, *Baryogenesis in the two-Higgs doublet model*, *JHEP* **11** (2006) 038 [hep-ph/0605242].

[52] K. Funakubo and E. Senaha, *Electroweak phase transition, critical bubbles and sphaleron decoupling condition in the MSSM*, *Phys. Rev. D* **79** (2009) 115024 [0905.2022].

[53] G. C. Dorsch, S. J. Huber, K. Mimasu and J. M. No, *The Higgs Vacuum Uplifted: Revisiting the Electroweak Phase Transition with a Second Higgs Doublet*, *JHEP* **12** (2017) 086 [1705.09186].

[54] P. Basler, M. Krause, M. Muhlleitner, J. Wittbrodt and A. Wlotzka, *Strong First Order Electroweak Phase Transition in the CP-Conserving 2HDM Revisited*, *JHEP* **02** (2017) 121 [1612.04086].

[55] J. Bernon, L. Bian and Y. Jiang, *A new insight into the phase transition in the early Universe with two Higgs doublets*, *JHEP* **05** (2018) 151 [1712.08430].

[56] M. Aoki, T. Komatsu and H. Shibuya, *Possibility of a multi-step electroweak phase transition in the two-Higgs doublet models*, *PTEP* **2022** (2022) 063B05 [2106.03439].

[57] S. Kanemura and M. Tanaka, *Strongly first-order electroweak phase transition by relatively heavy additional Higgs bosons*, *Phys. Rev. D* **106** (2022) 035012 [2201.04791].

[58] T. Biekötter, S. Heinemeyer, J. M. No, M. O. Olea-Romacho and G. Weiglein, *The trap in the early Universe: impact on the interplay between gravitational waves and LHC physics in the 2HDM*, 2208.14466.

[59] A. Ahriche, *What is the criterion for a strong first order electroweak phase transition in singlet models?*, *Phys. Rev. D* **75** (2007) 083522 [hep-ph/0701192].

[60] K. Fuyuto and E. Senaha, *Improved sphaleron decoupling condition and the Higgs coupling constants in the real singlet-extended standard model*, *Phys. Rev. D* **90** (2014) 015015 [1406.0433].

[61] K. Hashino, M. Kakizaki, S. Kanemura, P. Ko and T. Matsui, *Gravitational waves and Higgs boson couplings for exploring first order phase transition in the model with a singlet scalar field*, *Phys. Lett. B* **766** (2017) 49 [1609.00297].

[62] C.-W. Chiang, M. J. Ramsey-Musolf and E. Senaha, *Standard Model with a Complex Scalar Singlet: Cosmological Implications and Theoretical Considerations*, *Phys. Rev. D* **97** (2018) 015005 [1707.09960].

[63] C.-W. Chiang, Y.-T. Li and E. Senaha, *Revisiting electroweak phase transition in the standard model with a real singlet scalar*, *Phys. Lett. B* **789** (2019) 154 [1808.01098].

[64] G.-C. Cho, C. Idegawa and E. Senaha, *Electroweak phase transition in a complex singlet extension of the Standard Model with degenerate scalars*, *Phys. Lett. B* **823** (2021) 136787 [2105.11830].

[65] G.-C. Cho, C. Idegawa and E. Senaha, *CP-violating effects on gravitational waves in a complex singlet extension of the Standard Model with degenerate scalars*, *Phys. Rev. D* **106** (2022) 115012 [2205.12046].

[66] J. R. Espinosa and M. Quiros, *The Electroweak phase transition with a singlet*, *Phys. Lett. B* **305** (1993) 98 [hep-ph/9301285].

[67] J. R. Espinosa, T. Konstandin and F. Riva, *Strong Electroweak Phase Transitions in the Standard Model with a Singlet*, *Nucl. Phys. B* **854** (2012) 592 [1107.5441].

[68] M. Kakizaki, S. Kanemura and T. Matsui, *Gravitational waves as a probe of extended scalar sectors with the first order electroweak phase transition*, *Phys. Rev. D* **92** (2015) 115007 [1509.08394].

[69] K. Hashino, M. Kakizaki, S. Kanemura and T. Matsui, *Synergy between measurements of gravitational waves and the triple-Higgs coupling in probing the first-order electroweak phase transition*, *Phys. Rev. D* **94** (2016) 015005 [1604.02069].

[70] M. Cepeda et al., *Report from Working Group 2: Higgs Physics at the HL-LHC and HE-LHC*, *CERN Yellow Rep. Monogr.* **7** (2019) 221 [1902.00134].

[71] P. Bambade et al., *The International Linear Collider: A Global Project*, 1903.01629.

[72] C. Grojean and G. Servant, *Gravitational Waves from Phase Transitions at the Electroweak Scale and Beyond*, *Phys. Rev. D* **75** (2007) 043507 [hep-ph/0607107].

[73] N. Bartolo et al., *Science with the space-based interferometer LISA. IV: Probing inflation with gravitational waves*, *JCAP* **12** (2016) 026 [1610.06481].

[74] LISA collaboration, *Laser Interferometer Space Antenna*, 1702.00786.

[75] N. Seto, S. Kawamura and T. Nakamura, *Possibility of direct measurement of the acceleration of the universe using 0.1-Hz band laser interferometer gravitational wave antenna in space*, *Phys. Rev. Lett.* **87** (2001) 221103 [astro-ph/0108011].

[76] C. Delaunay, C. Grojean and J. D. Wells, *Dynamics of Non-renormalizable Electroweak Symmetry Breaking*, *JHEP* **04** (2008) 029 [0711.2511].

[77] J. R. Espinosa, T. Konstandin, J. M. No and M. Quiros, *Some Cosmological Implications of Hidden Sectors*, *Phys. Rev. D* **78** (2008) 123528 [0809.3215].

[78] C. Wainwright, S. Profumo and M. J. Ramsey-Musolf, *Gravity Waves from a Cosmological Phase Transition: Gauge Artifacts and Daisy Resummations*, *Phys. Rev. D* **84** (2011) 023521 [1104.5487].

[79] R.-G. Cai, M. Sasaki and S.-J. Wang, *The gravitational waves from the first-order phase transition with a dimension-six operator*, *JCAP* **08** (2017) 004 [1707.03001].

[80] M. Chala, C. Krause and G. Nardini, *Signals of the electroweak phase transition at colliders and gravitational wave observatories*, *JHEP* **07** (2018) 062 [1802.02168].

[81] O. Gould, J. Kozaczuk, L. Niemi, M. J. Ramsey-Musolf, T. V. I. Tenkanen and D. J. Weir, *Nonperturbative analysis of the gravitational waves from a first-order electroweak phase transition*, *Phys. Rev. D* **100** (2019) 115024 [1903.11604].

[82] K. Hashino, R. Jinno, M. Kakizaki, S. Kanemura, T. Takahashi and M. Takimoto, *Selecting models of first-order phase transitions using the synergy between collider and gravitational-wave experiments*, *Phys. Rev. D* **99** (2019) 075011 [1809.04994].

[83] R. Zhou, L. Bian and H.-K. Guo, *Connecting the electroweak sphaleron with gravitational waves*, *Phys. Rev. D* **101** (2020) 091903 [1910.00234].

[84] D. Croon, O. Gould, P. Schicho, T. V. I. Tenkanen and G. White, *Theoretical uncertainties for cosmological first-order phase transitions*, *JHEP* **04** (2021) 055 [2009.10080].

[85] R. Zhou and L. Bian, *Gravitational wave and electroweak baryogenesis with two Higgs doublet models*, *Phys. Lett. B* **829** (2022) 137105 [2001.01237].

[86] K. Enomoto, S. Kanemura and Y. Mura, *New benchmark scenarios of electroweak baryogenesis in aligned two Higgs double models*, *JHEP* **09** (2022) 121 [2207.00060].

[87] K. Hashino, S. Kanemura and T. Takahashi, *Primordial black holes as a probe of strongly first-order electroweak phase transition*, *Phys. Lett. B* **833** (2022) 137261 [2111.13099].

[88] K. Hashino and D. Ueda, *SMEFT effects on gravitational wave spectrum from electroweak phase transition*, 2210.11241.

[89] C. Grojean, G. Servant and J. D. Wells, *First-order electroweak phase transition in the standard model with a low cutoff*, *Phys. Rev. D* **71** (2005) 036001 [hep-ph/0407019].

[90] S. W. Ham and S. K. Oh, *Electroweak phase transition in the standard model with a dimension-six Higgs operator at one-loop level*, *Phys. Rev. D* **70** (2004) 093007 [hep-ph/0408324].

[91] D. Bodeker, L. Fromme, S. J. Huber and M. Seniuch, *The Baryon asymmetry in the standard model with a low cut-off*, *JHEP* **02** (2005) 026 [hep-ph/0412366].

[92] M. Postma and G. White, *Cosmological phase transitions: is effective field theory just a toy?*, *JHEP* **03** (2021) 280 [2012.03953].

[93] A. Falkowski and R. Rattazzi, *Which EFT*, *JHEP* **10** (2019) 255 [1902.05936].

[94] T. Cohen, N. Craig, X. Lu and D. Sutherland, *Is SMEFT Enough?*, *JHEP* **03** (2021) 237 [2008.08597].

[95] S. Kanemura, T. Kubota and E. Takasugi, *Lee-Quigg-Thacker bounds for Higgs boson masses in a two doublet model*, *Phys. Lett. B* **313** (1993) 155 [hep-ph/9303263].

[96] S. Kanemura and K. Yagyu, *Unitarity bound in the most general two Higgs doublet model*, *Phys. Lett. B* **751** (2015) 289 [1509.06060].

[97] F. Feruglio, *The Chiral approach to the electroweak interactions*, *Int. J. Mod. Phys. A* **8** (1993) 4937 [hep-ph/9301281].

[98] C. P. Burgess, J. Matias and M. Pospelov, *A Higgs or not a Higgs? What to do if you discover a new scalar particle*, *Int. J. Mod. Phys. A* **17** (2002) 1841 [hep-ph/9912459].

[99] B. Grinstein and M. Trott, *A Higgs-Higgs bound state due to new physics at a TeV*, *Phys. Rev. D* **76** (2007) 073002 [0704.1505].

[100] G. F. Giudice, C. Grojean, A. Pomarol and R. Rattazzi, *The Strongly-Interacting Light Higgs*, *JHEP* **06** (2007) 045 [hep-ph/0703164].

[101] G. Buchalla and O. Cata, *Effective Theory of a Dynamically Broken Electroweak Standard Model at NLO*, *JHEP* **07** (2012) 101 [1203.6510].

[102] A. Azatov, R. Contino and J. Galloway, *Model-Independent Bounds on a Light Higgs*, *JHEP* **04** (2012) 127 [1202.3415].

[103] R. Contino, M. Ghezzi, C. Grojean, M. Muhlleitner and M. Spira, *Effective Lagrangian for a light Higgs-like scalar*, *JHEP* **07** (2013) 035 [1303.3876].

[104] R. Alonso, M. B. Gavela, L. Merlo, S. Rigolin and J. Yepes, *The Effective Chiral Lagrangian for a Light Dynamical "Higgs Particle"*, *Phys. Lett. B* **722** (2013) 330 [1212.3305].

[105] G. Buchalla, O. Catà and C. Krause, *Complete Electroweak Chiral Lagrangian with a Light Higgs at NLO*, *Nucl. Phys. B* **880** (2014) 552 [1307.5017].

[106] F.-K. Guo, P. Ruiz-Femenía and J. J. Sanz-Cillero, *One loop renormalization of the electroweak chiral Lagrangian with a light Higgs boson*, *Phys. Rev. D* **92** (2015) 074005 [1506.04204].

[107] G. Buchalla, O. Cata, A. Celis and C. Krause, *Fitting Higgs Data with Nonlinear Effective Theory*, *Eur. Phys. J. C* **76** (2016) 233 [1511.00988].

[108] G. Buchalla, O. Cata, A. Celis, M. Knecht and C. Krause, *Complete One-Loop Renormalization of the Higgs-Electroweak Chiral Lagrangian*, *Nucl. Phys. B* **928** (2018) 93 [1710.06412].

[109] G. Buchalla, M. Capozi, A. Celis, G. Heinrich and L. Scyboz, *Higgs boson pair production in non-linear Effective Field Theory with full m_t-dependence at NLO QCD*, *JHEP* **09** (2018) 057 [1806.05162].

[110] R. Alonso, K. Kanshin and S. Saa, *Renormalization group evolution of Higgs effective field theory*, *Phys. Rev. D* **97** (2018) 035010 [1710.06848].

[111] S. Hawking, *Gravitationally collapsed objects of very low mass*, *Mon. Not. Roy. Astron. Soc.* **152** (1971) 75.

[112] B. J. Carr and S. W. Hawking, *Black holes in the early Universe*, *Mon. Not. Roy. Astron. Soc.* **168** (1974) 399.

[113] B. J. Carr, *The Primordial black hole mass spectrum*, *Astrophys. J.* **201** (1975) 1.

[114] H. Kodama, M. Sasaki and K. Sato, *Abundance of Primordial Holes Produced by Cosmological First Order Phase Transition*, *Prog. Theor. Phys.* **68** (1982) 1979.

[115] S. W. Hawking, I. G. Moss and J. M. Stewart, *Bubble Collisions in the Very Early Universe*, *Phys. Rev. D* **26** (1982) 2681.

[116] C. Gross, G. Landini, A. Strumia and D. Teresi, *Dark Matter as dark dwarfs and other macroscopic objects: multiverse relics?*, *JHEP* **09** (2021) 033 [2105.02840].

[117] M. J. Baker, M. Breitbach, J. Kopp and L. Mittnacht, *Primordial Black Holes from First-Order Cosmological Phase Transitions*, 2105.07481.

[118] M. J. Baker, M. Breitbach, J. Kopp and L. Mittnacht, *Detailed Calculation of Primordial Black Hole Formation During First-Order Cosmological Phase Transitions*, 2110.00005.

[119] T. H. Jung and T. Okui, *Primordial black holes from bubble collisions during a first-order phase transition*, 2110.04271.

[120] J. Liu, L. Bian, R.-G. Cai, Z.-K. Guo and S.-J. Wang, *Primordial black hole production during first-order phase transitions*, *Phys. Rev. D* **105** (2022) L021303 [2106.05637].

[121] K. Kawana and K.-P. Xie, *Primordial black holes from a cosmic phase transition: The collapse of Fermi-balls*, *Phys. Lett. B* **824** (2022) 136791 [2106.00111].

[122] P. Huang and K.-P. Xie, *Primordial black holes from an electroweak phase transition*, 2201.07243.

[123] K. Nishijima, *Charge Independence Theory of V Particles*, *Prog. Theor. Phys.* **13** (1955) 285.

[124] M. Gell-Mann, *The interpretation of the new particles as displaced charge multiplets*, *Nuovo Cim.* **4** (1956) 848.

[125] S. L. Glashow, *Partial Symmetries of Weak Interactions*, *Nucl. Phys.* **22** (1961) 579.

[126] S. Weinberg, *A Model of Leptons*, *Phys. Rev. Lett.* **19** (1967) 1264.

[127] A. Salam, *Weak and Electromagnetic Interactions*, *Conf. Proc. C* **680519** (1968) 367.

[128] G. H. Derrick, *Comments on nonlinear wave equations as models for elementary particles*, *J. Math. Phys.* **5** (1964) 1252.

[129] N. Cabibbo, *Unitary Symmetry and Leptonic Decays*, *Phys. Rev. Lett.* **10** (1963) 531.

[130] M. Kobayashi and T. Maskawa, *CP Violation in the Renormalizable Theory of Weak Interaction*, *Prog. Theor. Phys.* **49** (1973) 652.

[131] S. L. Glashow, J. Iliopoulos and L. Maiani, *Weak Interactions with Lepton-Hadron Symmetry*, *Phys. Rev. D* **2** (1970) 1285.

[132] M. E. Peskin and D. V. Schroeder, *An Introduction to quantum field theory*. Addison-Wesley, Reading, USA, 1995.

[133] B. W. Lee, C. Quigg and H. B. Thacker, *The Strength of Weak Interactions at Very High-Energies and the Higgs Boson Mass*, *Phys. Rev. Lett.* **38** (1977) 883.

[134] B. W. Lee, C. Quigg and H. B. Thacker, *Weak Interactions at Very High-Energies: The Role of the Higgs Boson Mass*, *Phys. Rev. D* **16** (1977) 1519.

[135] J. F. Gunion, H. E. Haber, G. L. Kane and S. Dawson, *The Higgs Hunter's Guide*, vol. 80. 2000.

[136] G. Degrassi, S. Di Vita, J. Elias-Miro, J. R. Espinosa, G. F. Giudice, G. Isidori et al., *Higgs mass and vacuum stability in the Standard Model at NNLO*, *JHEP* **08** (2012) 098 [1205.6497].

[137] N. G. Deshpande and E. Ma, *Pattern of Symmetry Breaking with Two Higgs Doublets*, *Phys. Rev. D* **18** (1978) 2574.

[138] K. G. Klimenko, *On Necessary and Sufficient Conditions for Some Higgs Potentials to Be Bounded From Below*, *Theor. Math. Phys.* **62** (1985) 58.

[139] M. Sher, *Electroweak Higgs Potentials and Vacuum Stability*, *Phys. Rept.* **179** (1989) 273.

[140] S. Nie and M. Sher, *Vacuum stability bounds in the two Higgs doublet model*, *Phys. Lett. B* **449** (1999) 89 [hep-ph/9811234].

[141] M. E. Peskin and T. Takeuchi, *Estimation of oblique electroweak corrections*, *Phys. Rev. D* **46** (1992) 381.

[142] I. Maksymyk, C. P. Burgess and D. London, *Beyond S, T and U*, *Phys. Rev. D* **50** (1994) 529 [hep-ph/9306267].

[143] J. Haller, A. Hoecker, R. Kogler, K. Mönig, T. Peiffer and J. Stelzer, *Update of the global electroweak fit and constraints on two-Higgs-doublet models*, *Eur. Phys. J. C* **78** (2018) 675 [1803.01853].

[144] CMS collaboration, *A portrait of the Higgs boson by the CMS experiment ten years after the discovery*, *Nature* **607** (2022) 60 [2207.00043].

[145] LHC Higgs Cross Section Working Group collaboration, *Handbook of LHC Higgs Cross Sections: 3. Higgs Properties*, 1307.1347.

[146] ATLAS collaboration, *Constraining the Higgs boson self-coupling from single- and double-Higgs production with the ATLAS detector using pp collisions at* $\sqrt{s} = 13$ *TeV*, 2211.01216.

[147] K. Enomoto, S. Kanemura and Y. Mura, *Electroweak baryogenesis in aligned two Higgs doublet models*, *JHEP* **01** (2022) 104 [2111.13079].

[148] P. Basler, M. Mühlleitner and J. Müller, *Electroweak Baryogenesis in the CP-Violating Two-Higgs Doublet Model*, 2108.03580.

[149] ACME collaboration, *Improved limit on the electric dipole moment of the electron*, *Nature* **562** (2018) 355.

[150] C. Abel et al., *Measurement of the Permanent Electric Dipole Moment of the Neutron*, *Phys. Rev. Lett.* **124** (2020) 081803 [2001.11966].

[151] S. Kanemura, M. Kubota and K. Yagyu, *Aligned CP-violating Higgs sector canceling the electric dipole moment*, *JHEP* **08** (2020) 026 [2004.03943].

[152] S. Kanemura, M. Kubota and K. Yagyu, *Testing aligned CP-violating Higgs sector at future lepton colliders*, *JHEP* **04** (2021) 144 [2101.03702].

[153] P. Basler, M. Mühlleitner and J. Wittbrodt, *The CP-Violating 2HDM in Light of a Strong First Order Electroweak Phase Transition and Implications for Higgs Pair Production*, *JHEP* **03** (2018) 061 [1711.04097].

[154] E. Senaha, *Radiative Corrections to Triple Higgs Coupling and Electroweak Phase Transition: Beyond One-loop Analysis*, *Phys. Rev. D* **100** (2019) 055034 [1811.00336].

[155] J. Braathen, S. Kanemura and M. Shimoda, *Two-loop analysis of classically scale-invariant models with extended Higgs sectors*, *JHEP* **03** (2021) 297 [2011.07580].

[156] M. A. Shifman, A. I. Vainshtein, M. B. Voloshin and V. I. Zakharov, *Low-Energy Theorems for Higgs Boson Couplings to Photons*, *Sov. J. Nucl. Phys.* **30** (1979) 711.

[157] ALEPH, DELPHI, L3, OPAL, LEP collaboration, *Search for Charged Higgs bosons: Combined Results Using LEP Data*, *Eur. Phys. J. C* **73** (2013) 2463 [1301.6065].

[158] D. Toussaint, *Renormalization Effects From Superheavy Higgs Particles*, *Phys. Rev. D* **18** (1978) 1626.

[159] S. Bertolini, *Quantum Effects in a Two Higgs Doublet Model of the Electroweak Interactions*, *Nucl. Phys. B* **272** (1986) 77.

[160] W. Grimus, L. Lavoura, O. M. Ogreid and P. Osland, *The Oblique parameters in multi-Higgs-doublet models*, *Nucl. Phys. B* **801** (2008) 81 [0802.4353].

[161] Particle Data Group collaboration, *Review of Particle Physics*, *Phys. Rev. D* **98** (2018) 030001.

[162] A. Pomarol and R. Vega, *Constraints on CP violation in the Higgs sector from the rho parameter*, *Nucl. Phys. B* **413** (1994) 3 [hep-ph/9305272].

[163] J. M. Gerard and M. Herquet, *A Twisted custodial symmetry in the two-Higgs-doublet model*, *Phys. Rev. Lett.* **98** (2007) 251802 [hep-ph/0703051].

[164] S. de Visscher, J.-M. Gerard, M. Herquet, V. Lemaitre and F. Maltoni, *Unconventional phenomenology of a minimal two-Higgs-doublet model*, *JHEP* **08** (2009) 042 [0904.0705].

[165] J. M. Cornwall, D. N. Levin and G. Tiktopoulos, *Uniqueness of spontaneously broken gauge theories*, *Phys. Rev. Lett.* **30** (1973) 1268.

[166] J. M. Cornwall, D. N. Levin and G. Tiktopoulos, *Derivation of Gauge Invariance from High-Energy Unitarity Bounds on the s Matrix*, *Phys. Rev. D* **10** (1974) 1145.

[167] S. Kanemura, T. Kasai and Y. Okada, *Mass bounds of the lightest CP even Higgs boson in the two Higgs doublet model*, *Phys. Lett. B* **471** (1999) 182 [hep-ph/9903289].

[168] J. R. Espinosa and M. Quiros, *Novel Effects in Electroweak Breaking from a Hidden Sector*, *Phys. Rev. D* **76** (2007) 076004 [hep-ph/0701145].

[169] D. Curtin, P. Meade and C.-T. Yu, *Testing Electroweak Baryogenesis with Future Colliders*, *JHEP* **11** (2014) 127 [1409.0005].

[170] T. Appelquist and J. Carazzone, *Infrared Singularities and Massive Fields*, *Phys. Rev. D* **11** (1975) 2856.

[171] B. Grzadkowski, M. Iskrzynski, M. Misiak and J. Rosiek, *Dimension-Six Terms in the Standard Model Lagrangian*, *JHEP* **10** (2010) 085 [1008.4884].

[172] R. Alonso, E. E. Jenkins, A. V. Manohar and M. Trott, *Renormalization Group Evolution of the Standard Model Dimension Six Operators III: Gauge Coupling Dependence and Phenomenology*, *JHEP* **04** (2014) 159 [1312.2014].

[173] B. Henning, X. Lu and H. Murayama, *How to use the Standard Model effective field theory*, *JHEP* **01** (2016) 023 [1412.1837].

[174] J. Ellis, M. Madigan, K. Mimasu, V. Sanz and T. You, *Top, Higgs, Diboson and Electroweak Fit to the Standard Model Effective Field Theory*, *JHEP* **04** (2021) 279 [2012.02779].

[175] V. Barger, T. Han, P. Langacker, B. McElrath and P. Zerwas, *Effects of genuine dimension-six Higgs operators*, *Phys. Rev. D* **67** (2003) 115001 [hep-ph/0301097].

[176] S. A. R. Ellis, S. Ipek and G. White, *Electroweak Baryogenesis from Temperature-Varying Couplings*, *JHEP* **08** (2019) 002 [1905.11994].

[177] R. Alonso, E. E. Jenkins and A. V. Manohar, *Geometry of the Scalar Sector*, *JHEP* **08** (2016) 101 [1605.03602].

[178] S. R. Coleman and E. J. Weinberg, *Radiative Corrections as the Origin of Spontaneous Symmetry Breaking*, *Phys. Rev. D* **7** (1973) 1888.

[179] S. Kanemura and R. Nagai, *A new Higgs effective field theory and the new no-lose theorem*, *JHEP* **03** (2022) 194 [2111.12585].

[180] G. Steigman, *Observational tests of antimatter cosmologies*, *Ann. Rev. Astron. Astrophys.* **14** (1976) 339.

[181] G. 't Hooft, *Computation of the Quantum Effects Due to a Four-Dimensional Pseudoparticle*, *Phys. Rev. D* **14** (1976) 3432.

[182] G. 't Hooft, *Symmetry Breaking Through Bell-Jackiw Anomalies*, *Phys. Rev. Lett.* **37** (1976) 8.

[183] P. B. Arnold and L. D. McLerran, *Sphalerons, Small Fluctuations and Baryon Number Violation in Electroweak Theory*, *Phys. Rev. D* **36** (1987) 581.

[184] K. Funakubo, A. Kakuto, S. Tao and F. Toyoda, *Sphalerons in the NMSSM*, *Prog. Theor. Phys.* **114** (2006) 1069 [hep-ph/0506156].

[185] A. Ahriche, *Sphalerons on Orbifolds*, *Eur. Phys. J. C* **66** (2010) 333 [0904.0700].

[186] A. Ahriche, T. A. Chowdhury and S. Nasri, *Sphalerons and the Electroweak Phase Transition in Models with Higher Scalar Representations*, *JHEP* **11** (2014) 096 [1409.4086].

[187] K. Fuyuto and E. Senaha, *Sphaleron and critical bubble in the scale invariant two Higgs doublet model*, *Phys. Lett. B* **747** (2015) 152 [1504.04291].

[188] X. Gan, A. J. Long and L.-T. Wang, *Electroweak sphaleron with dimension-six operators*, *Phys. Rev. D* **96** (2017) 115018 [1708.03061].

[189] M. Spannowsky and C. Tamarit, *Sphalerons in composite and non-standard Higgs models*, *Phys. Rev. D* **95** (2017) 015006 [1611.05466].

[190] S. Kanemura and M. Tanaka, *Higgs boson coupling as a probe of the sphaleron property*, *Phys. Lett. B* **809** (2020) 135711 [2005.05250].

[191] V. Q. Phong, P. H. Khiem, N. P. D. Loc and H. N. Long, *Sphaleron in the first-order electroweak phase transition with the dimension-six Higgs field operator*, *Phys. Rev. D* **101** (2020) 116010 [2003.09625].

[192] A. D. Linde, *Decay of the False Vacuum at Finite Temperature*, *Nucl. Phys. B* **216** (1983) 421.

[193] C. L. Wainwright, *CosmoTransitions: Computing Cosmological Phase Transition Temperatures and Bubble Profiles with Multiple Fields*, *Comput. Phys. Commun.* **183** (2012) 2006 [1109.4189].

[194] M. Fukugita and T. Yanagida, *Baryogenesis Without Grand Unification*, *Phys. Lett. B* **174** (1986) 45.

[195] L. Carson, X. Li, L. D. McLerran and R.-T. Wang, *Exact Computation of the Small Fluctuation Determinant Around a Sphaleron*, *Phys. Rev. D* **42** (1990) 2127.

[196] L. Carson and L. D. McLerran, *Approximate Computation of the Small Fluctuation Determinant Around a Sphaleron*, *Phys. Rev. D* **41** (1990) 647.

[197] S. J. Huber and T. Konstandin, *Gravitational Wave Production by Collisions: More Bubbles*, *JCAP* **09** (2008) 022 [0806.1828].

[198] C. Caprini et al., *Science with the space-based interferometer eLISA. II: Gravitational waves from cosmological phase transitions*, *JCAP* **04** (2016) 001 [1512.06239].

[199] J. R. Espinosa, T. Konstandin, J. M. No and G. Servant, *Energy Budget of Cosmological First-order Phase Transitions*, *JCAP* **06** (2010) 028 [1004.4187].

[200] P. Binetruy, A. Bohe, C. Caprini and J.-F. Dufaux, *Cosmological Backgrounds of Gravitational Waves and eLISA/NGO: Phase Transitions, Cosmic Strings and Other Sources*, *JCAP* **06** (2012) 027 [1201.0983].

[201] C. Caprini, R. Durrer and G. Servant, *The stochastic gravitational wave background from turbulence and magnetic fields generated by a first-order phase transition*, *JCAP* **12** (2009) 024 [0909.0622].

[202] J. M. Cline, A. Friedlander, D.-M. He, K. Kainulainen, B. Laurent and D. Tucker-Smith, *Baryogenesis and gravity waves from a UV-completed electroweak phase transition*, *Phys. Rev. D* **103** (2021) 123529 [2102.12490].

[203] L. Dolan and R. Jackiw, *Symmetry Behavior at Finite Temperature*, *Phys. Rev. D* **9** (1974) 3320.

[204] R. R. Parwani, *Resummation in a hot scalar field theory*, *Phys. Rev. D* **45** (1992) 4695 [hep-ph/9204216].

[205] P. B. Arnold and O. Espinosa, *The Effective potential and first order phase transitions: Beyond leading-order*, *Phys. Rev. D* **47** (1993) 3546 [hep-ph/9212235].

[206] Y. Hamada and K. Kikuchi, *Obtaining the sphaleron field configurations with gradient flow*, *Phys. Rev. D* **101** (2020) 096014 [2003.02070].

[207] V. Corbin and N. J. Cornish, *Detecting the cosmic gravitational wave background with the big bang observer*, *Class. Quant. Grav.* **23** (2006) 2435 [gr-qc/0512039].

[208] W.-H. Ruan, Z.-K. Guo, R.-G. Cai and Y.-Z. Zhang, *Taiji program: Gravitational-wave sources*, *Int. J. Mod. Phys. A* **35** (2020) 2050075 [1807.09495].

[209] TianQin collaboration, *TianQin: a space-borne gravitational wave detector*, *Class. Quant. Grav.* **33** (2016) 035010 [1512.02076].

[210] J. E. Camargo-Molina, R. Enberg and J. Löfgren, *A new perspective on the electroweak phase transition in the Standard Model Effective Field Theory*, *JHEP* **10** (2021) 127 [2103.14022].

[211] S. Weinberg, *Gauge and Global Symmetries at High Temperature*, *Phys. Rev. D* **9** (1974) 3357.

[212] S. Kanemura, R. Nagai and M. Tanaka, *Electroweak phase transition in the nearly aligned Higgs effective field theory*, *JHEP* **06** (2022) 027 [2202.12774].

[213] P. H. Damgaard, A. Haarr, D. O'Connell and A. Tranberg, *Effective Field Theory and Electroweak Baryogenesis in the Singlet-Extended Standard Model*, *JHEP* **02** (2016) 107 [1512.01963].

[214] J. de Vries, M. Postma, J. van de Vis and G. White, *Electroweak Baryogenesis and the Standard Model Effective Field Theory*, *JHEP* **01** (2018) 089 [1710.04061].

[215] T. Harada, C.-M. Yoo and K. Kohri, *Threshold of primordial black hole formation*, *Phys. Rev. D* **88** (2013) 084051 [1309.4201].

[216] J. C. Niemeyer and K. Jedamzik, *Dynamics of primordial black hole formation*, *Phys. Rev. D* **59** (1999) 124013 [astro-ph/9901292].

[217] I. Musco, J. C. Miller and L. Rezzolla, *Computations of primordial black hole formation*, *Class. Quant. Grav.* **22** (2005) 1405 [gr-qc/0412063].

[218] I. Musco and J. C. Miller, *Primordial black hole formation in the early universe: critical behaviour and self-similarity*, *Class. Quant. Grav.* **30** (2013) 145009 [1201.2379].

[219] K. Hashino, S. Kanemura, T. Takahashi and M. Tanaka, *Probing first-order electroweak phase transition via primordial black holes in the effective field theory*, 2211.16225.

[220] M. S. Turner, E. J. Weinberg and L. M. Widrow, *Bubble nucleation in first order inflation and other cosmological phase transitions*, *Phys. Rev. D* **46** (1992) 2384.

[221] M. E. Carrington and J. I. Kapusta, *Dynamics of the electroweak phase transition*, *Phys. Rev. D* **47** (1993) 5304.

[222] E. W. Kolb and M. S. Turner, *The Early Universe*, vol. 69. 1990, 10.1201/9780429492860.

[223] D. Croon, D. McKeen, N. Raj and Z. Wang, *Subaru-HSC through a different lens: Microlensing by extended dark matter structures*, *Phys. Rev. D* **102** (2020) 083021 [2007.12697].

[224] H. Niikura, M. Takada, S. Yokoyama, T. Sumi and S. Masaki, *Constraints on Earth-mass primordial black holes from OGLE 5-year microlensing events*, *Phys. Rev. D* **99** (2019) 083503 [1901.07120].

[225] P. Tisserand, L. Le Guillou, C. Afonso, J. Albert, J. Andersen, R. Ansari et al., *Limits on the macho content of the galactic halo from the eros-2 survey of the magellanic clouds*, *Astronomy & Astrophysics* **469** (2007) 387.

[226] S. A. Johnson, M. Penny, B. S. Gaudi, E. Kerins, N. J. Rattenbury, A. C. Robin et al., *Predictions of the nancy grace roman space telescope galactic exoplanet survey. ii. free-floating planet detection rates*, *The Astronomical Journal* **160** (2020) 123.

[227] G. W. Anderson and L. J. Hall, *The Electroweak phase transition and baryogenesis*, *Phys. Rev. D* **45** (1992) 2685.

[228] A. Eichhorn, J. Lumma, J. M. Pawlowski, M. Reichert and M. Yamada, *Universal gravitational-wave signatures from heavy new physics in the electroweak sector*, *JCAP* **05** (2021) 006 [2010.00017].

[229] J. Liu, Z.-K. Guo and R.-G. Cai, *Primordial Black Holes from Cosmic Domain Walls*, *Phys. Rev. D* **101** (2020) 023513 [1908.02662].

[230] C.-M. Yoo, T. Harada and H. Okawa, *Threshold of Primordial Black Hole Formation in Nonspherical Collapse*, *Phys. Rev. D* **102** (2020) 043526 [2004.01042].

[231] J. Ellis, M. Lewicki and J. M. No, *On the Maximal Strength of a First-Order Electroweak Phase Transition and its Gravitational Wave Signal*, *JCAP* **04** (2019) 003 [1809.08242].